Communicating the Impacts of Potential Future Climate Change on the Expected Frequency of Extreme Rainfall Events in Cook County, Illinois

Momcilo Markus, James Angel, Gregory Byard, Chen Zhang, Zoe Zaloudek, Sally McConkey

May 2016

Communicating the Impacts of Potential Future Climate Change on the Expected Frequency of Extreme Rainfall Events in Cook County, Illinois

Principal Investigators:
Momcilo Markus
James Angel
Gregory Byard
Chen Zhang
Zoe Zaloudek
Sally McConkey

Abstract

A novel methodology for determining future rainfall frequency is described in this report. Isohyetal maps illustrate how heavy precipitation may change in the future, but the results have a high level of uncertainty expressed as very wide confidence limits. Uncertainty in possible future conditions is much greater than the uncertainty identified for current commonly used precipitation analyses. The resulting isohyetal maps do not replace existing sources, such as Illinois State Water Survey (ISWS) Bulletin 70 (Huff and Angel, 1989) or National Oceanic and Atmospheric Administration (NOAA) Atlas 14 (Bonnin et al., 2006). Presently, the ISWS is updating Bulletin 70 (Huff and Angel, 1989) for subregions of Illinois. Some of these updates will include projected rainfall frequency.

The key objectives of this study are to i) design a framework to translate future climate scenarios into a product that engineers and planners can use to quantify the impact of climate change, and ii) demonstrate how climate model output can be used to inform and plan adaptive strategies for stormwater and floodplain management. The framework in this study is illustrated using the observed and projected rainfall data in Cook County, Illinois, providing a road map to evaluate climate change impacts on urban flooding and a plan for adaptation.

Numerous studies attempt to identify the implications of climate change with respect to hydrologic extremes (e.g., IPCC, 2007; CCSP, 2008; Milly et al., 2008). These studies project future climate conditions with more frequent extreme precipitation events in many regions around the world, including parts of the United States. In particular, it has been projected that northeastern Illinois, including the Chicago metropolitan area, will experience more frequent and more intense rainfall events in the future (Markus et al., 2012), which will lead to more intense and more frequent urban flooding events and to increased human, environmental, and economic risks. Thus, various planning and management measures need to be considered by urban communities which are responsible for administering ordinances governing the construction and maintenance of stormwater management systems, and for floodplain management to address public safety concerns, property damage, and economic interruption from intense precipitation. In these efforts, effective communication of climate change impacts on urban watersheds/sewer sheds is needed. Data should be delivered at the watershed level in a form that can be incorporated in watershed planning at the community level. Delivery of useful climate change information is critical for community planning and adaptation to changing climate conditions.

It is common practice that future climate projections, which are based on global circulation models (GCM), are downscaled to finer temporal and spatial scales using statistical or dynamical downscaling models. However, watershed-scale climate data generated by climate models still do not provide precipitation data in a format useful for community engineers and planners to prepare, mitigate, and adapt to future conditions. Furthermore, city managers and decision makers need quantifiable future risk to demonstrate the need for adaptive actions, such as retrofitting storm sewers and other water conveyance structures or adopting higher regulatory design standards within the community. This is not offered by the present climate modeling outputs. In this research, a method is designed to analyze and express climate data in a format that can be readily used to assess future extreme precipitation events in models commonly used for sizing stormwater infrastructure and identifying flooding potential. In this method, future conditions climate data are analyzed to prepare precipitation maps for selected design storm frequencies which can be used to model future climate conditions of stormwater runoff and flood risk.

This report presents a newly designed research framework to determine future conditions rainfall frequency maps, illustrating it in Cook County, Illinois, for the 24-hour duration rainfall event and for a range of

recurrence intervals (also called return periods). Engineers commonly use these maps to determine the appropriate return period rainfall amount by interpolating between the isohyetals to evaluate options for storm and flood water management. Impacts of future climate conditions can then be convincingly demonstrated using conventional engineering to show changes in flooding frequency and extent, as well as damage comparisons associated with changing intense precipitation. Using standard and familiar models with future conditions precipitation scenarios facilitates communication of quantifiable future risk and supports community decision makers so they can plan, mitigate, and adapt to future conditions. This directly supports climate adaptation and mitigation by providing an understandable method for community engineers and planners to demonstrate the impact of climate change at the local level and develop specific adaptation strategies that will reduce future risk.

Acknowledgements

TABLE OF CONTENTS

This Page Left Intentionally Blank

Introduction

Understanding the interaction of the climate with the built environment is paramount to ensuring resilient communities and mitigating exposure to risk. In their Fourth Assessment Report, the Intergovernmental Panel for Climate Change (IPCC, 2007) discussed the science behind the warming of the climate system, illustrated observed effects of this warming on natural systems, and described possible mitigation strategies. Additionally, the U.S. Climate Change Science Program (CCSP) published a report documenting weather and climate extremes for the United States (CCSP, 2008). The report provides scientific evidence that the observed increases in climate extremes, such as higher temperatures and heavy storms, are related to increases in anthropogenic emissions and indicate that climate change could cause more severe rainstorms and flooding in the future.

The National Research Council, Committee on Hydrologic Science (2011) reported that "…assumptions on the statistical distribution of hydrologic events used to analyze hydrologic extremes are predicted on stationarity, yet the recent record shows that this assumption is not accurate. Furthermore, the nature of hydrologic extremes is convolved with land cover change, urbanization, and the operation of water management facilities such as dams, irrigation works, wells, and diversions." They further reported that "…lack of interaction [among climate science, water science, and engineering applications communities] has not only limited fundamental research on climate extremes but also impeded the translation of new and potentially useful outputs from scientists into the planning and management realm. Risk to the nation's infrastructure from water-related extremes is a function of not only the climate-change induced hydrologic hazards but also the exposure of assets (and their value) to these extremes, as humans continue to settle and build in hydrologically dangerous settings such as floodplains and river deltas. Without substantially greater interchange of research findings and ideas across these three communities as well as further understanding of the various dimensions of the risk, the design of effective climate change adaptation strategies will remain unrealized."

The potential impacts of climate change on extreme hydrologic events have been projected to increase in the Midwest and in particular in the vicinity of Chicago, Illinois. Schuster et al. (2012) used statistically-downscaled and bias-corrected precipitation projections for the state of Wisconsin derived from 14 General Circulation Models (GCMs) to assess the projected precipitation changes for the mid-21st century. The resulting risk assessment was performed on the basis of regional risk equations, showing a moderate but significant increase in heavy rainfall. Although with noted uncertainty, comparable increases were obtained based on a study by Markus et al. (2012). While these ranges likely offer a reasonable first approximation of the future heavy rainfall and the corresponding flooding, it does not fully account for the uncertainty range. To better quantify the uncertainty, the approach described in this study utilizes an ensemble of multiple models and scenarios based on dynamical and statistical downscaling and projects rainfall frequency for Cook County in Illinois.

Hydrologic Significance

The design of storm sewers, sizing of bridges, and determination of flood inundation areas are performed using extreme event design storms: precipitation events that have an expected intensity, duration, and frequency. For urban flooding studies (Winters et al., 2015), the parameters of the design storm precipitation are calculated by statistical analysis of rain gage data, and then spatially interpolated to create isohyetals

such as those published by the National Oceanic and Atmospheric Administration (NOAA) in Atlas 14 (Bonnin et al., 2006). In Illinois, isohyetals published in Bulletin 70 (Huff and Angel, 1989) are commonly used for floodplain and stormwater modeling (IDNR-OWR, 1996). An example of 24-hour duration 100-year event rainfall depths (isohyetals) from Bulletin 71 (Huff and Angel, 1992) is shown in Figure 1. Although with a much larger scale than the scale in this project (Cook County, Illinois), the map shows a significant spatial decreasing trend from southwest to northeast. In addition to the general trend, there are areas with large variability in rainfall depths, such as those located southwest of Lake Michigan, including Cook County. Similar projected isohyetals, representing future climatic conditions, can be used as input to hydrologic and hydraulic models to create potential future flood inundation maps. These maps can be used by various stakeholders, including the Federal Emergency Management Agency (FEMA), state and local governments for infrastructure design and stormwater ordinance, and others (CH2MHILL, 2009; HDR, 2011; MWH, 2009).
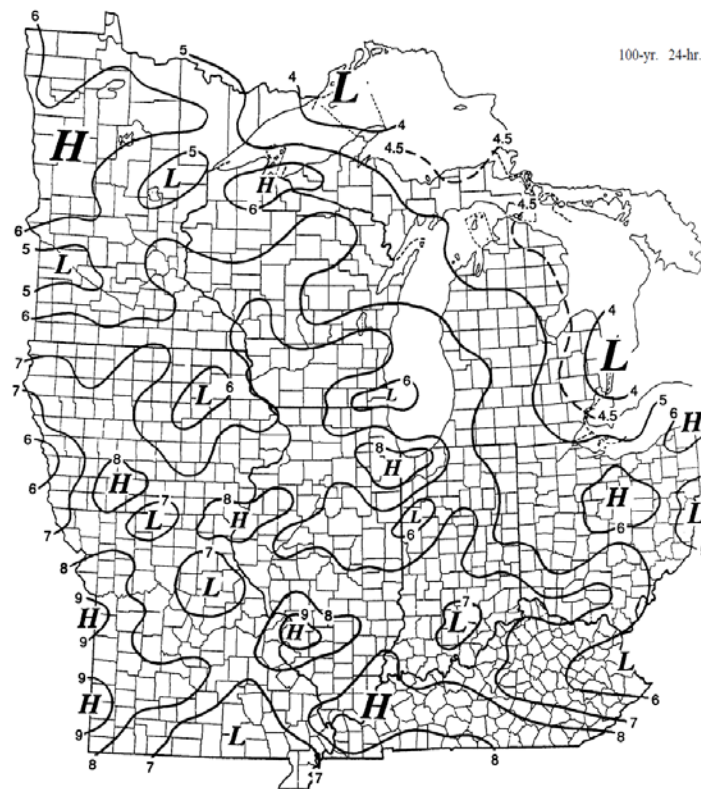
Figure 1. Example of 24-hour 100-year rainfall depths (isohyetals) in inches from ISWS Bulletin 71 (Huff and Angel, 1992)

Statistical analyses in current standards, such as those published in Atlas 14 (Bonnin et al., 2006), are based on the assumption of the stationarity of the precipitation data and do not account for climate change. Comparatively, some authors (Markus et al., 2007) detect trends in heavy rainfall observations and adjust for them (Huff and Angel, 1989). Moreover, climate studies indicate that the intensity and frequency of heavy storms is likely to increase in this region (Winters et al., 2015). Thus, using only statistics of the past observed rainfall in urban drainage infrastructure design will likely underestimate future storms and floods, as well as their confidence limits. The effects of the projected climates on extreme rainfall have to be taken into account, but extrapolation of trends beyond the observed record is not recommended. Instead, this

study uses climate model outputs as suggested by many scientists (Guo and Senior, 2006; Collins and Knight, 2007; Sanchez et al., 2009; Schuster et al., 2012).

Study Framework

Climate models generally do not produce results in a format usable by floodplain and stormwater managers. This report describes a new approach in which the projected precipitation frequency results are prepared in a map and/or tabular format typically used by regulatory and municipal agencies. As outlined in Figure 2, the GCM climate model outputs (e.g., rainfall) for future time horizons are first downscaled (dynamically or statistically) to the spatio-temporal scale usable by water engineers. Once these downscaled outputs are bias corrected, they serve as inputs to statistical frequency analysis.

Multiple climate models and scenarios result in high uncertainties (Markus et al., 2012). These uncertainties often discourage efforts to quantify the effects of climate change on heavy rainfall, as the confidence limits around the projected rainfall quantiles could be much larger than those of the observed rainfall. To account for these potentially significant changes in heavy rainfall and flooding, a framework is designed to account for the uncertainties resulting from using different climate scenarios, model structures, precipitation downscaling methods, and observed data to calibrate these models. This framework gives a probabilistic estimate of future heavy rainfall events including confidence limits for each projected rainfall quantile. The confidence limits offer a range of probable magnitudes of a particular event, such as 100-year 24-hour rainfall, and could serve as a tool for urban floodplain and stormwater managers to possibly adopt more stringent urban drainage standards by applying suitable safety factors (e.g., Hennegriff, 2007).
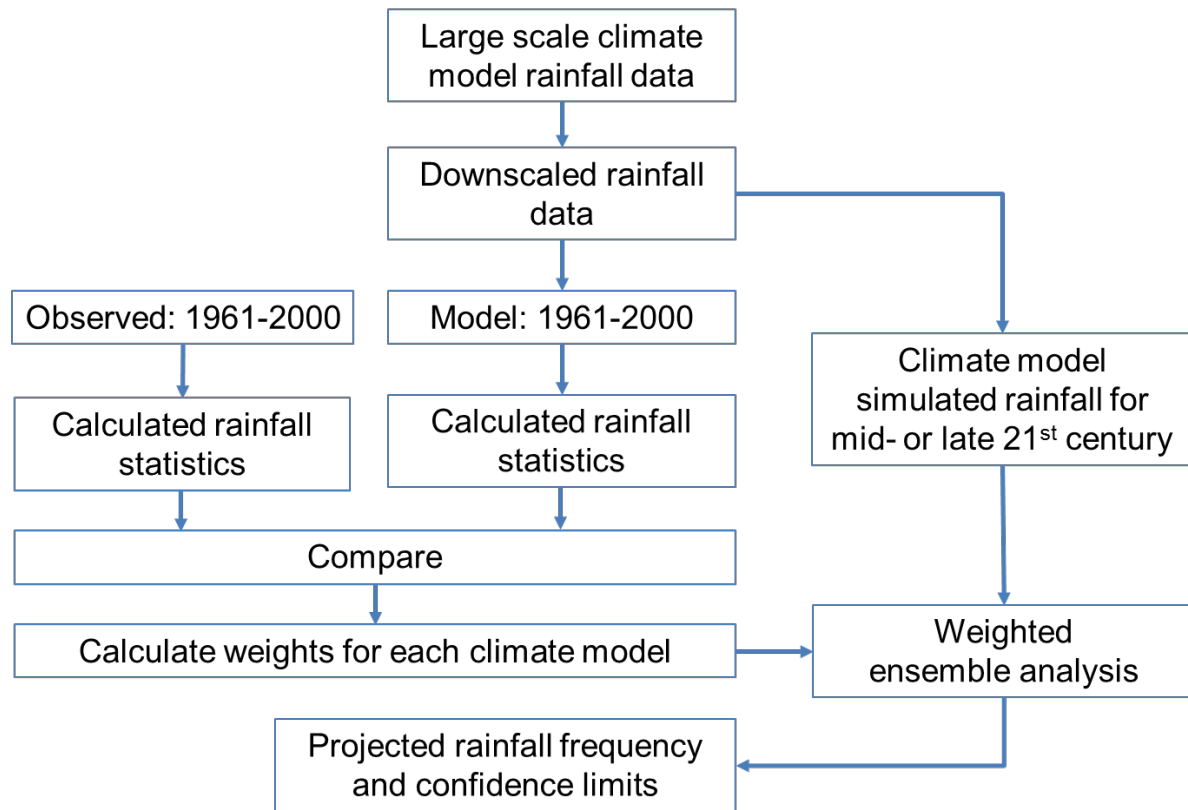
Figure 2. Schematic of the methodology used in this study. For 3 representative IPCC CMIP3 climate scenarios (B1, A1B, and A2) each climate model was tested. The models providing extremes closer to the observed ones, have higher credibility (i.e., higher weights) for their applications in future projections.

Cook County, Illinois, a highly urbanized area with over 120 communities (including Chicago), was chosen to illustrate the study framework. The Metropolitan Water Reclamation District of Greater Chicago (MWRDGC) establishes a countywide stormwater management program to provide Cook County with effective rules, regulations, and projects that will reduce the potential for stormwater damage to life, public health, safety, property, and the environment. Nineteen stormwater management goals have been developed by the District for the Cook County Stormwater Management Plan (CCSMP). The goals extend from protecting new and existing development from flooding to preventing the loss of water quality and habitat. Although MWRDGC has authorized watershed plans based on highly detailed hydrologic and hydraulic models for major watersheds in Cook County (http://www.mwrd.org/irj/portal/anonymous? NavigationTarget=navurl://89537fd445b81b3b34c467db5124cefe, accessed November 15, 2015), these models were completed and calibrated to existing conditions. These models are used to plan for storm sewer infrastructure upgrading necessitated by changes in heavy rainfall; however, climate data to design and prepare for changing conditions are not available.

Twenty-four-hour duration isohyetals are presented for the 100-, 50-, 25-, 10-, 5-, and 2-year recurrence intervals (often called return periods) for the future climate conditions. These conditions are projected from global climate models downscaled to smaller spatial (1/8 deg.) and temporal (1 day) increments for the Cook County area. Engineers commonly use these extreme events for stormwater and floodplain studies, including but not limited to these examples: the 100-year event is used to prepare Flood Insurance Rate Maps (FEMA, 2009), the 100-, 50-, 25-, and 10-year events are recommended for computing average annualized losses (FEMA, 2012), the 100- and 2-year events are suggested to design onsite storage facilities

(MWRDGC, 2009), and the 5- and 2-year events are commonly used to design stormwater infrastructure (Winters et al., 2015). The protocol developed for translating regional climate model outputs to consumable products that engineers and planners can use can be applied in other geographic areas.

Observed Rainfall Data

Raingage data that were reviewed for this analysis included databases from the National Oceanic and Atmospheric Administration (NOAA) National Centers of Environmental Information (NCEI) (formerly National Climate Data Center, NCDC), the Midwestern Regional Climate Center (MRCC), and the Illinois State Water Survey (ISWS). Observed precipitation data were analyzed on the basis of spatial distribution, gaged period of record, and data quality and completeness.

Data from NOAA-NCEI, in general, provide gages with the longest period of record, with several gage records beginning prior to 1900. Data from the Cook County Precipitation Network (CCPN) of the ISWS provides the most complete and spatially dense data source within Cook County, but the gage period of record begins in 1989.

In order to adequately capture both the temporal and spatial aspects of precipitation in the Chicago Metropolitan area, rain gages from both the NOAA-NCEI network and ISWS CCPN were merged into a single dataset. Because of the high quality and long gage record, all NOAA-NCEI gages in the region that included at least 20 years of record and were at least a 90 percent complete during the period of record were included. To avoid a high number of short-term gages available in the ISWS-CCPN from unduly biasing the temporal record, all of the 25 ISWS-CCPN gages are not included. Use of the network could, however, supplement the NOAA-NCEI record's spatial coverage of the region. ISWS-CCPN gages that did not fall within 10 km of a NOAA-NCEI station are considered for inclusion, with CCPN stations 7, 8, 15, 19, and 20 ultimately selected. Stations selected for this study are shown in Figure 3 and listed in Table 1.
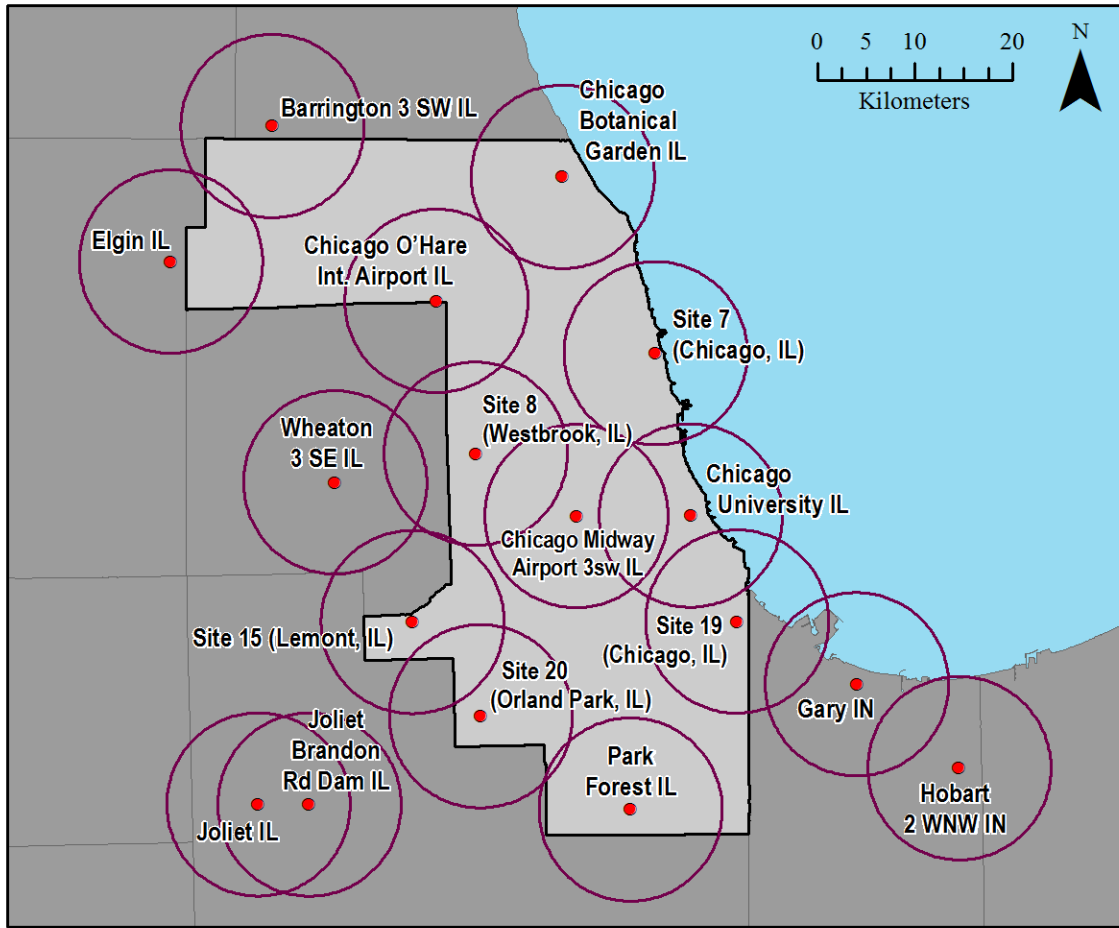
Figure 3. Location of stations including a 10 km radius buffer

Table 1. Raingages used in this study

#	Site Name	Station	Elevation (m)	Latitude	Longitude	Period of Record
1	Barrington 3 SW IL	GHCND:USC00110442	266.7	42.12	-88.16	Nov 1962 – Nov 2014
2	Chicago Botanical Garden IL	GHCND:USC00111497	192.0	42.14	-87.79	Oct 1981 – Nov 2014
3	Chicago Midway Airport 3sw IL	GHCND:USC00111577	189.0	41.73	-87.78	Mar 1928 – Nov 2014
4	Chicago O'Hare Int. Airport IL	GHCND:USW00094846	201.8	41.99	-87.93	Nov 1958 – Nov 2014
5	Chicago University IL	GHCND:USW00014892	181.1	41.78	-87.60	Jan 1926 – Oct 1994
6	Elgin IL	GHCND:USC00112736	232.6	42.06	-88.29	Feb 1898 – Nov 2014
7	Gary IN	GHCND:USC00123213	182.9	41.62	-87.38	Jun 1936 – Jan 1979
8	Hobart 2 WNW IN	GHCND:USC00124008	195.1	41.54	-87.29	Jul 1919 – Feb 2000
9	Joliet Brandon Rd Dam IL	GHCND:USC00114530	165.5	41.50	-88.10	Jun 1943 – Nov 2014
10	Joliet IL	GHCND:USW00014834	181.1	41.50	-88.17	Nov 1893 – Nov 1974
11	Park Forest IL	GHCND:USC00116616	216.4	41.49	-87.68	Jun 1952 – Nov 2014
12	Wheaton 3 SE IL	GHCND:USC00119221	207.3	41.81	-88.07	May 1895 – Dec 2011
13	Site 7 (Chicago, IL)	CCPN: Site 7	N/A	41.94	-87.65	Oct 1989 – Sep 2013
14	Site 8 (Westbrook, IL)	CCPN: Site 8	N/A	41.84	-87.88	Oct 1989 – Sep 2013
15	Site 15 (Lemont, IL)	CCPN: Site 15	N/A	41.68	-87.97	Oct 1989 – Sep 2013
16	Site 19 (Chicago, IL)	CCPN: Site 19	N/A	41.68	-87.54	Oct 1989 – Sep 2013
17	Site 20 (Orland Park, IL)	CCPN: Site 20	N/A	41.59	-87.88	Oct 1989 – Sep 2013

Many raingage records, including most of those in the NOAA-NCEI network within the Chicago Metropolitan area are daily raingages. Gaged intervals (e.g., 7 am to 7 am, 8 am to 8 am, etc.) have often been based on the ease of gage operation and maintenance and the availability of personnel to retrieve records from the field. To account for storm events occurring in two "gage days," rainfall is typically converted from daily precipitation values to 24-hour precipitation (Weiss, 1964). Past analyses have been consistent regarding this conversion. NOAA Atlas 14 (Bonnin et al., 2006), Technical Paper-40 (Hershfield, 1961), NOAA Atlas 2 (Miller et al., 1973), ISWS Bulletin 46 (Huff and Neill, 1959) and ISWS Bulletin 70 (Huff and Angel, 1989) all found a conversion equal to 1.13 to convert from 1 day to 24-hour precipitation.

Climate Model Precipitation Data

The scientific community has developed potential future emission scenarios to assess the future climatic response. The Intergovernmental Panel on Climate Change (IPCC) developed the Special Report on Emission Scenarios (SRES) to revise earlier scenarios based on additional data and advancements in the scientific understanding of climate response to emissions. The report provides for a range of climate driving forces including demographic change, technological advancement, and economic development, to be tested. The range of driving forces is to help advance understanding of key climatic factors, their impact, potential societal responses, and uncertainties associated with climate projections under future emission scenarios (Nakicenovic et al., 2000). https://www.ipcc.ch/pdf/special-reports/spm/sres-en.pdf

Climate models not only vary in spatial and temporal resolution, but also vary in complexity and modeled natural and anthropogenic greenhouse gas constituents. Depending on their complexity, models may

include constituents such as CO_2, CH_4, N_2O, SO_2, NO_x, CO, NH_3, C_2H_4O, C_2H_5OH, C_2H_6O, SO_4, NH_4NO_3, various fluorinated gases and ozone-depleting substances, black, organic, and volatile organic carbons, as well as some aerosols and dust. Although numerous atmospheric constituents contribute to global warming and climate change, carbon dioxide (CO_2) is considered the most important greenhouse gas emitted by humans, responsible for most of the global warming.

CMIP3 and CMIP5 Data

The World Climate Research Program's (WCRP's) Coupled Model Intercomparison Project (CMIP) was created by the global community of climate modelers to produce consistent model-generated data sets for climate change impact studies. The third-phase CMIP dataset (CMIP3) supports the IPCC's Fourth Assessment Report (AR4; IPCC 2007), while the fifth phase, CMIP5, supports the IPCC Fifth Assessment Report (AR5; IPCC 2013). Basic information on CMIP3 and CMIP5 is presented in Table 2. While the CMIP5 model output is quickly becoming the *de facto* standard for climate projections (Lukas et al., 2014), CMIP5 does not invalidate CMIP3. In fact, these two projections are similar, and while CMIP5 is newer and superior in some aspects, CMIP3 has been validated for nearly a decade, unlike the newer CMIP5. Lukas et al. (2014) writes: "It is also important to note that it took the climate science community several years to comprehensively examine and diagnose the results of the CMIP3 models, and that process is still ongoing for the CMIP5 models. Thus, while we have reason to believe the CMIP5 output is better than CMIP3 in some respects, at this stage the CMIP3 output has been more fully vetted." However, some authors lean towards using the CMIP5 data. Flato et al. (2013) writes: "There is medium evidence (single multi-model study) and medium agreement (as inter-model difference is large) that CMIP5 models tend to simulate more intense and thus more realistic precipitation extremes than CMIP3, which could be partly due to generally higher horizontal resolution. There is medium evidence and high agreement that CMIP3 models tend to underestimate the sensitivity of extreme precipitation intensity to temperature." Some authors (Kunkel et al., 2016) suggest using both CMIP3 and CMIP5 as a compromise.

Table 2. Key characteristics of CMIP3 and CMIP5 model projections (modified from Lukas et al., 2014)

Characteristic	CMIP3	CMIP5
Emissions scenarios	Special Report on Emissions Scenarios (SRES) B1, A1B, A2 (IPCC, 2007)	Representative Concentration Pathways (RCP) 2.6, 4.5, 6.0, 8.5 (IPCC, 2013)
Historical climate	1880–2000	1850–2005
Projection period	2001–2100	2006–2100+
Number of modeling centers	16	30
Number of models	22	55
Number of model simulations/projections	120	250
Spatial resolutions (average grid cell size)	60–300 miles (median: 160 mi.)	40–160 miles (median: 90 mi.)
Time-scale of archived data	Monthly	Daily and monthly
Decadal prediction	No	2010–2035

To facilitate communication of climatic responses to certain driving forces, CMIP3 scenarios are grouped by the IPCC into four "storylines" with each representing "different demographic, social, economic, technological, and environmental developments" (IPCC, 2007). The A1 scenario assumes rapid economic growth followed by a decline after 2050 due to the introduction of new and more efficient technologies. This scenario has three sub-categories: fossil intensive (A1FI), non-fossil energy sources (A1T), or a

balance across all energy sources (A1B). The A2 assumes regionally oriented economic development and slower economic growth. The B1 scenario is a low-emission scenario with rapid change in economic structures toward a service and information economy, with clean and resource-efficient technologies.

The newer source, CMIP5, however, is not based on development scenarios. Instead, it is based on the final effects of development expressed by the representative concentration pathways (RCPs). RCPs are based on four greenhouse gas concentration trajectories. The greenhouse effect causes global warming which is quantified through a radiative forcing, and expressed as watts per square meter (W/m^2). The four RCPs are RCP2.6, RCP4.5, RCP6, and RCP8.5. They are named after a possible range of radiative forcing values in the year 2100 relative to pre-industrial values (+2.6, +4.5, +6.0, and +8.5 W/m^2, respectively). Although global warming is caused by several greenhouse gas emissions, carbon-dioxide (CO_2) is the primary greenhouse gas that is contributing to recent climate change. CO_2 concentrations (CMIP3 and CMIP5) are illustrated in Figure 4.
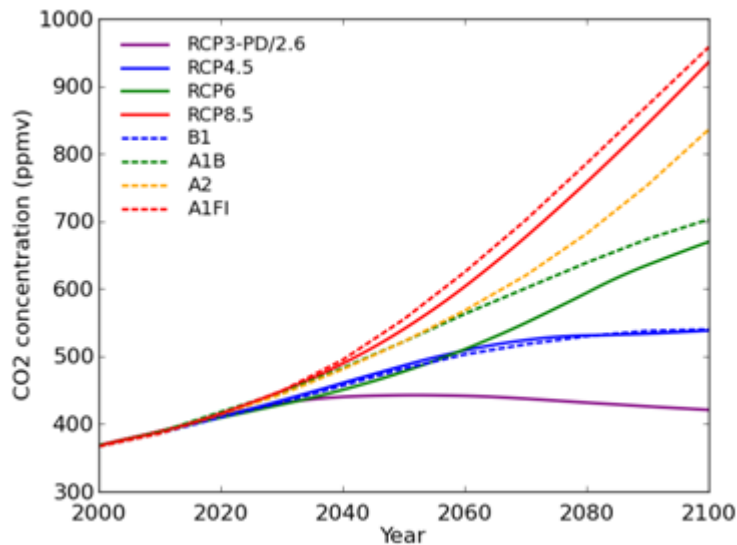
Figure 4. CO_2 Concentration Pathways based on CMIP3 IPCC and CMIP5 IPCC (http://www.climatechangeinaustralia.gov.au/en/climate-projections/climate-futures-tool/experiments/)

The first step in this study was to review several available sources of data, including both CMIP3 and CMIP5, and to select the most appropriate data sources based on preliminary data analysis, as described below in "Climate Model Data Selection for this Study."

Climate Model Data Selection for this Study

The following data sources are applied in this study: CMIP5-Statistically Downscaled-World Climate Research Programme (WCRP) (Meehl et al., 2007; Taylor et al., 2011) (Table 3), CMIP5-Dynamically Downscaled-Oak Ridge National Lab (ORNL), described in Oubeidillah et al. (2013) and Ashfaq et al. (2010, 2013) (Table 5), and CMIP3-Statistically Downscaled-University of Wisconsin-Madison (UW), (Notaro et al., 2014) (Table 4).

Table 3. Statistically Downscaled CMIP5 data by World Climate Research Programme (WCRP), indicating models, scenarios, and the number of runs used in this study (Meehl et al., 2007; Taylor et al., 2011)

Model Scenarios	RCP4.5	RCP8.5
ACCESS1-0	1	1
BCC-CSM1-1	1	1
CANESM2	5	5
CCSM4	2	2
CESM1-BGC	1	1
CNNM-CM5	1	1
CSIRO-MK3-6-0	10	10
GFDL-CM3	0	1
GFDL-ESM2G	1	1
GFDL-ESM2M	1	1
INMCM4	1	1
IPSL-CM5A-LR	4	4
IPSL-CM5A-MR	1	1
MIROC-ESM	1	1
MIROC-ESM-CHEM	1	1
MIROC5	3	3
MPI-ESM-LR	3	3
MPI-ESM-MR	3	1
MRI-CGCM3	1	1
NORESM1-M	1	1

Table 4. Dynamically Downscaled CMIP5 data by Oak Ridge National Laboratory (ORNL), indicating models, scenarios, and the number of runs in this study (Oubeidillah, et al., 2013; Ashfaq et al., 2010, 2013)

	RCP8.5
ACCESS	1
BCC-CSM	1
CCSM4	1
CMCC-CM	1
FGOALS	1
GFDL_ESM2M	1
IPSL-CM5A-LR	1
MIROC5	1
MPI-ESM-MR	1
MRI-CGCM3	1
NORESM1-M	1

Table 5. Statistically Downscaled CMIP3 data by the University of Wisconsin (UW), indicating models, scenarios, and the number of runs in this study. (Notaro et al., 2014)

	A1B	A2	B1
CCCMA_CGCM3_1	1	1	1
CCCMA_CGCM3_1_T63	1	0	1
CNRM_CM3	1	1	1
CSIRO_MK3_0	1	1	1
CSIRO_MK3_5	1	1	1
GFDL_CM2_0	1	1	1
GISS_AOM	1	0	1
GISS_MODEL_E_R	1	1	1
IAP_FGOALS1_0_G	1	0	1
MIROC3_2_HIRES	1	0	1
MIUB_ECHO_G	1	1	1
MPI_ECHAM5	1	1	1
MRI_CGCM2_3_2A	1	1	1

Climate model data selection for this study was based on preliminary data analysis for each of the three available data sources, WCRP, ORNL, and UW, as shown in Tables 3-5. Data sources with higher hindcast accuracy, i.e., the accuracy of simulation of the past observed data, are considered more reliable and more appropriate as no additional downscaling or bias correction were considered for this analysis. As the focus of this study is on high extremes, the annual maximum daily rainfall data based on each data source are compared with observed data in the study area. The comparison results are described below.

- The WCRP data (Meehl et al., 2007; Taylor et al., 2011) is found to have a large negative bias in annual maximum series (AMS). This bias per each year at O'Hare is shown in Figure 5 for the 1960-2014 period. Bias per model is also significant. The observed annual maxima has an average of 2.87 in (7.29 cm), while the model-based average ranged between 1.41 in and 1.73 in (3.58 cm and 4.39 cm).
- The ORNL data have a similar negative bias, meaning that the models underestimate the observed peaks for the historical period. The observed average for the 1966-2005 period is 2.77 in (7.04 cm) and the models range between 1.91 in (4.85 cm) and 2.28 in (5.79 cm).
- It is found that the UW data are the only data source reviewed without a significant overall average bias. Although some of the UW models have positive biases of up to 60 percent at some sites, and negative biases at some other sites of up to -40 percent, most models at most of the sites have absolute biases of less than 20 percent. Figure 6 shows the results for each model, and Figure 7 for each site based on this data source. Models are listed in Table 5, and sites are described in Table 1. For these reasons, the UW data source is adopted for this study.
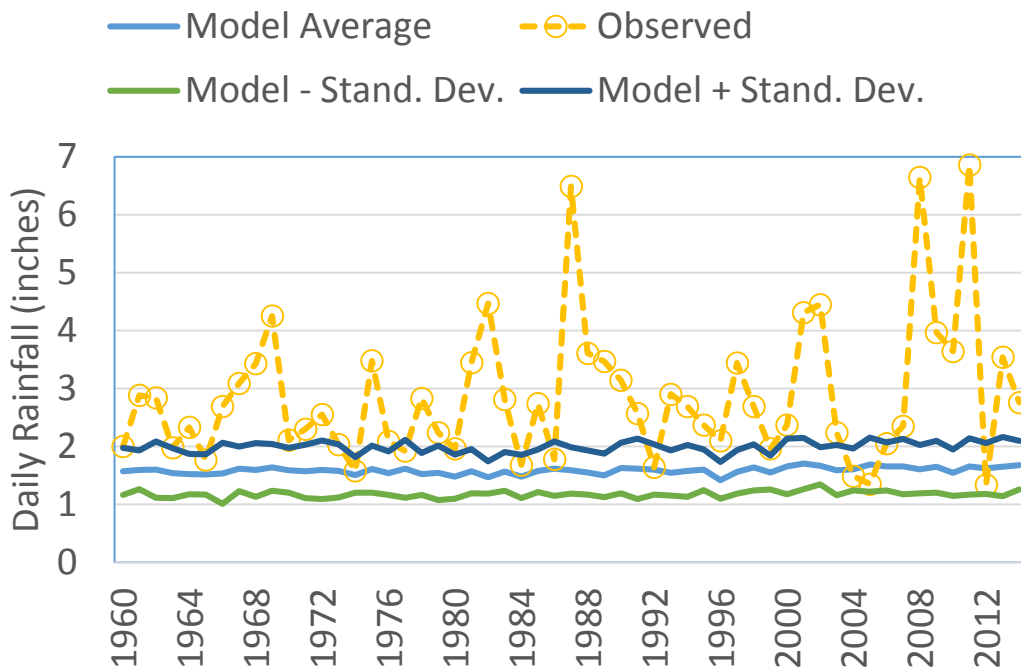
Figure 5. Observed and CMIP5-based statistically downscaled (WCRP) annual maximum daily rainfall at O'Hare showing an apparent bias
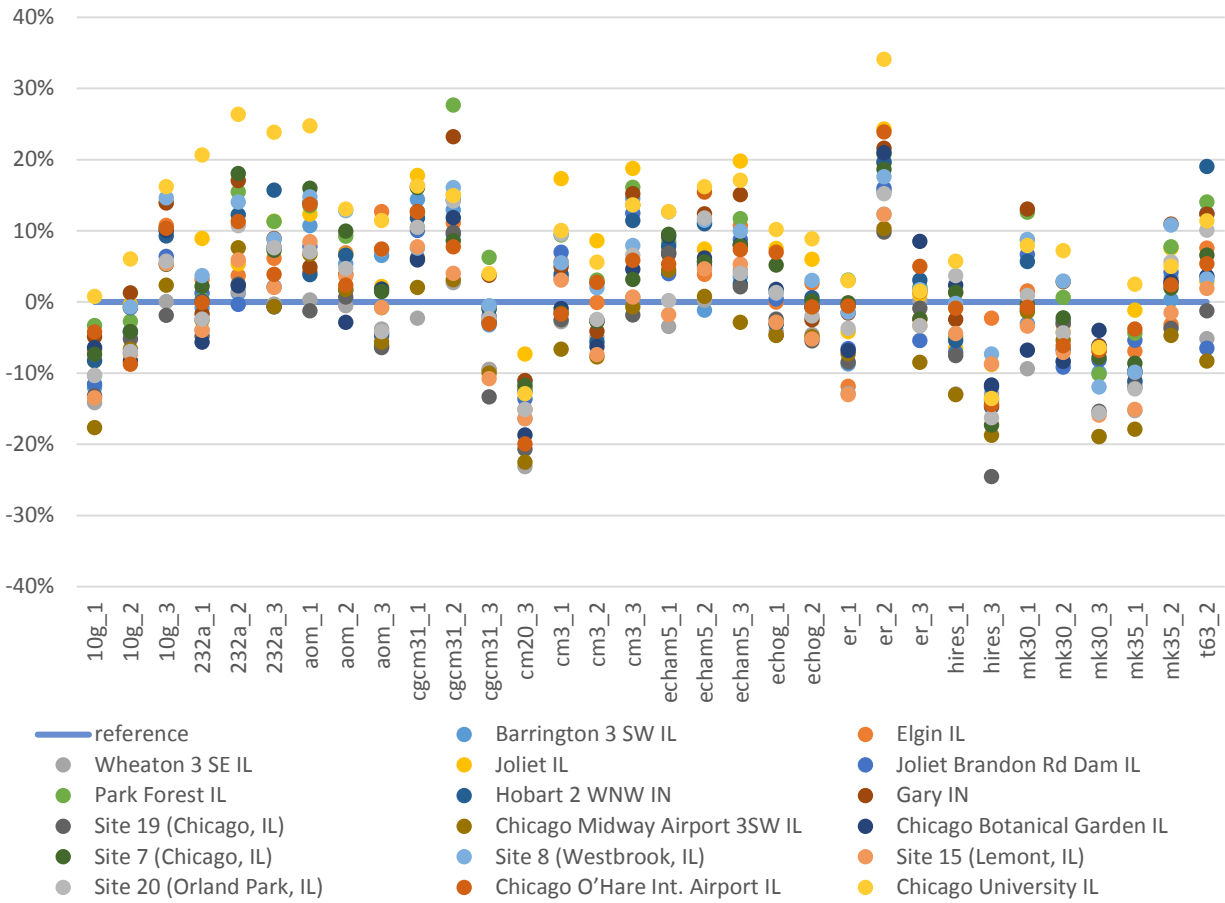
Figure 6. Relative CMIP3 statistical downscaling (UW) model departures from observations for each model (Period: 1961-2000) in AMS
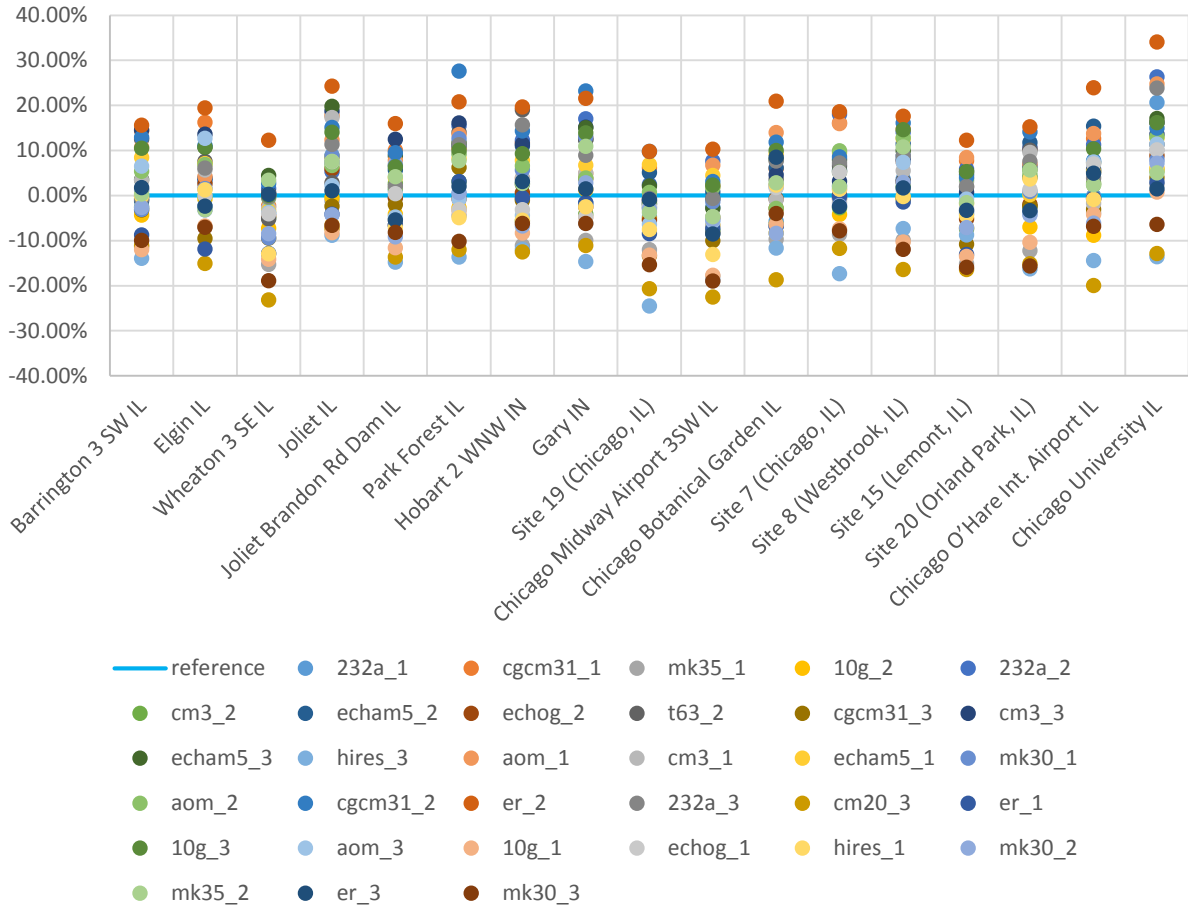
Figure 7. Relative CMIP3 statistical downscaling (UW) model departures from observations for each site (Period: 1961-2000) in AMS

The adopted CMIP3 UW data are statistically downscaled with special attention paid to the central and eastern United States, especially the Great Lakes Region, by Notaro et al. (2014). The downscaled data include daily maximum temperature, minimum temperature, and precipitation at 0.1°×0.1° resolution. The statistically downscaled data cover the entire Chicago metropolitan area. In addition to modeling the historic period from 1961 to 2000, three climate scenarios (A1B, A2, and B1) are included with estimates for 2046 to 2065 and from 2081 to 2100. The data include the results of 13 GCMs. The present study uses 32 runs from 13 of those models to determine weights for each model run.

Methodology

An increasing frequency of heavy rainfall events has been a visible expression of climate change across the United States in recent decades. The upper Midwest, including the Chicago area, has been hit especially hard, experiencing intensity increases of over 30 percent since the late 1950s (Karl et al., 2009). This crisis motivates the development of novel approaches in analysis of past and projected precipitation. This project

uses an innovative statistical approach based on the L-moments method and weighted ensemble to determine the present rainfall frequency and projected changes in heavy precipitation events by the mid- and late-21st century. The study also designs a methodology to account for uncertainties based on various models and climate scenarios, resulting in confidence limits for frequency estimates for the past, and the two representative future horizons. These approaches are described below.

Precipitation Frequency Analysis using L-Moments

Using the standard methodology adopted by NOAA based on L-Moments (Hosking, 2000; Hosking and Wallis, 1997), we compute 24-hour point rainfall depths representing 100-, 50-, 25-, 10-, 5-, and 2-year events at each rain gage. The magnitude of a 100-year event is often calculated based on less than 100 years of observed data. Regional frequency analysis based on L-moments alleviates this problem by trading space for time (Hosking and Wallis, 1997), i.e., by using data from several sites to estimate event frequencies at one site. Past research results (Vogel and Fennessey, 1993) indicate that regional frequency analysis based on the L-moments method has several advantages, such as robustness and better identification of the parent distribution compared to standard estimation techniques, particularly for regional studies (e.g., Markus et al., 2007, Markus and McConkey, 2007, Hejazi and Markus, 2009). The L-moments method uses the discordancy measure (Hosking and Wallis, 1997) to identify unusual sites in a region and the heterogeneity measure to assess if the region is homogeneous. The next step is to find which statistical distribution best fits the region among the following 10 distributions (Hosking, 2000): Exponential, Gamma, Gumbel, Normal, Generalized Pareto, Generalized Extreme Value, Generalized Logistic, Generalized Normal, Pearson Type 3, and Wakeby. Generally, a distribution with the smallest goodness-of-fit-measure zDIST (Hosking and Wallis, 1997) is selected. This measure is defined as $z^{DIST} = \dfrac{(\tau_4^{DIST} - t_4^R + B_4)}{\sigma_4}$ where τ_4^{DIST} is the fitted L-kurtosis for any distribution, t_4^R is the observed regional average L-kurtosis, σ_4 is the standard deviation of t_4^R, and $B_4 = \dfrac{1}{N}\sum_{m=1}^{N}(t_4^{[m]} - t_4^R)$ is the bias in the same regional average L-kurtosis. N is the large number of realizations of a region. The fit is declared to be adequate if the absolute value of zDIST is less than 1.64 (Hosking and Wallis, 1997). Once the distribution is selected and the parameters calculated, design precipitation values are estimated.

Hosking (1990) defined L-moments as linear combinations of probability weighted moments (PWMs), denoted as β_r. For a probability distribution with cumulative distribution function F(x), unbiased estimators (b$_r$) of the first three PWMs (β_r) are defined by Hosking and Wallis (1997):

$$b_r = n^{-1}\binom{n-1}{r}^{-1}\sum_{j=r+1}^{n}\binom{j-1}{r}x_{j:n}$$

where x$_{j:n}$ denotes the jth smallest number in the sample of size n.

For estimating p unknown parameters of a selected distribution, the method of L-moments obtains parameter estimates by equating first p sample L-moments to the corresponding population quantities, i.e., $\lambda_i = \ell_i$, i=1, 2, 3, 4, τ=t, τ_3=t3, and τ_4=t4. For various distributions, Hosking and Wallis (1997) provided expressions for distribution parameters in terms of L-moments.

To construct 90 percent confidence limits, 1,000 synthetic datasets having the same statistical features were generated using a Monte Carlo simulation technique (Hosking and Wallis, 1997), where each synthetic dataset produces a quantile. The upper confidence limit separates the upper 5 percent and the lower 95 percent, and similarly, the lower confidence limit separates the lower 5 percent from the top 95 percent.

The frequency estimates can be calculated based on either the partial duration series (PDS) or annual maximum series (AMS). As the PDS approach involves various data preparation issues, it was deemed impractical for this study. On the other hand, the AMS approach underestimates quantiles, producing a negative bias, particularly for smaller (e.g., 2-, 5-, and 10-year) recurrence intervals. In this study, we adopt the AMS approach, and similar to Perica et al. (2011), remove the bias by the Langbein's (Langbein, 1949) formula. Langbein's formula was developed to transform PDS-based average recurrence interval (ARI) to AMS-based annual exceedance probability (AEP): $AEP = 1 - exp\left(-\frac{1}{ARI}\right)$. Thus after conversion, equivalent frequencies used in this study based on AMS are: 2.54-, 5.52-, 10.51-, 25-, 50-, and 100-years, which corresponds to the PDS based 2-, 5-, 10-, 25-, 50-, and 100-years. For example, the unbiased estimate of a 2-year recurrence interval rainfall can be calculated using the AMS approach for a recurrence interval of 2.54 years.

The AMS daily data are observed every day at a fixed time which varies by rain gage (for details on the monitoring data used in this study, please see the "Observed Rainfall Data" section, earlier in this narrative). All frequency estimates based on daily data are multiplied by 1.13 (daily to 24-hour conversion, as described in "Observed Rainfall Data," and 1.04 (grid to point adjustment factor). The grid to point adjustment factor is calculated as an inverse of the areal reduction factor defined in Miller et al. (1973).

Frequency estimates are provided for three future climate scenarios (A1B, A2, B1) for two future periods, 2046-2065 (mid-century), and 2081-2100 (late-century). The weight set derived from historical data is applied to corresponding model results to get weighted point estimates for 24-hour for 2-, 5-, 10-, 25-, 50- and 100-year precipitation events for different climate scenarios for the two time horizons. It should be noted that for the CMIP3 UW data, under A2 climate scenario, there are only 23 model runs as compared to 32 model runs of the other scenarios. To account for this difference, the weight set for scenario A2 is re-normalized first and then is applied to get the final product.

Weighted Ensemble Methodology

Climate models produce generally variable results with regard to rainfall and other variables. To account for modeling variability, many studies suggest a multi-model (ensemble) approach (Raisanen and Palmer, 2001; Sanchez et al., 2009; Sun et al., 2011). Following this methodology, an average prediction of these models is assumed to be the most likely outcome, while the standard deviation among the models represents the variability of these outcomes. It is often assumed that all models have equal weights, regardless of their hindcast accuracy, i.e., the accuracy of simulation of the past observed data. However, not all models are equally successful in reproducing observed climate parameters. Some models are more accurate, while some others can be very inaccurate. It can be argued that if a climate model has poor hindcast accuracy, then it is unlikely that the future prediction would be accurate. On the other hand, if the hindcast has good accuracy, then one can have some confidence in the model, although it is certainly possible that the forecast will be poor. While the risks associated with assigning model weights have been recognized (Haughton et al., 2015), numerous applications argue in favor of the weighted approach and demonstrate its benefits (Raisanen and Ylhaisi, 2012: Sanchez et al., 2009). To account for model accuracy we designed a weighted

ensemble approach (Figure 2) in which we assigned higher weights to more accurate models and lower weights to the poorer performing models. It should be noted that the skill of the model and thus the weight assigned will vary depending on the location of the observed data, e.g., the same model results downscaled in a different geographical location could result in different weights.

There is no widely accepted set of metrics to evaluate climate model performance (Gleckler et al. 2008) because of the difficulties in developing weights for models based on observed data (Knutti et al, 2010). In their study, Christensen et al. (2010) describe a multi-objective approach to determining weights. These objectives include large-scale circulation patterns, meso-scale seasonal mean temperature and precipitation, probability distribution function of daily and monthly temperature and precipitation, extremes in temperature and precipitation recurrence intervals, long-term trends in temperature, and annual cycle in temperature and precipitation. Murphy et al. (2004) use a climate prediction index (CPI) as an objective tool to calculate weights for different models. CPI reflects the relative ability of the models to reproduce observed climate variables, and uses a suite of climate variables. Some other studies determine weights based on specific model performances, such as Wilby and Harris (2006) who weigh models by performance at reproducing annual low-flow series. Nonetheless, Christensen et al. (2010) suggest metrics that are more tied to the needs of some specific impact study. Similarly, Knutti (2010) suggests that the selection of a metric should depend on the application.

In the next step of this study, the statistical frequency estimates based on the model-generated data are compared with those based on observed data to determine model weights for the ensemble analysis. Models producing frequency estimates closer to the estimates based on the observed data are considered more reliable for their use in future projections than the models producing inaccurate estimates.

Following Christensen et al. (2010) and Knutti (2010), the weights in this study are defined through the agreement between the observed and model-based cumulative distribution functions based on annual maximum daily precipitation series for the 1961-2000 period. Weights for each model are calculated based on averaged goodness-of-fit between the observed- and model-based estimates of 2-, 5-, 10-, 25-, 50, and 100-year rainfall amounts. Goodness-of-fit (d) between model-based and observation-based frequencies for each model is defined as an average percent deviation of a particular model from observation estimates. Since model estimates are based on gridded data while observation estimates are based on point data, an empirical conversion factor is introduced to get comparable results. This factor is related to grid size and event duration. In our study, the selected point-to-grid conversion factor is 0.96 (Miller et al., 1973).

Weights w for each model are determined using the tricube weight function defined by Tukey (1977):

$$
w = \begin{cases} \left(1 - \left(\frac{d}{h}\right)^3\right)^3, & if \ |d| \le h \\ 0, & if \ |d| > h \end{cases}
$$

where h is the half window width defined as one standard deviation of the whole series of average percent deviation for different models. This standard deviation is determined by calculating the percent deviation (d) between the modeled and observed frequency estimates averaged for all recurrence intervals for a particular model. Next, one standard deviation (h) of the resulting series is calculated. Symbol d, the average percent deviation of a particular model from observation estimates is calculated as:

$$
d = \frac{\sum_{i=1}^{n_{station}} \sum_{j=1}^{n_{event}} \frac{model_{i,j} - obs_{i,j}}{obs_{i,j}} * 100\%}{n_{station} * n_{event}}
$$

Where $n_{station}$ is the number of stations (17), n_{event} is the number of events (2-, 5-, 10-, 25-, 50-, and 100-year events, equal to 6). Weights for different model estimates are normalized such that the average weight equals 1, as required in the equations calculating the weighted frequency estimates.

Confidence Intervals

Our best estimates of the precipitation quantiles are the mean values based on ensemble, but this single value does not provide our level of confidence in these estimates. Our level of confidence is expressed through the confidence limits (CL), which are a measure of uncertainty of these estimates. CL represents two values (the upper CL and the lower CL) between which the true value of the precipitation quantile would lie under a certain confidence level. For example, if the confidence level is 90 percent, we are 90 percent confident that the true value for the quantile is between these confidence limits (Figure 8). The higher the confidence level, the wider the confidence limits. Also, it should be noted that the confidence limits are not necessarily equidistant from the estimates, as in Atlas 14, Volume 9 (Perica et al., 2013), as the distribution used for determining the CL is not necessarily symmetrical.
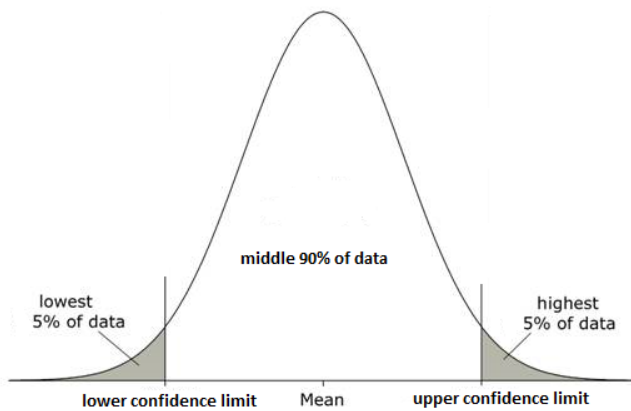
Figure 8. A distribution of calculated quantiles showing the lower and upper confidence limits

The results in this study vary primarily depending on model selection and climate scenario. The results of this study also provide a measure of the sampling variability of model parameters on the estimated frequencies. For each downscaled climate model data, a Monte Carlo simulation procedure (Hosking and Wallis, 1997) provides confidence intervals that account for uncertainties in distribution parameters (proportional to the data length) as well as the impact of inter-station dependence. These confidence limits are superimposed with confidence limits describing the variability of results based on different models. The final results are presented separately for several climate scenarios. For each scenario, an ensemble of outputs of different models is statistically analyzed in a weighted ensemble mode. Because the distribution of each rainfall quantile is generally non-symmetrical, the best-fit distribution and its parameters are determined based on the weighted mean, weighted variance, and weighted skewness. Weighted mean, variance, and skewness can be calculated as follows (Rimoldini, 2014):

Weighted mean: $\mu = \frac{1}{V_1}\sum_{i=1}^{n} w_i x_i$ where i denotes each model, x_i is the model output (i.e. 100-year 24-hour rainfall for model i), n is the number of models and w_i are the model weights.

Weighted variance: $\sigma^2 = \frac{\sum_{i=1}^{n} w_i(x_i-\bar{x})^2}{\frac{n-1}{n}\sum_{i=1}^{n} w_i}$ where n is the number of non-zero weights

Weighted skewness $\gamma = \frac{K_3}{K_2^{\frac{3}{2}}}$ where $V_p = \sum_{i=1}^{n} w_{i,}^{p}$, $p = 1,2,3$. and

$$K_3 = \frac{V_1^3}{V_1^3-3V_1V_2+2V_3}k_3; \quad K_2 = \frac{V_1^2}{V_1^2-V_2}k_2; \quad k_2 = \frac{1}{V_1}\sum_{i=1}^{n} w_i(x_i-\mu)^2 \quad k_3 = \frac{1}{V_1}\sum_{i=1}^{n} w_i(x_i-\mu)^3$$

Results

This study uses downscaled climate model-based simulated gridded daily rainfall to determine 24-hour point rainfall for each raingage. In the next step, the frequencies are estimated for each point and are spatially interpolated/extrapolated using the spline fitting method to create isohyetals for the 24-hour duration corresponding to 100-, 50-, 25-, 10-, 5-, and 2-year events.

Model weights have been determined based on the above described method. It should be noted that the models have been developed at different centers based on different sets of assumptions, and also that they were continuously being improved with time based on their performance. Groups of models with similar assumptions inherited from their earlier versions are considered similar compared to groups of models with different assumptions. These similarities among the models based on evolution or genealogy of the models used in this and other studies (Tebaldi and Knutti, 2007; Masson and Knutti, 2011; Sanderson et al., 2015) are expected to affect the weights. However, our analysis did not reveal significant correlations among the rainfall frequency estimates from different models, and thus the correlation of model genealogy is not considered in this study. A graphic presentation of model weights is shown in Figure 9. The figure indicates that some models have higher weights (close to 2.0), such as CSIRO_MK3_0, MIUB_ECHO_G and CNRM_CM3, while some other models, such as MPI_ECHAM5 and GFDL_CM2_0 have insignificant weights (equal or close to zero).
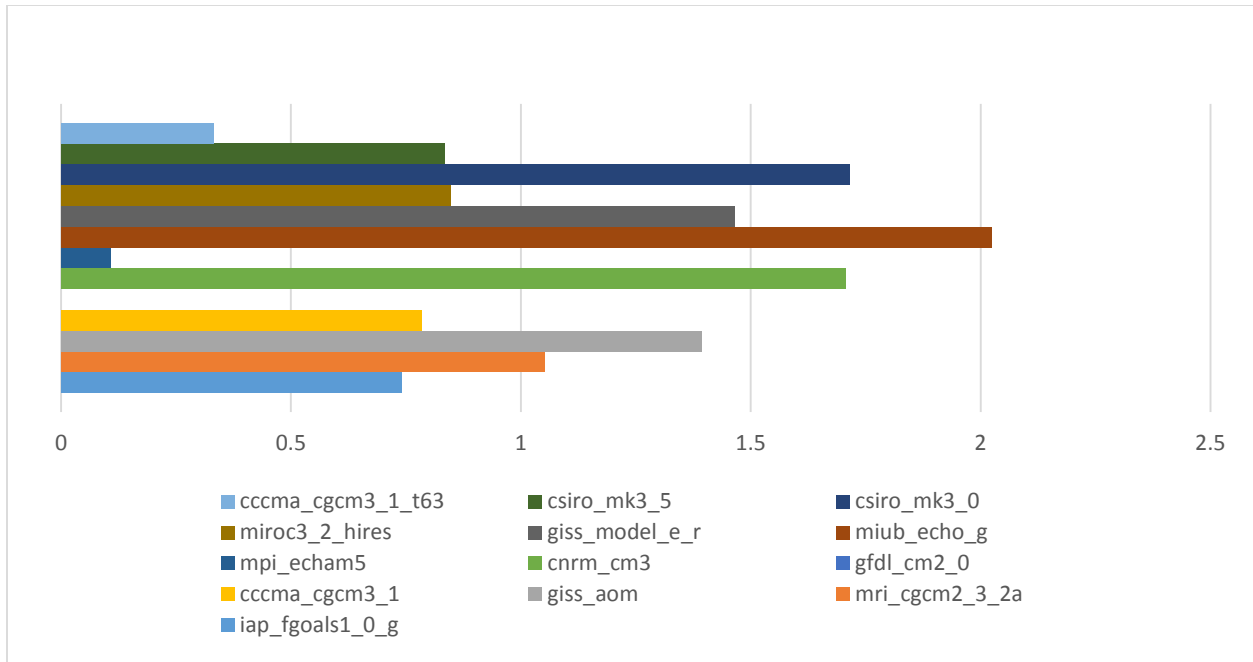
Figure 9. Model Weights for the data adopted in this study (UW)

Final results are shown graphically in Appendix A-D and Appendix F (isohyetal maps, Figures 10-39) and numerically in Appendix E (Tables 7-14). Interpolations are directly translated from the Spline interpolation function within GIS without manual adjustments. Figures 10-15 show projected isohyetal lines for 2-, 5-, 10-, 25-, 50-, and 100-year events, respectively, for mid- and late-21st century.

In general, these figures show that the projected isohyetals are higher than the published sources [Bulletin 70 (Huff and Angel, 1989) and Atlas 14 (Bonnin et al., 2006)], depending on the recurrence interval, time horizon, and the assumed climate scenario. For example, in some parts of the county, the relative increase in 24-hour rainfall for 2-year recurrence interval exceeds 40 percent for late-21st century and scenarios B1 and A1B (Figure 23). On the other hand, in some other cases, the difference is negative. For example, for mid-21st century and for 100-year recurrence interval, the 24-hour rainfall amounts projected based on B1 and A2, are 5 percent smaller than those published in Bulletin 70 (Figure 20). It should be noted, however, that this relative decrease is shown only in the southeastern corner of the county, and that other areas show increases of up to 20 percent.

In addition, although the projected isohyetals maintain similar in spatial variability to previously published sources, the projected isohyetals exhibit less of a north-south spatial gradient. While the published sources show less rainfall in the northern parts of Cook County, and higher in the south, the projected isohyetal maps do not show any significant spatial trend. As a result, the relative difference between the projected and published rainfall in the northern parts of the county is higher than the increase in the south. The differences between the projected and published rainfall are shown in Appendix B and C. The larger increase in the north is consistent with projections given by Markus et al. (2012) and recently observed trends found by Winters et al. (2015).

Changes to the upper 90 percent confidence limits are shown in Appendix F. Figures 34-35 show the differences between projected 2-year, 24-hour 90 percent upper confidence interval isohyetals for mid- and

20

late-21st century and Atlas 14 (Bonnin et al., 2006), respectively. These results are expressed as absolute differences (top row charts in the figures) and percent differences (bottom row charts in the figures). In these figures, three columns show results for 3 IPCC CMIP3 climate scenarios (B1, A1B, and A2). The projected upper confidence limits for 2-year recurrence interval generally exceed the confidence limits based on Atlas 14 by as much as 35 and 50 percent for the mid- and late-21st century, thus indicating greater uncertainty, respectively (Figures 34-35). These results are very comparable with those for 10-year recurrence interval (Figures 36-37). However, for the 100-year recurrence interval, the upper confidence limits are as much as 65 and 80 percent higher than Atlas 14, for the mid- and late-21st century, respectively (Figures 38-39). These results show that the confidence limits are wider for rare events than for more frequent events. Also, these limits are wider for late-21st century than for the mid-21st century.

It should be recognized that the previous comparisons between the proposed method and the published sources, for both frequency estimates and confidence limits, are based on different data and methods, and the results need to be interpreted with caution. Nonetheless, the differences between these two sets of frequency estimates and confidence limits can serve as initial estimates of the amounts of uncertainty added based on climate models and climate scenarios. Future studies should refine the results of uncertainty analysis by comparing the hindcast accuracy and hindcast confidence limits of each ensemble of models with those of the projected data.

Summary and Conclusions

The research described in this report illustrates a methodology for calculating future rainfall frequency. These results should not replace design rainfalls described in the ISWS Bulletin 70 (Huff and Angel, 1989) or NOAA Atlas 14 (Bonnin et al., 2006). The ISWS is analyzing the data and tools necessary for an updated Bulletin 70 (Huff and Angel, 1989), which will include projected rainfall frequency for subregions of Illinois.

This study describes a new methodology for frequency analysis of projected rainfall and applies it to a gaging network in Cook County, in northeastern Illinois. Two of three data sources for model-based past and projected rainfall tested in this study (WCRP and ORNL) considerably underestimated rainfall extremes, while the third source (UW) did not have a significant bias, but had a large spread of biases for different climate models. This result is somewhat consistent with Janssen et al. (2014) and Wuebbles et al. (2014), who found that a majority of climate models underestimate the historical and projected trends in heavy rainfall, resulting in underestimation of projected extremes. The source with the smallest bias (UW) was adopted to calculate projected rainfall frequencies in this study.

Results for 24-hour precipitation events and for a range of 6 frequencies between the 2-year event and 100-year event generally show higher heavy rainfall events when compared with presently used sources, ISWS Bulletin 70 (Huff and Angel, 1989) and NOAA Atlas 14 (Bonnin et al., 2006). Although the data and methods in Bulletin 70 (Huff and Angel, 1989) and Atlas 14 (Bonnin et al., 2006) are different from the data and methods used in this study, the increases appear to be significant enough to indicate that heavy rainfall will increase in the mid- and late-21st century. Additionally, these increases are more pronounced in the northern part of the county, which is consistent with the findings of Markus et al. (2012).

The confidence limits for rainfall frequency projections are significantly larger than those based on past observed data in Atlas 14 (Bonnin et al., 2006), as shown in Appendix F. In addition to the uncertainties reported in Atlas 14 (Bonnin et al., 2006), which include parameter estimation uncertainty bounds, the

current projected uncertainties provided in this analysis include those based on modeling variability. The inclusion of modeling variability leads to large confidence limits for each scenario and time horizon. These new limits are expected to get smaller as additional data are gathered and more accurate climate models are developed. At this point, these limits could serve as justification for water managers to adopt somewhat more stringent standards for urban flood protection by applying appropriate safety factors, similar to Hennegriff (2007).

Uncertainties in these analyses are significant due to inherent uncertainties in climate prediction processes, absence of longer monitoring datasets, and relatively short data records to validate climate models. Future efforts should be geared towards continuous monitoring of relevant climate variables, as well as development and validation of climate models. These efforts would in turn reduce the epistemic uncertainty and thus provide more accurate projections of heavy rainfall.

References

Ashfaq, M., S. Ghosh, S-C Kao, L. C. Bowling, P. Mote, D. Touma, S. A. Rauscher, and N. S. Diffenbaugh. 2013. Near-term acceleration of hydroclimatic change in the western U.S. *Journal of Geophysical Research*. doi: 10.1002/jgrd.50816.

Ashfaq, M., L. C. Bowling, K. Cherkauer, J. S. Pal, and N. S. Diffenbaugh. 2010. Influence of climate model biases and daily-scale temperature and precipitation events on hydrological impacts assessment: A case study of the United States. *Journal of Geophysical Research-Atmos*. 115: D14116. doi:10.1029/2009JD012965.

Bonnin, G., D. Martin, B. Lin, T. Parzybok, M. Yekta, and D. Riley. 2006. *Precipitation-Frequency Atlas of the United States, Atlas 14 Volume 2 Version 3.0*. National Oceanic and Atmospheric Administration, National Weather Service, Silver Springs, Maryland.

Climate Change Science Program (CCSP). 2008. *Weather and Climate Extremes in a Changing Climate. Regions of Focus: North America, Hawaii, Caribbean, and U.S. Pacific Islands.* A Report by the U.S. Climate Change Science Program and the Subcommittee on Global Change Research. Department of Commerce, NOAA's National Climatic Data Center, Washington, D.C., 164 pp.

CH2MHILL. 2009, August. *Detailed Watershed Plan for the Calumet –Sag Channel Watershed, Final Report prepared for Metropolitan Water Reclamation District of Greater Chicago.* (http://www.mwrd.org/pv_obj_cache/pv_obj_id_B7EB07819A404EB370B004B00FB00C8A0EB33400/filename/CalSag-DWP.pdf (accessed November 15, 2015).

Collins, M., and S. Knight. 2007. Ensembles and probabilities: a new era in the prediction of climate change, *Philosophical Transactions of the Royal Society A*, pp. 1471–2962

FEMA (Federal Emergency Management Agency). 2009. *Hazus: FEMA's Methodology for Estimating Potential Losses from Disasters*. http://www.fema.gov/hazus.

Federal Emergency Management Agency. 2012. *Hazus-MH, Estimating Potential Losses from Disasters*. (http://www.fema.gov/media-library-data/20130726-1603-20490-6084/hazus_mh_2012.pdf (accessed March 31, 2016).

Flato, G., J. Marotzke, B. Abiodun, P. Braconnot, S. C. Chou, W. Collins, P. Cox, F. Driouech, S. Emori, V. Eyring, C. Forest, P. Gleckler, E. Guilyardi, C. Jakob, V. Kattsov, C. Reason, and M. Rummukainen. 2013. Evaluation of climate models. In *Climate Change 2013: The Physical Science Basis. Contribution of Working Group I to the Fifth Assessment Report of the Intergovernmental Panel on Climate Change* [Stocker, T.F., D. Qin, G.-K. Plattner, M. Tignor, S.K. Allen, J. Boschung, A. Nauels, Y. Xia, V. Bex and P.M. Midgley (eds.)]. Cambridge University Press, Cambridge, UK and New York, NY, USA.

Gleckler, P. J., K. E. Taylor, and C. Doutriaux. 2008. Performance metrics for climate models. *J. Geophys. Res*. 113: D06104. doi:10.1029/2007JD008972.

Guo, Y., and M. J. Senior. 2006. Climate model simulation of point rainfall frequency characteristics. *J. Hydrol. Eng*. 11(6):547–554.

Haughton, N., G. Abramowitz, A. Pitman, and S. J. Phipps. 2015. Weighting climate model ensembles for mean and variance estimates. *Clim Dyn* 45:3169–3181.

HDR. 2011. *Detailed Watershed Plan for the North Branch of the Chicago River and Lake Michigan Watershed. Final Report prepared for Metropolitan Water Reclamation District of Greater Chicago,* January 2011. https://www.mwrd.org/irj/go/km/docs/documents/MWRD/internet/protecting_the_environment/Stormwater_Management/htm/North_Branch_Chicago_River_Watershed/North_Branch_Chicago_River_DWP.htm.

Hejazi, M., and M. Markus. 2009. Impacts of urbanization and climate variability on floods in northeastern Illinois. *J. Hydrol. Eng*. doi:10.1061/(ASCE)HE.1943-5584.0000020.

Hennegriff, W. 2007. Climate change and floods: Findings and adaptation strategies for flood protection in Baden-Württemberg. *Water Science and Technology* 56(4): 35–44.

Hershfield, D. M. 1961. *Technical Paper 40: Rainfall Frequency Atlas of the United States for Duration from 30 Minutes to 24 Hours and Return Periods from 1 to 100 Years*. Soil Conservation Service, U.S. Department of Agriculture.

Hosking, J. R. M. 1990. L-moments: Analysis and estimation of distributions using linear combinations of order statistics, *J. R. Stat. Soc., Ser. B* 52(1):105–124.

Hosking, J. R. M. 2000. *FORTRAN routines for use with the method of L-moments*, Version 3.03. Research Report RC20525 (90933), IBM Research Division, New York: T. J. Watson Research Center, Yorktown Heights.

Hosking, J. R.M., and J. R. Wallis. 1997. *Regional frequency analysis: An approach based on L-moments*. Cambridge, U.K.: Cambridge Univ. Press.

Huff, F. A. and J. R. Angel. 1989. *Frequency Distributions and Hydroclimatic Characteristics of Heavy Rainstorms in Illinois*, Bulletin 70. Illinois State Water Survey, Champaign, IL.

Huff, F. A. and J. R. Angel. 1992. *Rainfall Frequency Atlas of the Midwest,* Bulletin 71. Illinois State Water Survey, Champaign, IL.

Huff, F. A. and J. C. Neill. 1959. *Frequency Relations for Storm Rainfall in Illinois*, Bulletin 46. Illinois State Water Survey, Champaign, IL.

Illinois Department of Natural Resources Office of Water Resources. 1996, March. Floodplain Map Revision Manual: How to Revise Regulatory Floodplain Map Studies and Get Map Revision Concurrence from IDNR-OWR. Schaumburg, Illinois.

IPCC. 2007. Climate change 2007: The physical science basis. In Solomon S, Qin D, Manning M, Marquis M, Averyt K, Tignor MMB, Miller HL Jr, Chen Z (eds.) *Contribution of Working Group I to the Fourth Assessment Report of the IPCC.* New York: Cambridge University Press. 996 pp.

IPCC. 2013. *Climate Change 2013: The Physical Science Basis. Contribution of Working Group I to the Fifth Assessment Report of the Intergovernmental Panel on Climate Change* [Stocker, T.F., D. Qin, G.-K. Plattner, M. Tignor, S.K. Allen, J. Boshung, A. Nauels, Y. Xia, V. Bex and P.M. Midgley (eds.)]. Cambridge University Press, Cambridge, United Kingdom and New York, NY, USA, 1535 pp. doi:10.1017/CBO9781107415324.

Janssen E., D. J. Wuebbles, K. E. Kunkel, S. C. Olsen, and A. Goodman. 2014. Observational- and model-based trends and projections of extreme precipitation over the contiguous United States. *Earth's Future* 2:99–113.

Karl, T. R., J. T. Melillo, and T. C. Peterson. 2009. *Global Climate Change Impacts in the United States.* Cambridge University Press, 189 pp.

Knutti, R. 2010. The end of model democracy? *Climatic Change* 102(3–4): 395–404, doi:10.1007/s10584-010-9800-2.

Knutti, R., R. Furrer, C. Tebaldi, J. Cermak, and G.A. Meehl. 2010. Challenges in combining projections from multiple climate models, *J. Clim.*, 23:2739–2758, http://dx.doi.org/10.1175/2009JCLI3361.1

Kunkel, K. E., R. Moss, and A. Parris. 2016. Innovations in science and scenarios for assessment. *Climatic Change* 135(1):55–68.

Langbein, W.B. 1949. Annual floods and the partial-duration flood series, *Trans. Am. Geophys. Union,* 30 (1949), p. 379

Lukas, J., J. Barsugli, N. Doesken, I. Rangwala, and K. Wolter. 2014. *Climate Change in Colorado. A Synthesis to Support Water Resources Management and Adaptation.* Tech. Rep., University of Colorado Boulder.

Markus M., J. R. Angel, L. Yang, and M. I. Hejazi. 2007. Changing estimates of design precipitation in northeastern Illinois: Comparison between different sources and sensitivity analysis. *J. Hydrology* 347(1-2):211–222.

Markus, M., and S. McConkey. 2007. *Quantifying the Impact of Land Cover Change and of Climate Change on Floods in Northeastern Illinois.* Final report for the Illinois-Indiana Sea Grant, http://www.iisgcp.org/research/projects/coast/markusrcm0504.pdf.

Markus, M., D. J. Wuebbles, X. –Z. Liang, K. Hayhoe, and D. A. R. Kristovich. 2012. Diagnostic analysis of future climate scenarios applied to urban flooding in the Chicago metropolitan area. Climatic Change 111(3):879–902.

Masson, D. and R. Knutti. 2011. Climate model genealogy. *Geophys Res Lett* 38:L08703. doi:10.1029/2011GL046864.

Meehl, G. A., C. Covey, T. Delworth, M. Latif, B. Mcavaney, J.F.B. Mitchell, R. J. Stouffer, and K. E. Taylor. 2007. The WCRP CMIP3 multimodel dataset: A new era in climate change research. *Bulletin of the American Meteorological Society* 88(9):1383-1394.

Miller, J. F., R. H. Frederick, and R .J. Tracey. 1973. *Precipitation Frequency Atlas of Wester United States.* NOAA Atlas 2, National Weather Service, Silver Spring, MD.

Milly, P.C.D., J. Betancourt, M. Falkenmark, R. M. Hirsch, Z. W. Kundzewicz, D. P. Lettenmaier, and R. J. Stouffer. 2008. Stationarity is dead: Whither water management? *Science* 319:573–574.

MWH. 2009. *Detailed Watershed Plan for the Upper Salt Creek Watershed, Final Report Prepared for Metropolitan Water Reclamation District of Greater Chicago*, November 2009.

http://www.mwrd.org/pv_obj_cache/pv_obj_id_5E3C156DEC13B6707EEA0BD18B6A77B314E31F00/filename/Final_Upper_Salt_Creek_DWP.pdf (accessed November 13, 2015).

Metropolitan Water Reclamation District of Greater Chicago (MWRDGC). 2009. *Technical Guidance Manual Public Review Draft.* 9-24-2009. http://www.mwrd.org/pv_obj_cache/pv_obj_id_D9771FC25B20AC0EAE0FDF08FD3DA195B35B8700/filename/10_Draft_TGM_Article_5.pdf (accessed November 15, 2015).

Murphy, J. M., D. M. H. Sexton, D. N. Barnett, G. S. Jones, M. J. Webb, M. Collins, and D. A. Stainforth. 2004. Quantification of modelling uncertainties in a large ensemble of climate change simulations. *Nature* 430:768–772.

Nakicenovic, N., J. Alcamo, G. Davis, H.J.M. de Vries, J. Fenhann, S. Gaffin, K. Gregory, A. Grubler, T.Y. Jung, T. Kram, E.L. La Rovere, L. Michaelis, S. Mori, T. Morita, W. Papper, H. Pitcher, L. Price, K. Riahi, A. Roehrl, H-H. Rogner, A. Sankovski, M. Schlesinger, P. Shukla, S. Smith, R. Swart, S. van Rooijen, N. Victor, and Z. Dadi. N. Nakicenovic and R. Swart (Eds.), UK. pp 570. *Special Report on Emissions Scenarios*, IPCC, Cambridge University Press, Cambridge, UK, 2000. pp. 570.

Nakicenovic, N., O. Davidson, G. Davis, A. Gru¨bler, T. Kram, E. L. La Rovere, B. Metz, T. Morita, W. Pepper, H. Pitcher, A. Sankovski, P. Shukla, R. Swart, R. Watson, and Z. Dadi. 2000. *Summary for policymakers, emissions scenarios: a special report of IPCC working group III.* IPCC, Geneva, Switzerland

National Research Council (NRC). 2011. *Global Change and Extreme Hydrology, Testing Conventional Wisdom*. Committee on Hydrologic Science, The National Academies Press, Washington D.C., www.nap.edu.

Notaro, M., D. Lorenz, C. Hoving, and M. Schummer. 2014. Twenty-first century projections of snowfall and winter severity across central-eastern North America. *J. Climate* 27: 6526–6550.

Oubeidillah, A. A., S. –C Kao, M. Ashfaq, B. S. Naz, and G. Tootle. 2013. A large-scale, high-resolution hydrological model parameter dataset for climate change impact assessment for the conterminous United States. *Hydrol. Earth Syst. Sci.*, 18:67–84, doi:10.5194/hess-18-67-2014.

Perica, S., S. Dietz, S. Heim, L. Hiner, K. Maitaria, D. Martin, S. Pavlovic, I. Roy, C. Trypaluk, D. Unruh, F. Yan, M. Yekta, T. Zhao, G. Bonnin, D. Brewer, L. Chen, T. Parzybok, and J. Yarchoan. 2011. NOAA Atlas 14 Volume 6 Version 2.0, *Precipitation Frequency Atlas of the United States*.

Perica, S., D. Martin, S. Pavlovic, I. Roy, M. St. Laurent, C. Trypaluk, D. Unruh, M. Yekta, and G. Bonnin. 2013. *Precipitation-Frequency Atlas of the United States, Atlas 14 Volume 9 Version 2.0*, National Oceanic and Atmospheric Administration, National Weather Service, Silver Spring, Maryland.

Raisanen, J., and T. N. Palmer. 2001. A probability and decision-model analysis of a multimodel ensemble of climate change simulations. *J. Clim*. 14(15): 3212–3226.

Raisanen, J., Ylhaisi, J.S. 2012. Can model weighting improve probabilistic projections of climate change? *Clim Dyn* 39:1981–1998.

Rimoldini, L. 2014. Weighted skewness and kurtosis unbiased by sample size and Gaussian uncertainties, *Astron. Comput.*, 5, pp. 1–8, http://dx.doi.org/10.1016/j.ascom.2014.02.001

Sanchez, E., R. Romera, M. A. Gaertner, C. Gallardo, and M. Castro. 2009. A weighting proposal for an ensemble of regional climate models over Europe driven by 1961–2000 ERA40 based on monthly precipitation probability density functions. *Atmos. Sci. Lett.* 10, 241–248.

Sanderson, B. M., R. Knutti, and P. Caldwell. 2015. A representative democracy to reduce nterdependency in a multimodel ensemble. *J. Climate* 28:5171–5194.

Schuster, Z. T., K. W. Potter, and D. S. Liebl, 2012. Assessing climate change impacts on precipitation and flood damage in Wisconsin, *Journal of Hydrologic Engineering*. doi:10.1061/(ASCE)HE.1943-5584.0000513.

Sun, F., M. L. Roderick, W. H. Lim, and G. D. Farquhar. 2011. Hydroclimatic projections for the Murray-Darling Basin based on an ensemble derived from Intergovernmental Panel on Climate Change AR4 climate models. *Water Resour. Res.*, 47: W00G02. doi:10.1029/2010WR009829.

Taylor, K. E., R. J. Stouffer, and G. A. Meehl. 2011. *A Summary of the CMIP5 Experiment Design*. January 22, 2011, 33 pp., available at: http://cmippcmdi.llnl.gov/cmip5/docs/Taylor_CMIP5_design.pdf.

Tebaldi, C., and R Knutti. 2007. The use of the multi-model ensemble in probabilistic climate projections, *Philos. Trans. Roy. Soc. A: Math., Phys. Eng. Sci.*, 365 (1857), pp. 2053–2075.

Tukey, J. W. 1977. *Exploratory data analysis*. Addison-Wesley: Reading, Massachusetts.

Vogel, R. M., and N. M. Fennessey. 1993. L moment diagrams should replace product moment diagrams. *Water Resour. Res*. 29(6):1745–1752.

Weiss, L. L. 1964. Ratio of True to Fixed-interval Maximum Rainfall. *Journal of Hydraulic Division of ASCE* 90:78–82.

Wilby, R. L., and I. Harris. 2006. A framework for assessing uncertainties in climate change impacts: Low-flow scenarios for the River Thames, UK, *Water Resour. Res.*, 42, W02419, doi:10.1029/2005WR004065.

Winters, B. A., J. R. Angel, C. Ballerine, J. Byard, A. Flegel, D. Gambill, E. Jenkins, S. McConkey, M. Markus, B. A. Bender, and M. J. O'Toole. 2015. *Report for the Urban Flooding Awareness Act*. Springfield, IL: Illinois Department of Natural Resources, Springfield, Illinois. http://hdl.handle.net/2142/78150

Wuebbles, D., G. Meehl, K. Hayhoe, T. Karl, K. Kunkel, B. Santer, M. Wehner, B. Colle, E. Fishcer, R. Fu, A. Goodman, E. Janssen, V. Kharin, H. Lee, W. Li, L. Long, S. Olsen, Z. Pan, A. Seth, J. Sheffield, and L. Sun. 2014. CMIP5 climate model analysis, *Am. Meteorol. Soc.*, 95(4):571–583.

Appendix A. Projected Isohyetal Maps for Cook County (2-year, 5-year, 10-year, 25-year, 50-year, and 100-year recurrence intervals)
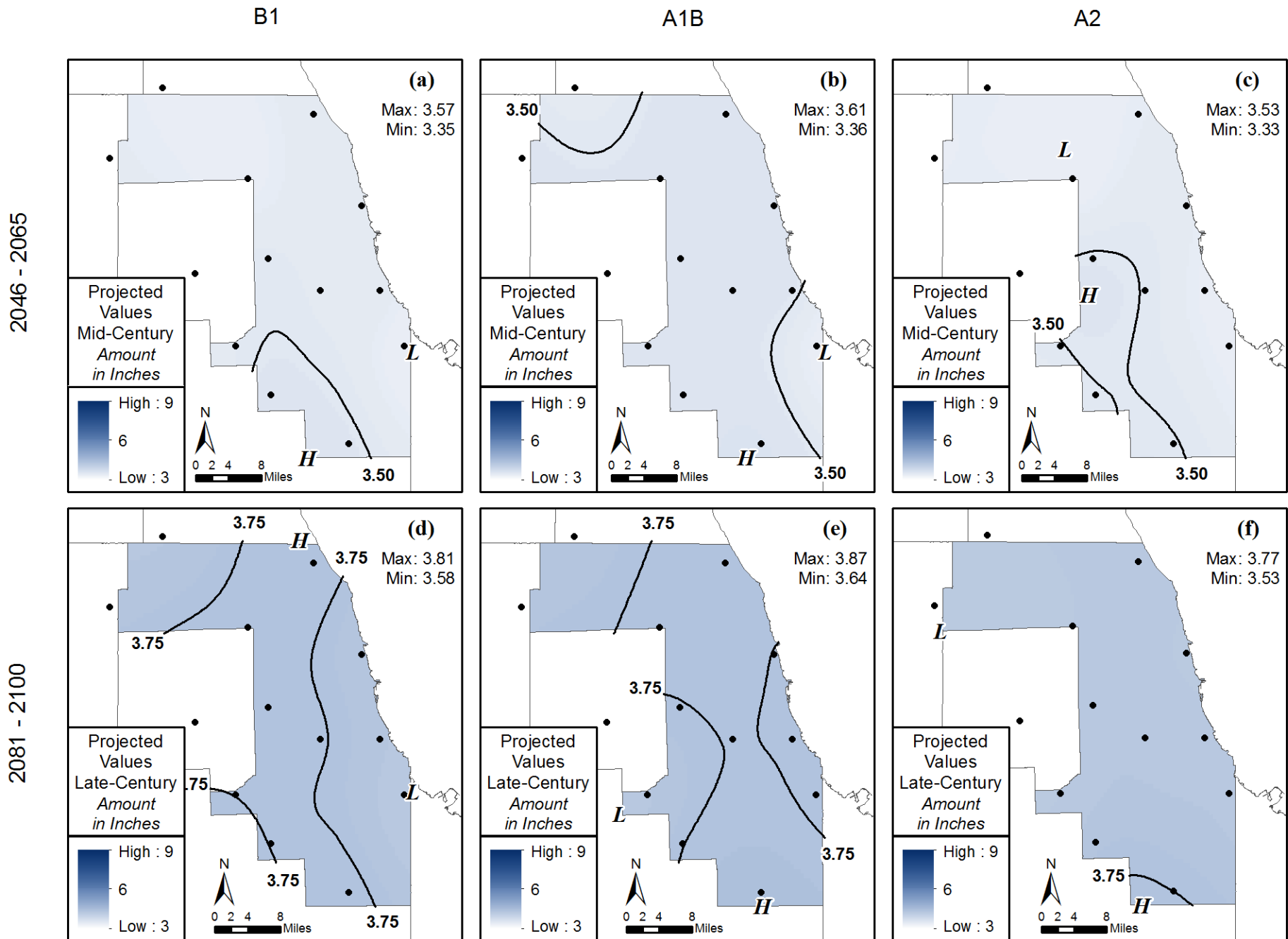
Figure 10. Projected 2-year, 24-hour isohyetals. Top row represents mid-21st century, and bottom row is late-21st century. Three columns show results for 3 IPCC CMIP3 climate scenarios (B1, A1B, and A2).
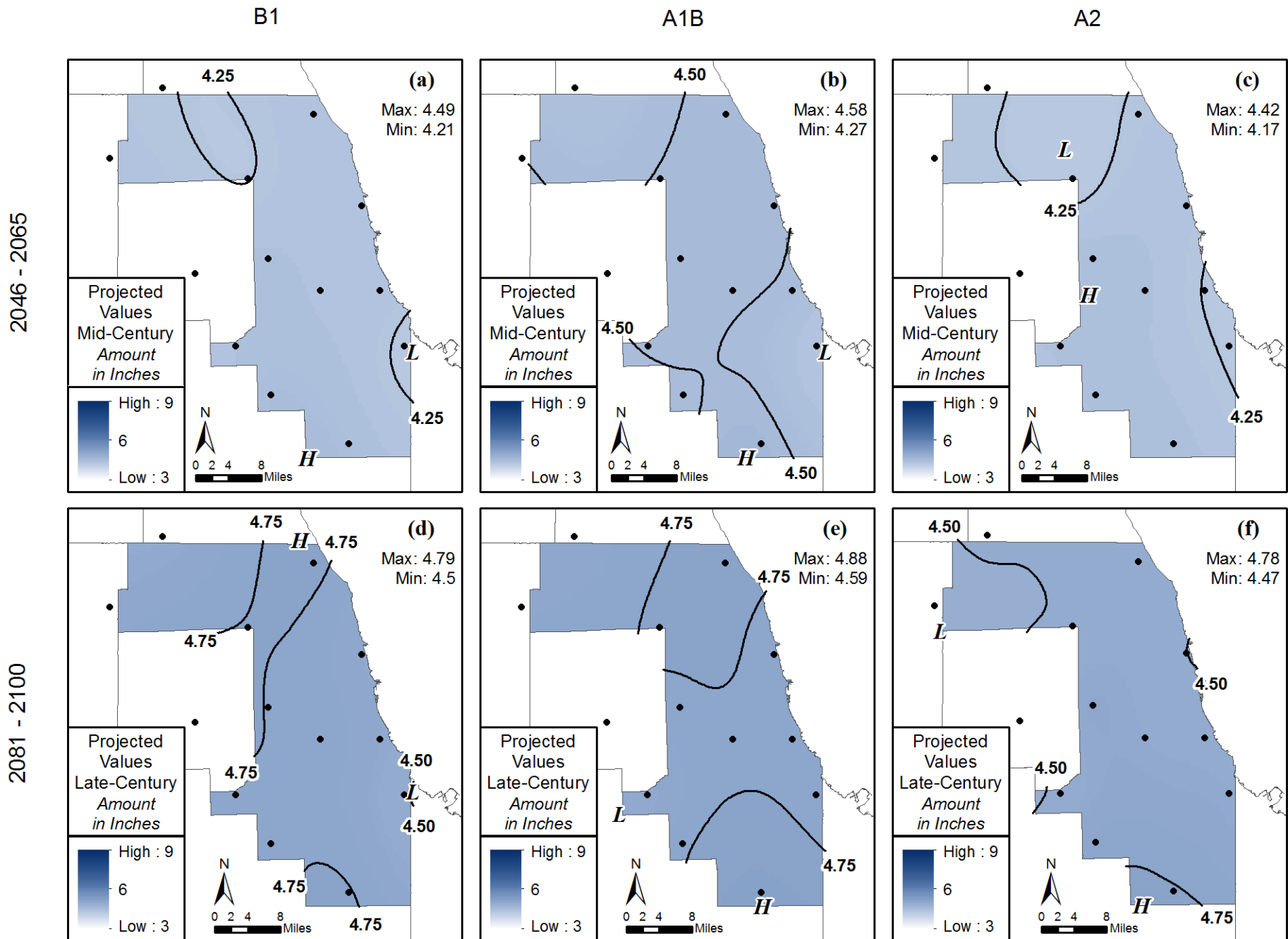
Figure 11. Projected 5-year, 24-hour isohyetals. Top row represents mid-21st century, and bottom row is late-21st century. Three columns show results for 3 IPCC CMIP3 climate scenarios (B1, A1B, and A2).
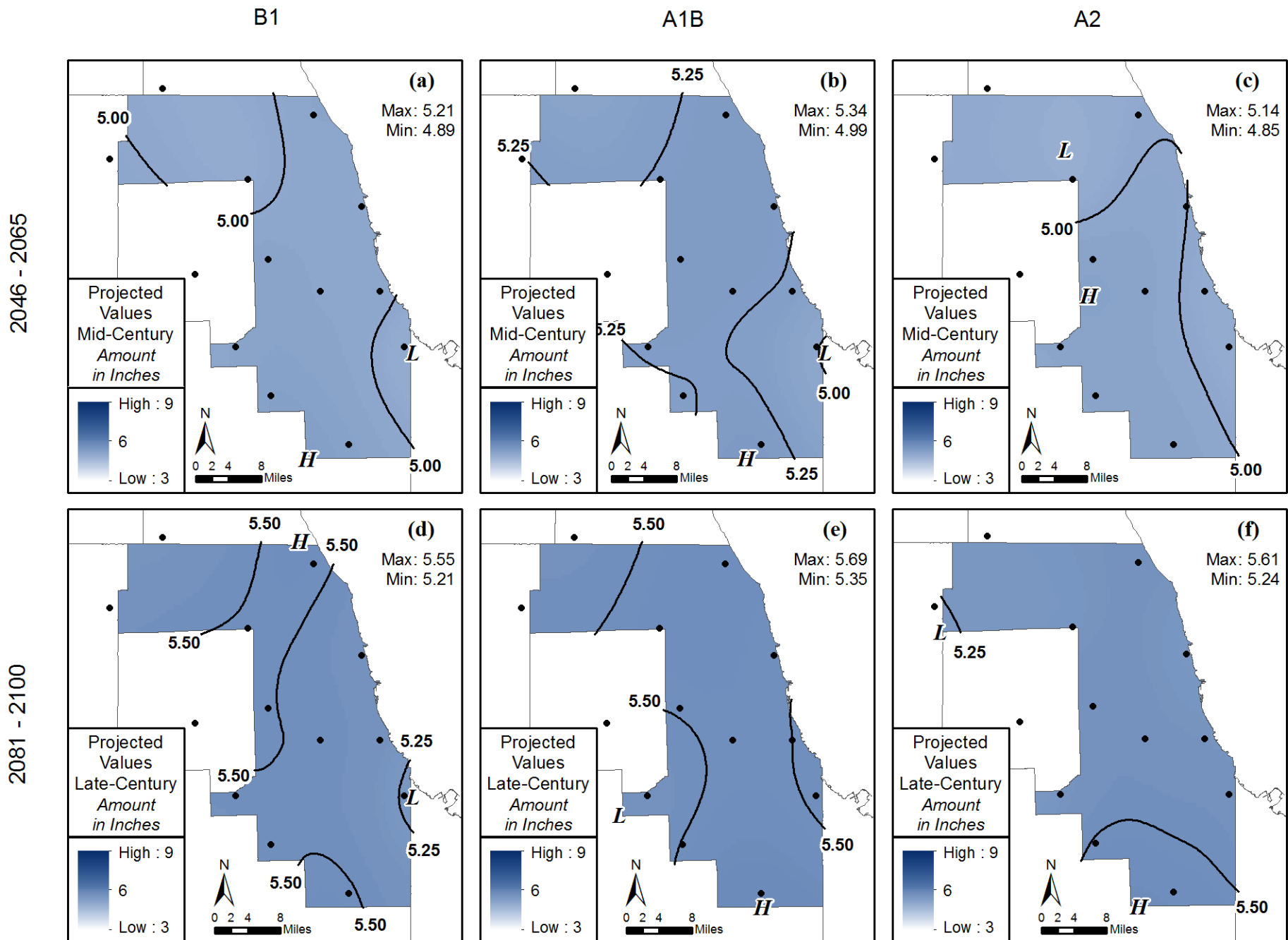
Figure 12. Projected 10-year, 24-hour isohyetals. Top row represents mid-21st century, and bottom row is late-21st century. Three columns show results for 3 IPCC CMIP3 climate scenarios (B1, A1B, and A2).
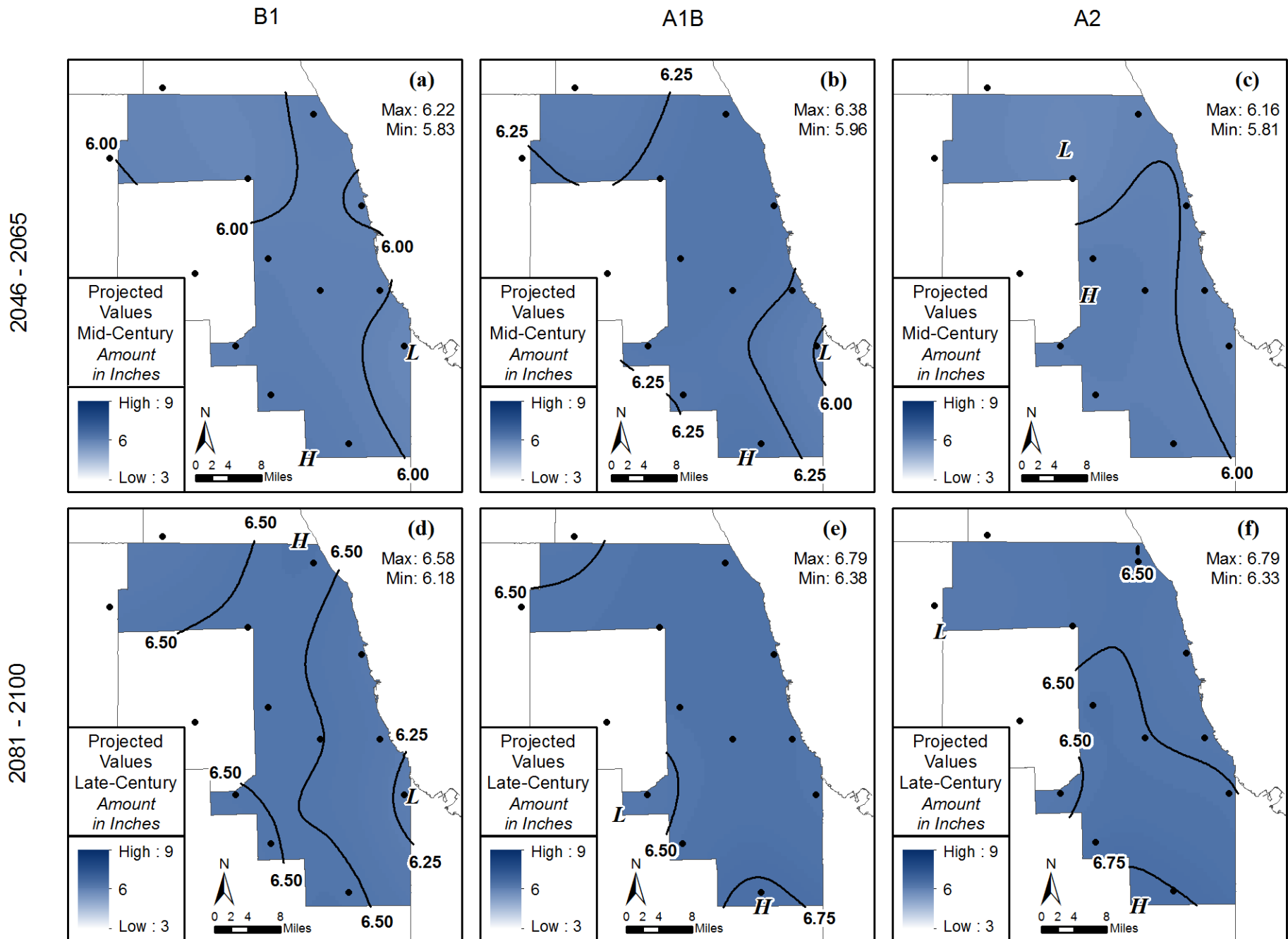
Figure 13. Projected 25-year, 24-hour isohyetals. Top row represents mid-21st century, and bottom row is late-21st century. Three columns show results for 3 IPCC CMIP3 climate scenarios (B1, A1B, and A2).
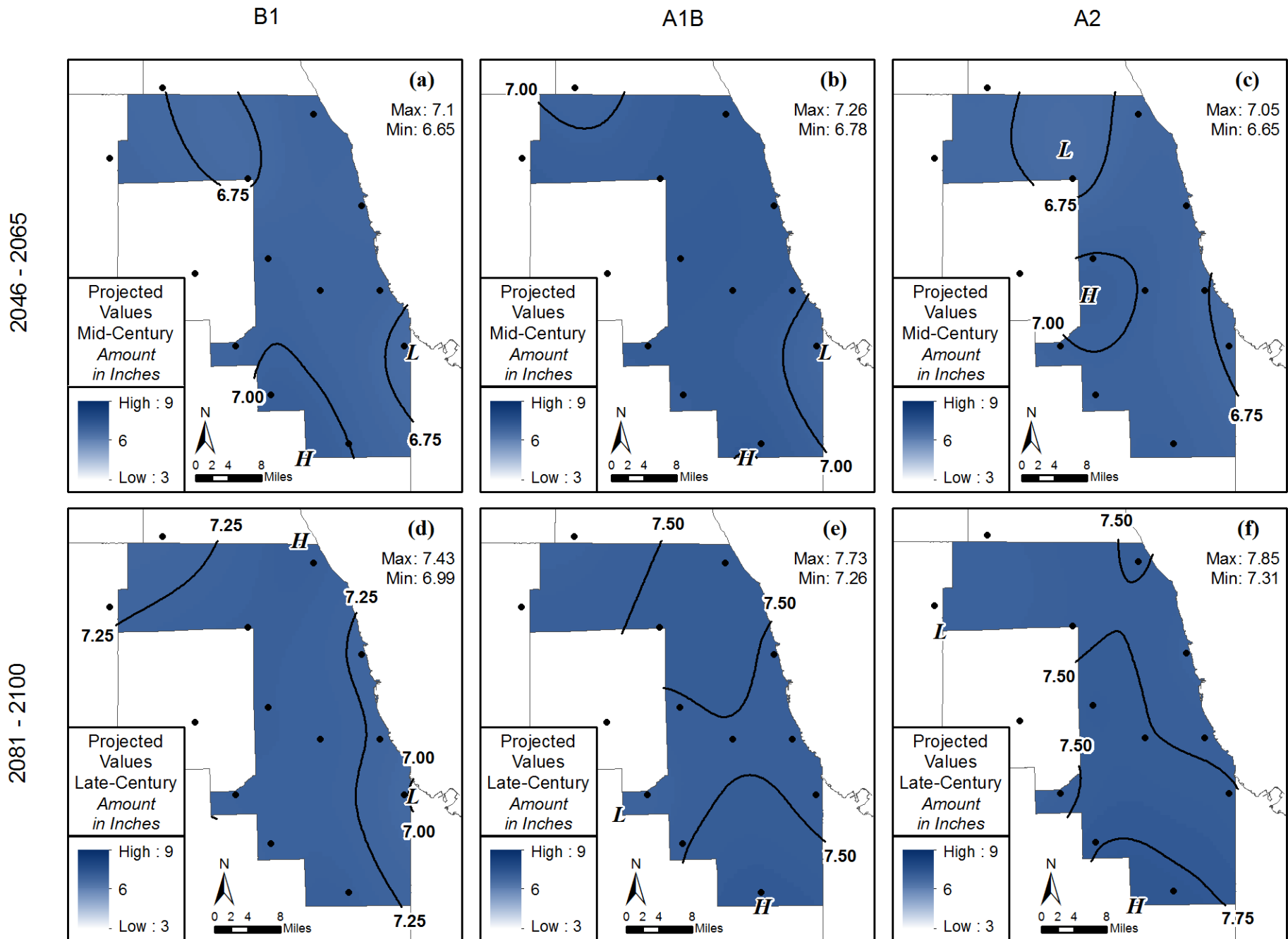
Figure 14. Projected 50-year, 24-hour isohyetals. Top row represents mid-21st century, and bottom row is late-21st century. Three columns show results for 3 IPCC CMIP3 climate scenarios (B1, A1B, and A2).
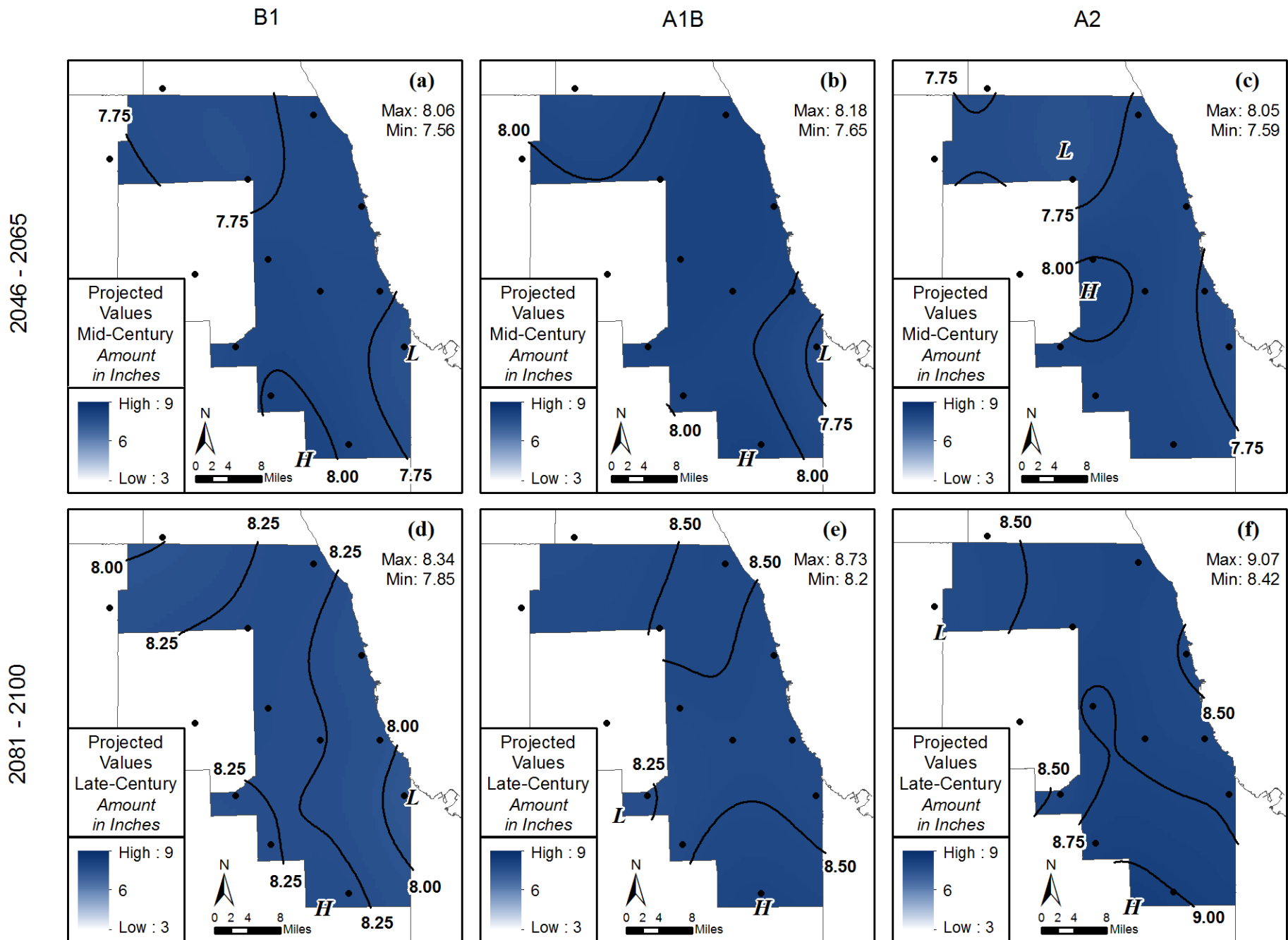
Figure 15. Projected 100-year, 24-hour isohyetals. Top row represents mid-21st century, and bottom row is late-21st century. Three columns show results for 3 IPCC CMIP3 climate scenarios (B1, A1B, and A2).

Appendix B. Comparisons of Projected Isohyetals with Bulletin 70 Isohyetal Maps for Cook County (2-year, 10-year and 100-year recurrence intervals)
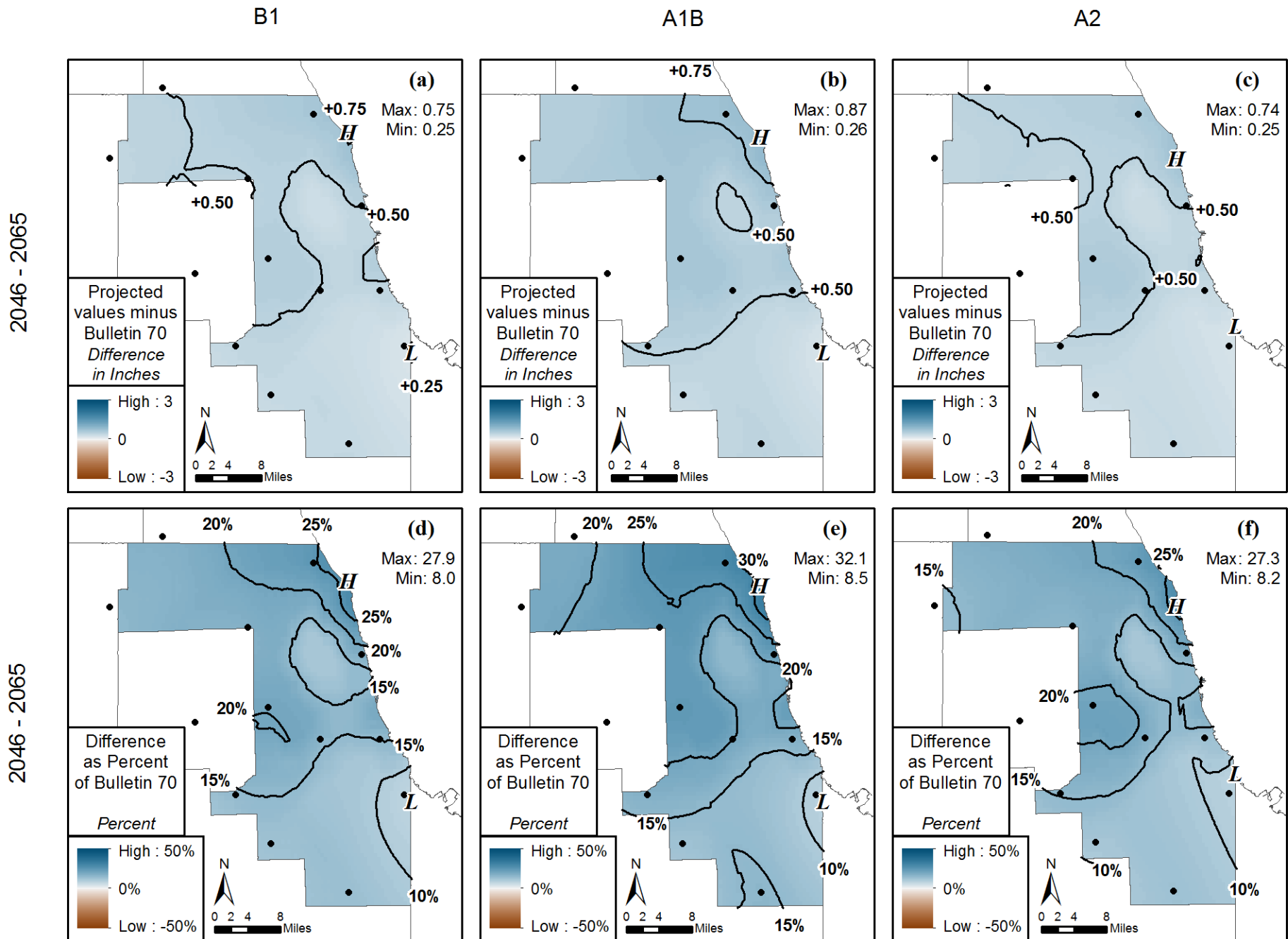
Figure 16. Differences between projected 2-year, 24-hour isohyetals for mid-21st century and Bulletin 70 (Huff and Angel, 1989). Top row shows absolute differences in inches, and the bottom row shows percent differences. Three columns show results for 3 IPCC CMIP3 climate scenarios (B1, A1B, and A2).
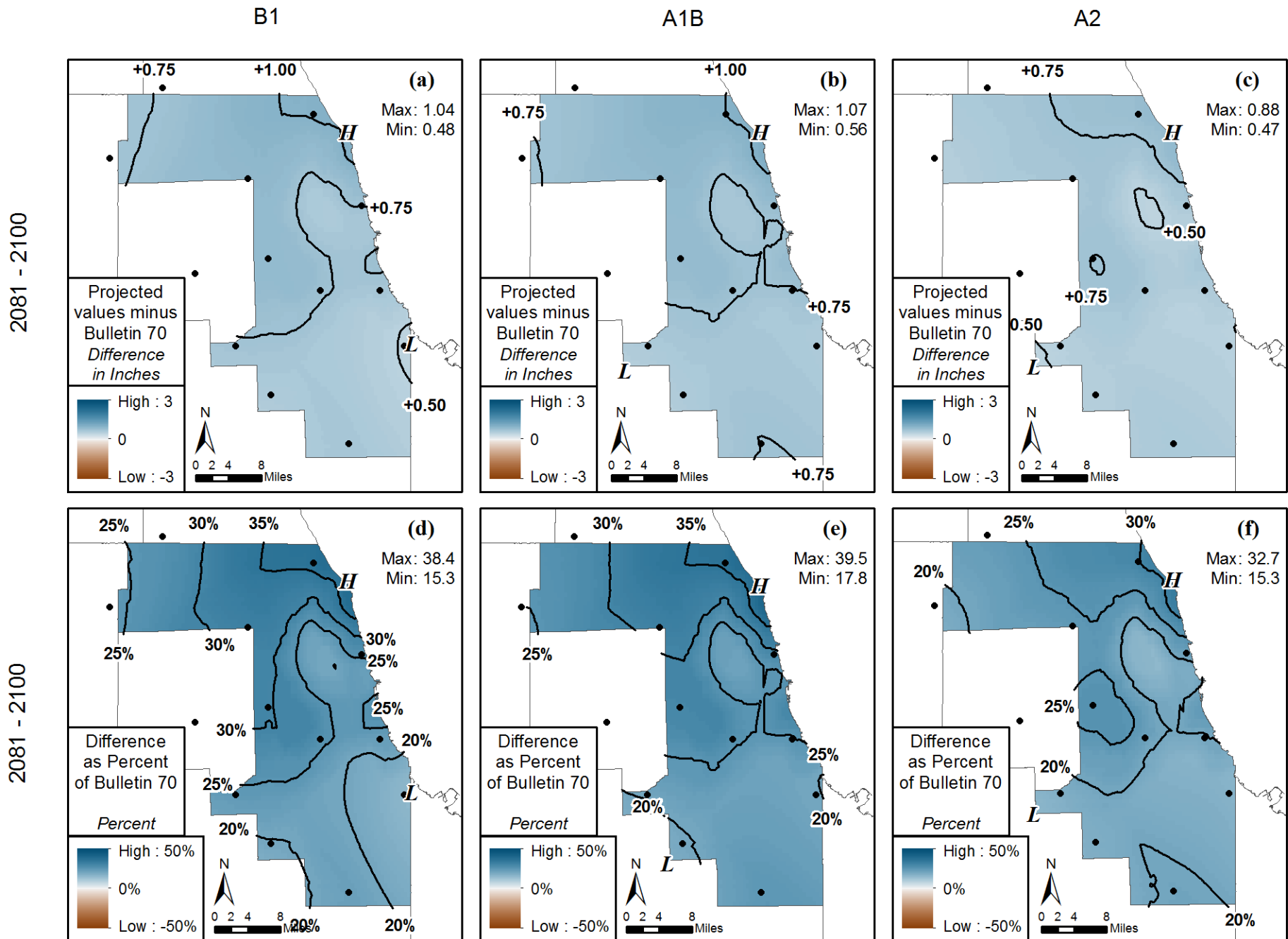
Figure 17. Differences between projected 2-year, 24-hour isohyetals for late-21st century and Bulletin 70 (Huff and Angel, 1989). Top row shows absolute differences in inches, and the bottom row shows percent differences. Three columns show results for 3 IPCC CMIP3 climate scenarios (B1, A1B, and A2).
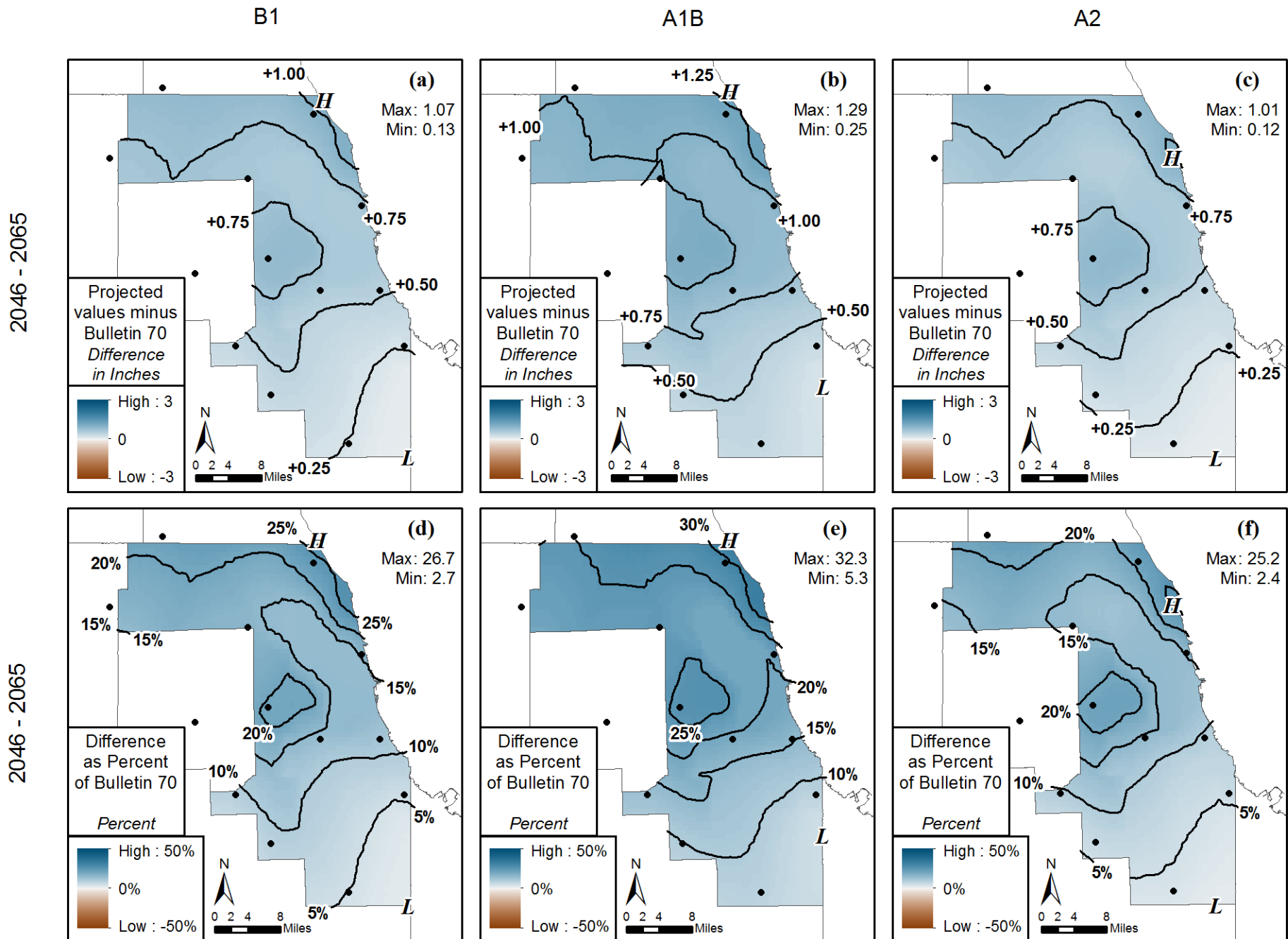
Figure 18. Differences between projected 10-year, 24-hour isohyetals for mid-21st century and Bulletin 70 (Huff and Angel, 1989). Top row shows absolute differences in inches, and the bottom row shows percent differences. Three columns show results for 3 IPCC CMIP3 climate scenarios (B1, A1B, and A2).
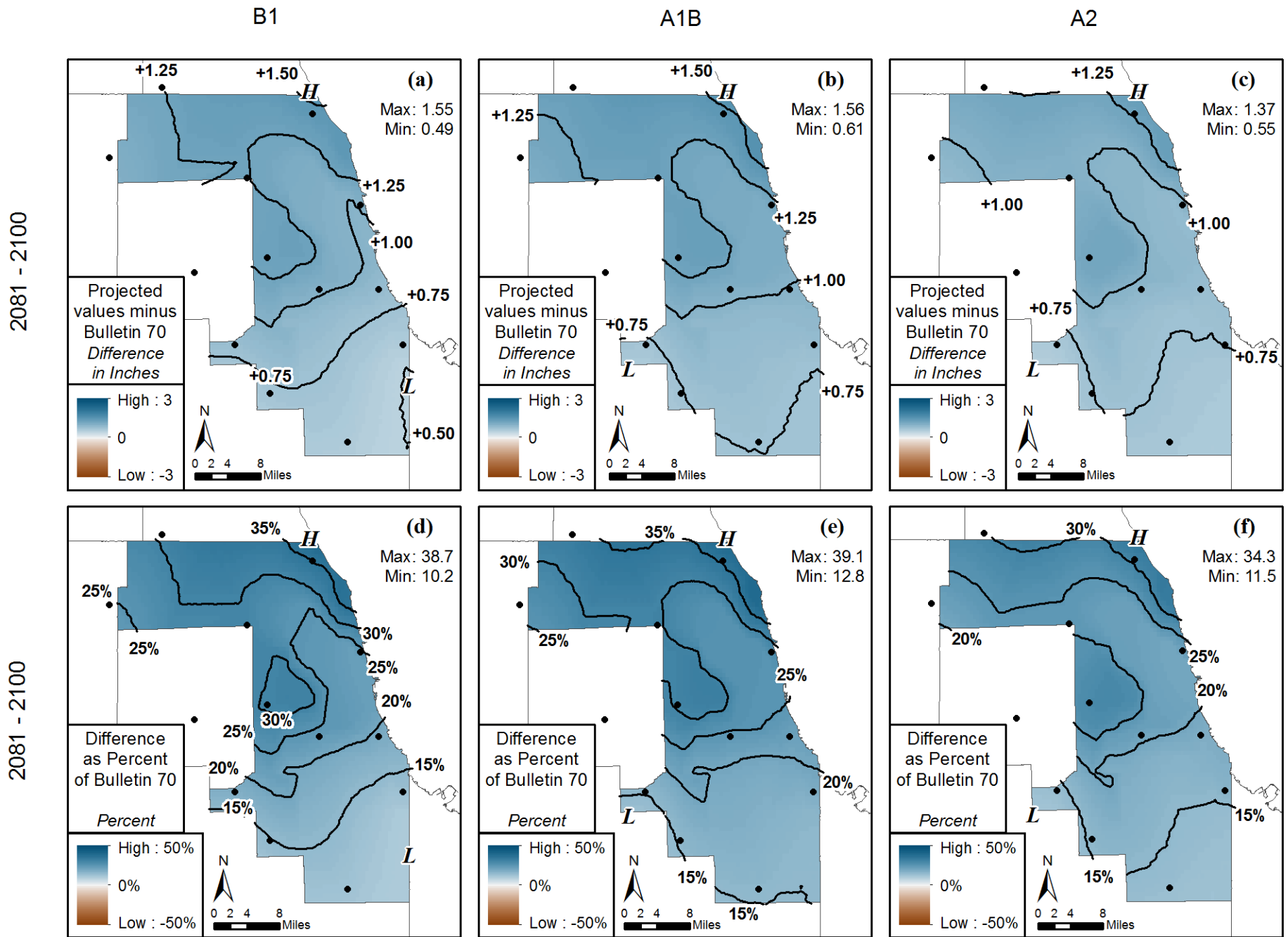
Figure 19. Differences between projected 10-year, 24-hour isohyetals for late-21st century and Bulletin 70 (Huff and Angel, 1989). Top row shows absolute differences in inches, and the bottom row shows percent differences. Three columns show results for 3 IPCC CMIP3 climate scenarios (B1, A1B, and A2).
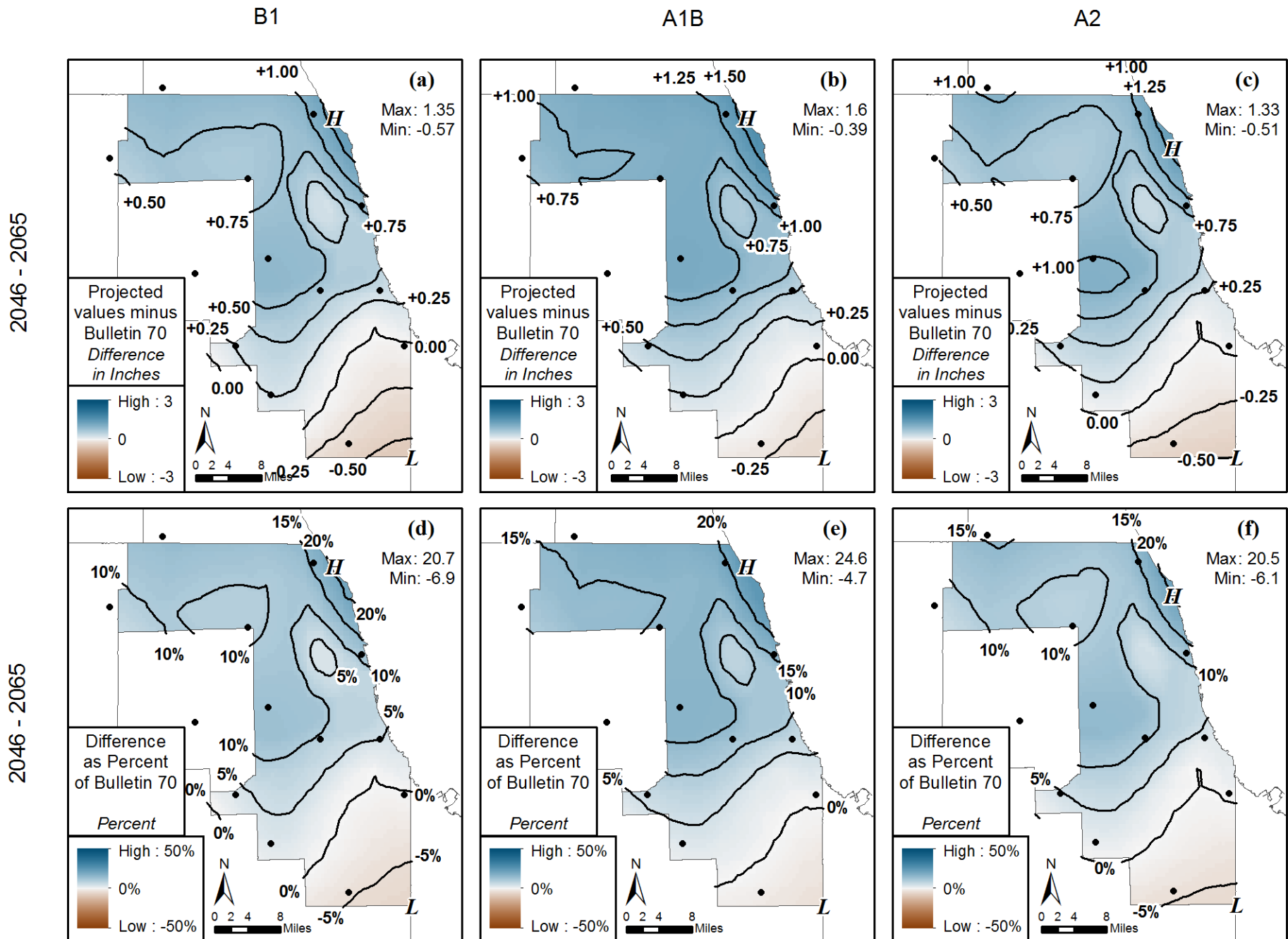
Figure 20. Differences between projected 100-year, 24-hour isohyetals for mid-21st century and Bulletin 70 (Huff and Angel, 1989). Top row shows absolute differences in inches, and the bottom row shows percent differences. Three columns show results for 3 IPCC CMIP3 climate scenarios (B1, A1B, and A2).
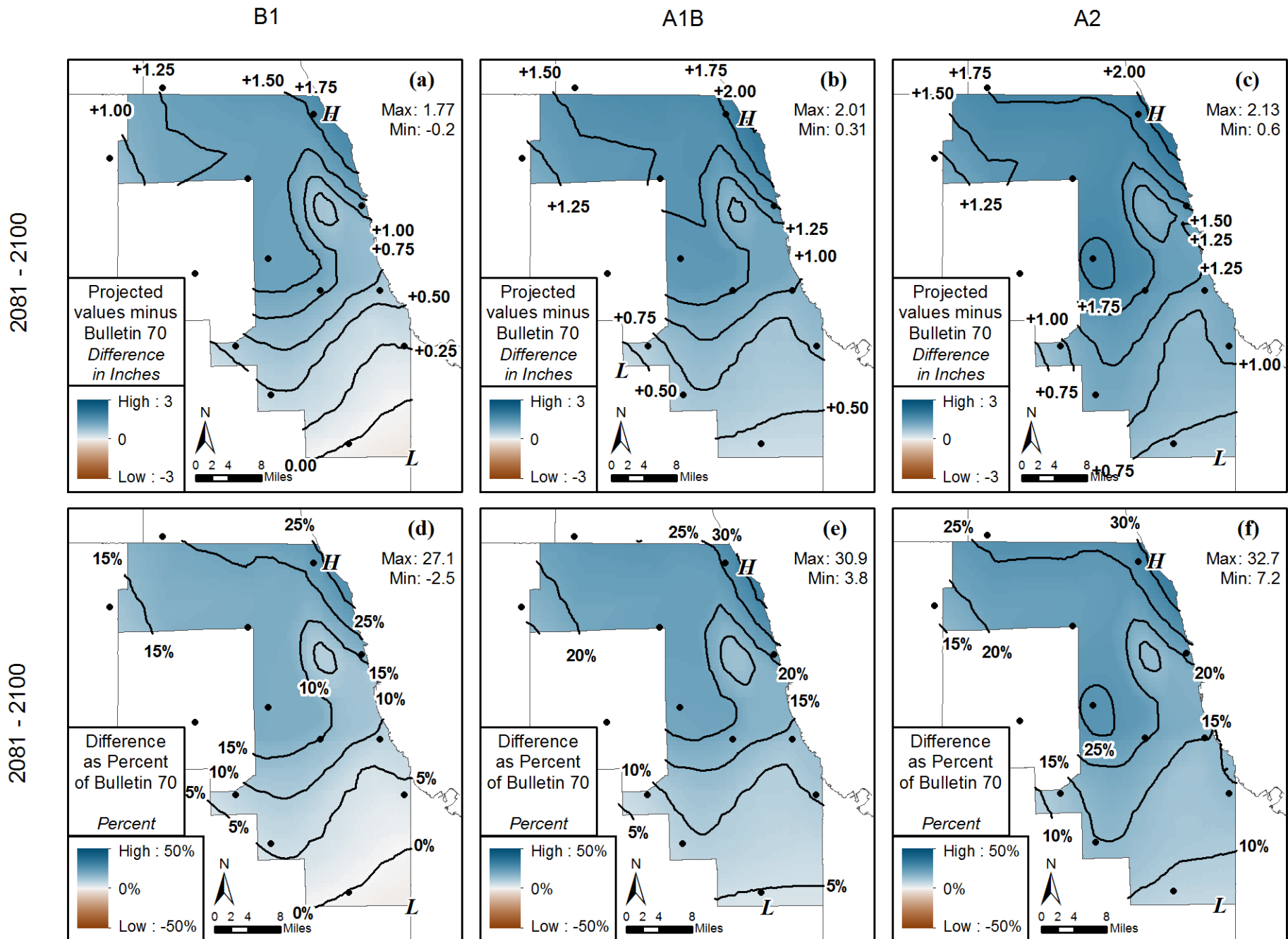
Figure 21. Differences between projected 100-year, 24-hour isohyetals for late-21st century and Bulletin 70 (Huff and Angel, 1989). Top row shows absolute differences in inches, and the bottom row shows percent differences. Three columns show results for 3 IPCC CMIP3 climate scenarios (B1, A1B, and A2).

Appendix C. Comparisons of Projected Isohyetals with NOAA Atlas 14 Isohyetal Maps for Cook County (2-year, 10-year, and 100-year recurrence intervals)
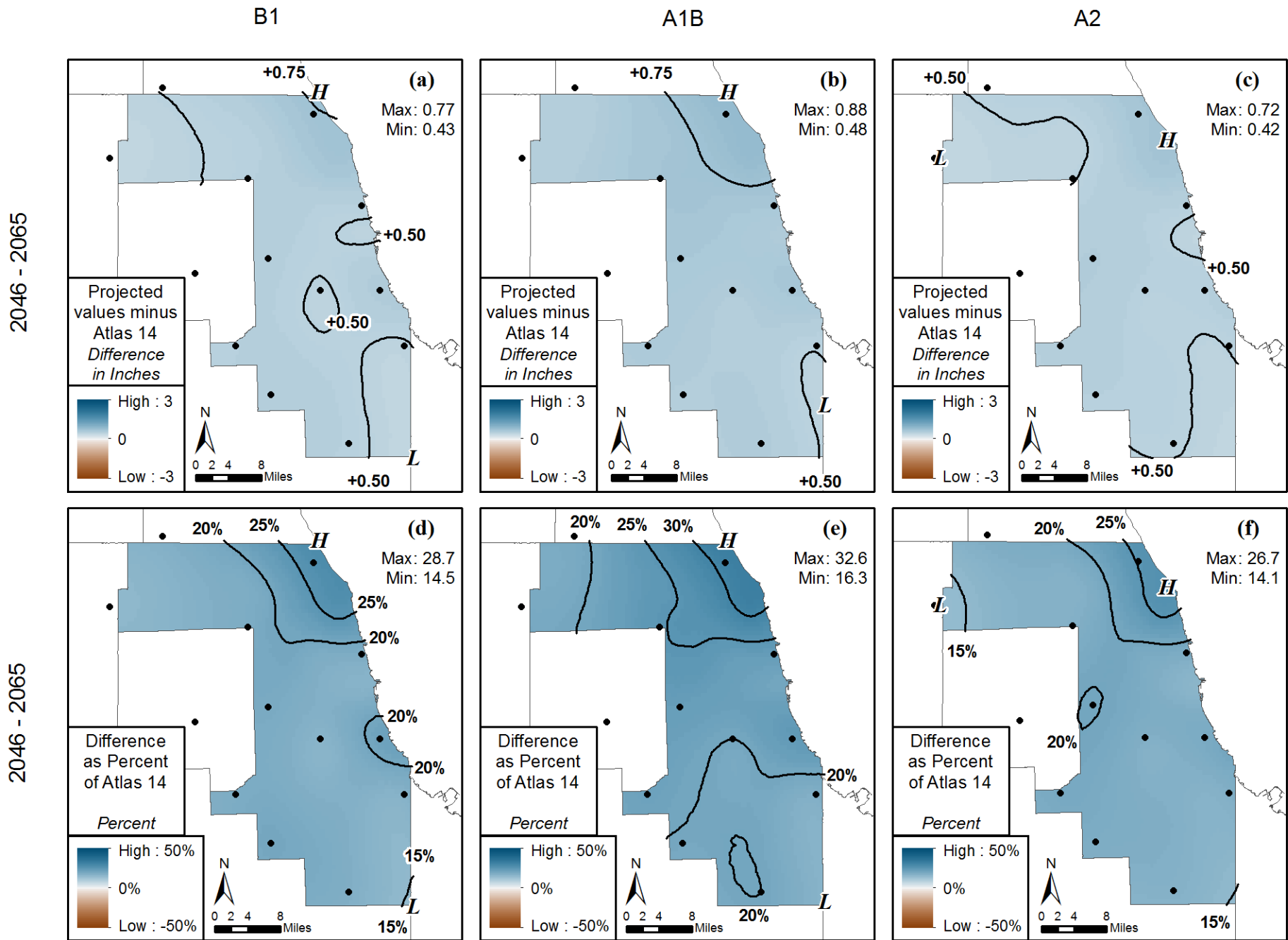
Figure 22. Differences between projected 2-year, 24-hour isohyetals for mid-21st century and Atlas 14 (Bonnin et al. 2006). Top row shows absolute differences in inches, and the bottom row shows percent differences. Three columns show results for 3 IPCC CMIP3 climate scenarios (B1, A1B, and A2).

43
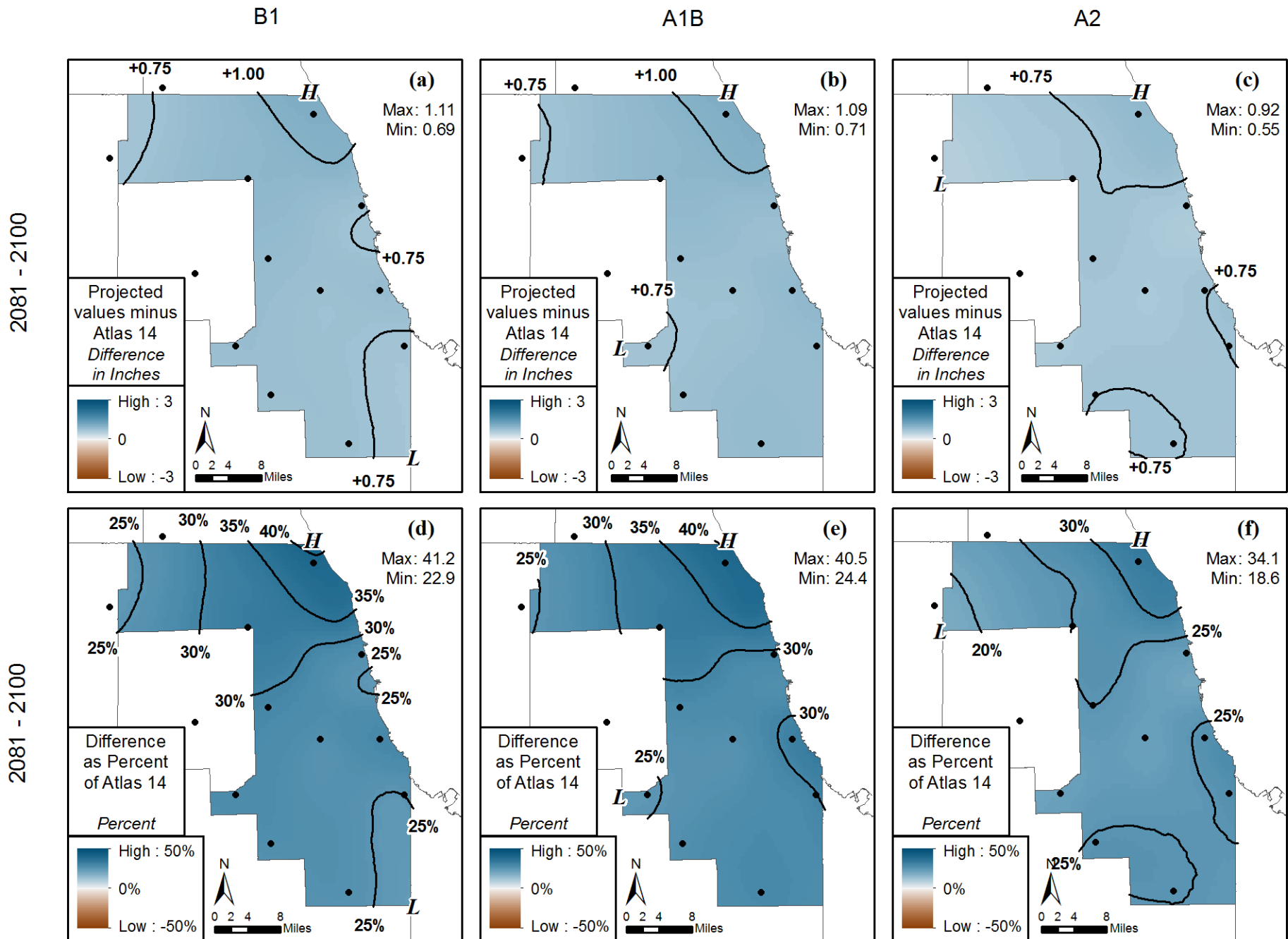
Figure 23. Differences between projected 2-year, 24-hour isohyetals for late-21st century and Atlas 14 (Bonnin et al. 2006). Top row shows absolute differences in inches, and the bottom row shows percent differences. Three columns show results for 3 IPCC CMIP3 climate scenarios (B1, A1B, and A2).

44
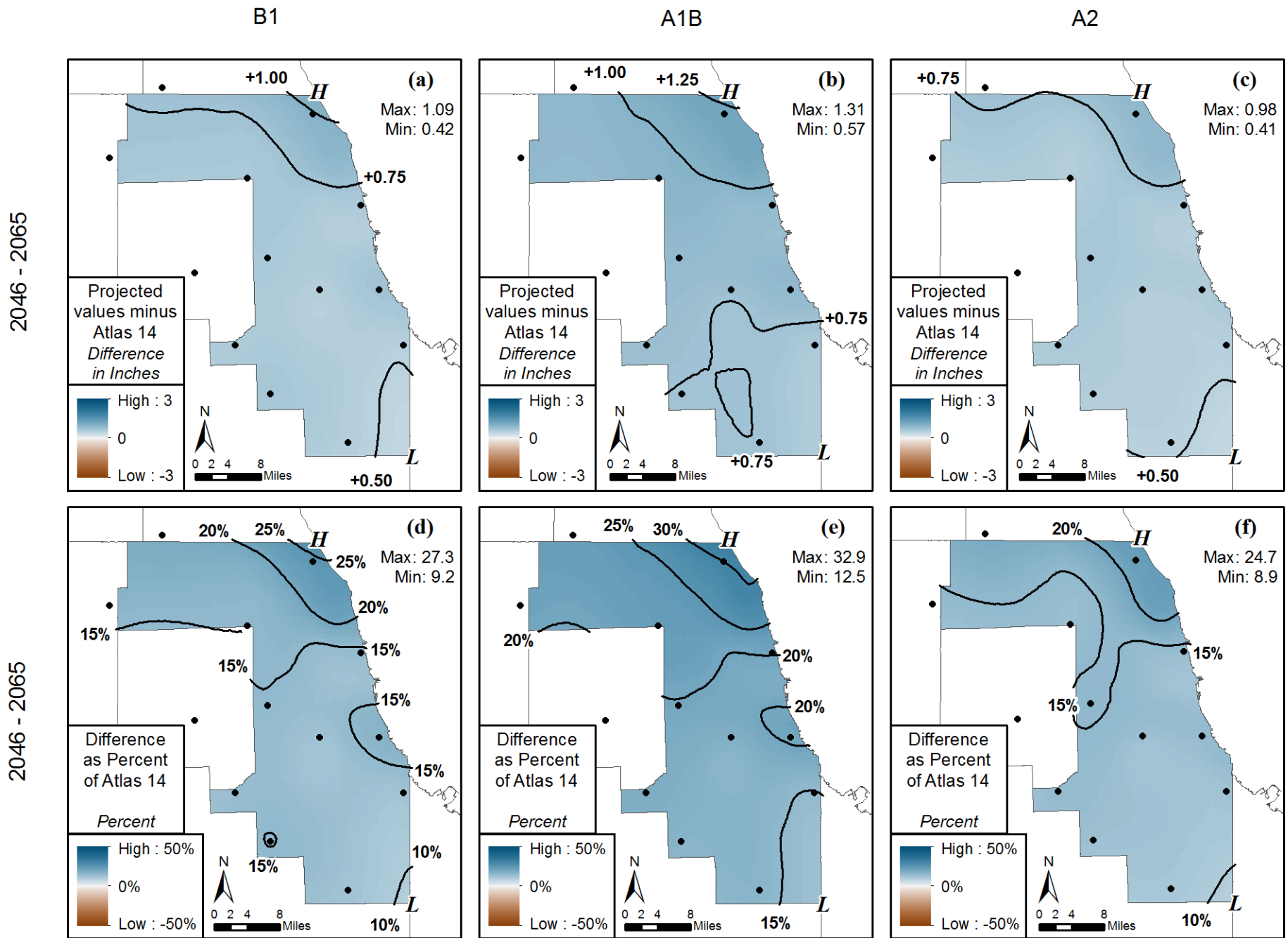
Figure 24. Differences between projected 10-year, 24-hour isohyetals for mid-21st century and Atlas 14 (Bonnin et al. 2006). Top row shows absolute differences in inches, and the bottom row shows percent differences. Three columns show results for 3 IPCC CMIP3 climate scenarios (B1, A1B, and A2).
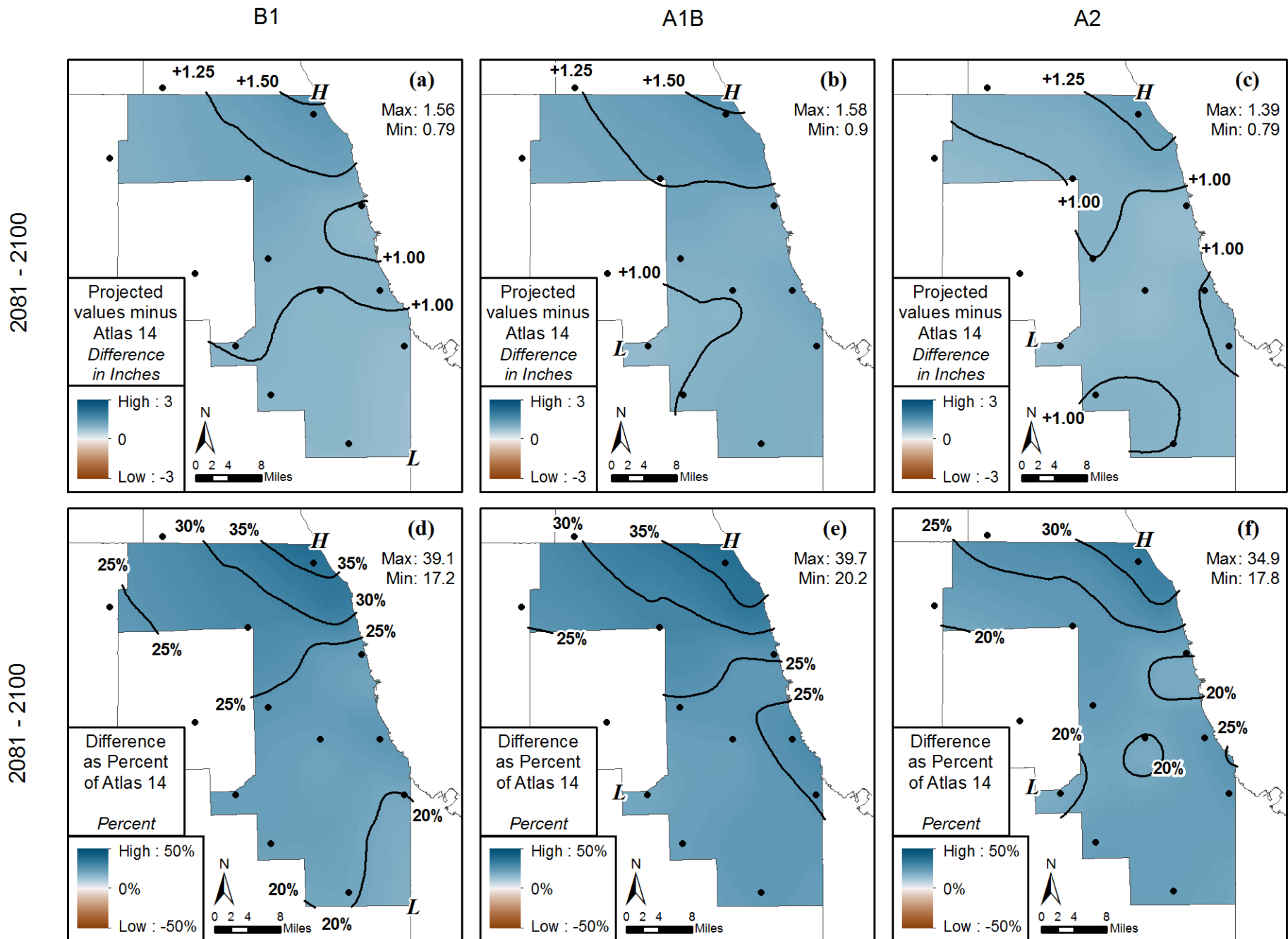
Figure 25. Differences between projected 10-year, 24-hour isohyetals for late-21st century and Atlas 14 (Bonnin et al. 2006). Top row shows absolute differences in inches, and the bottom row shows percent differences. Three columns show results for 3 IPCC CMIP3 climate scenarios (B1, A1B, and A2).
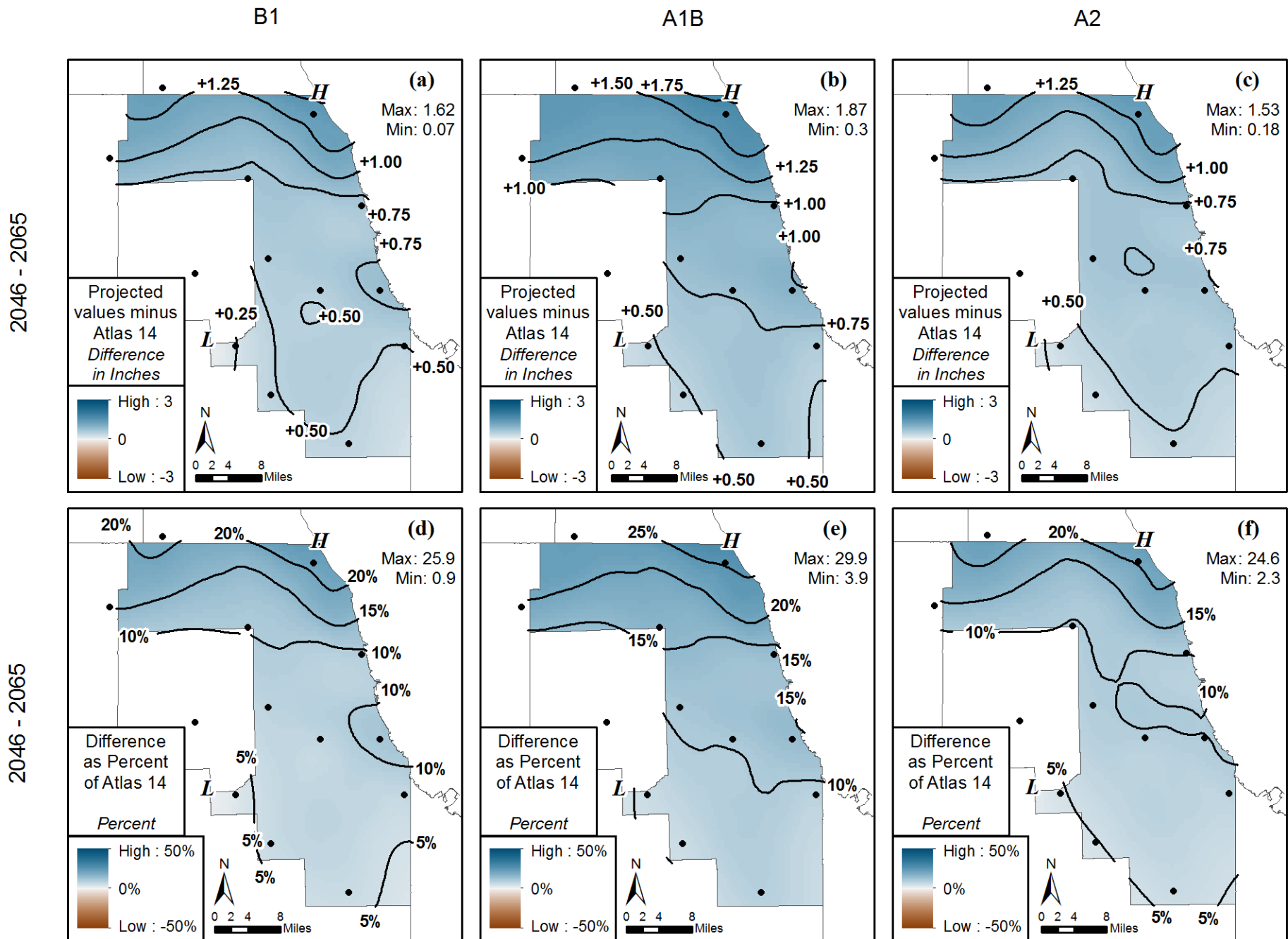
Figure 26. Differences between projected 100-year, 24-hour isohyetals for mid-21st century and Atlas 14 (Bonnin et al. 2006). Top row shows absolute differences in inches, and the bottom row shows percent differences. Three columns show results for 3 IPCC CMIP3 climate scenarios (B1, A1B, and A2).
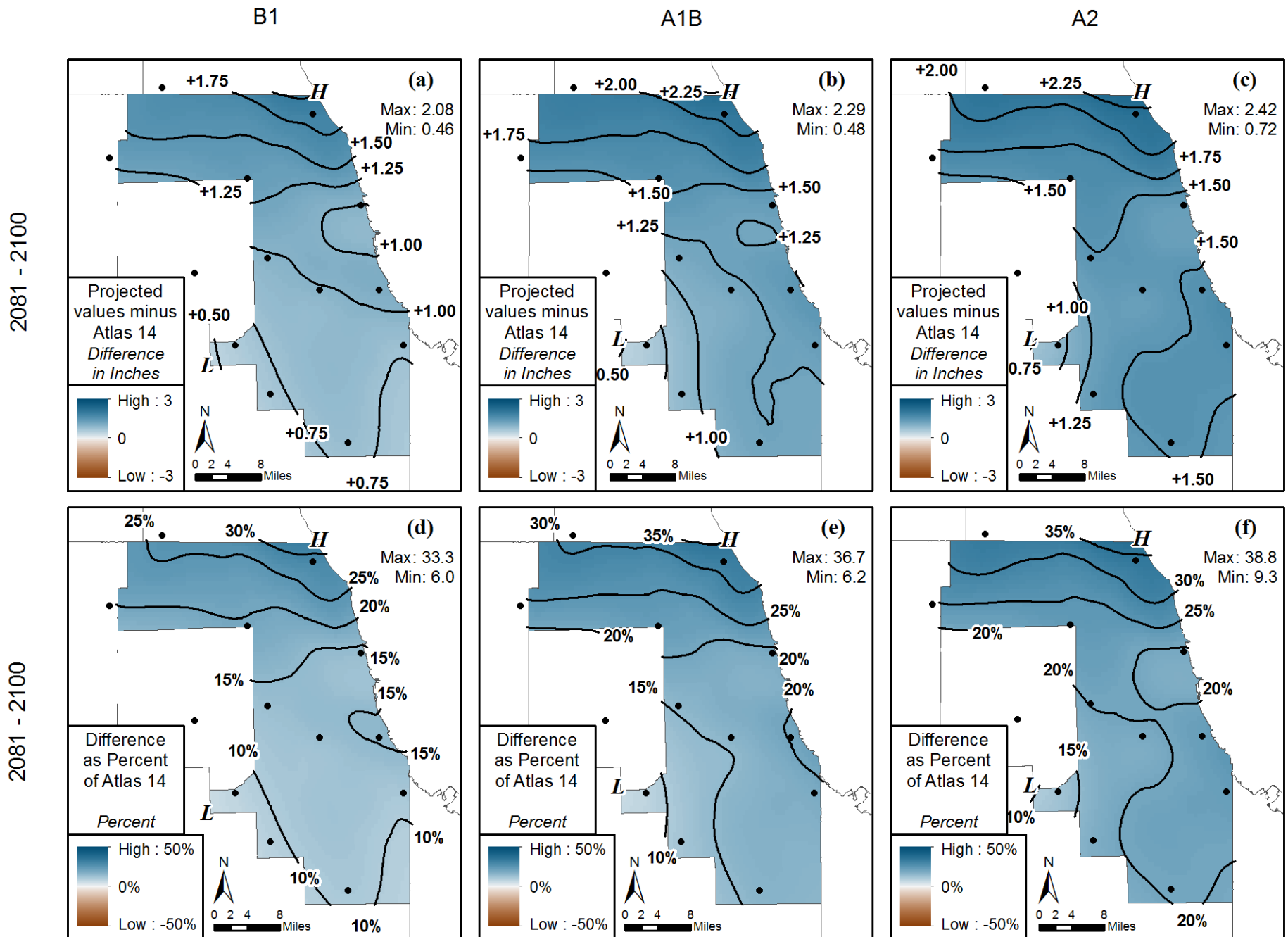
Figure 27. Differences between projected 100-year, 24-hour isohyetals for late-21st century and Atlas 14 (Bonnin et al. 2006). Top row shows absolute differences in inches, and the bottom row shows percent differences. Three columns show results for 3 IPCC CMIP3 climate scenarios (B1, A1B, and A2).

Appendix D. Comparisons of Projected Isohyetals with Hindcast Isohyetal Maps for Cook County (2-year, 10-year, and 100-year recurrence intervals)
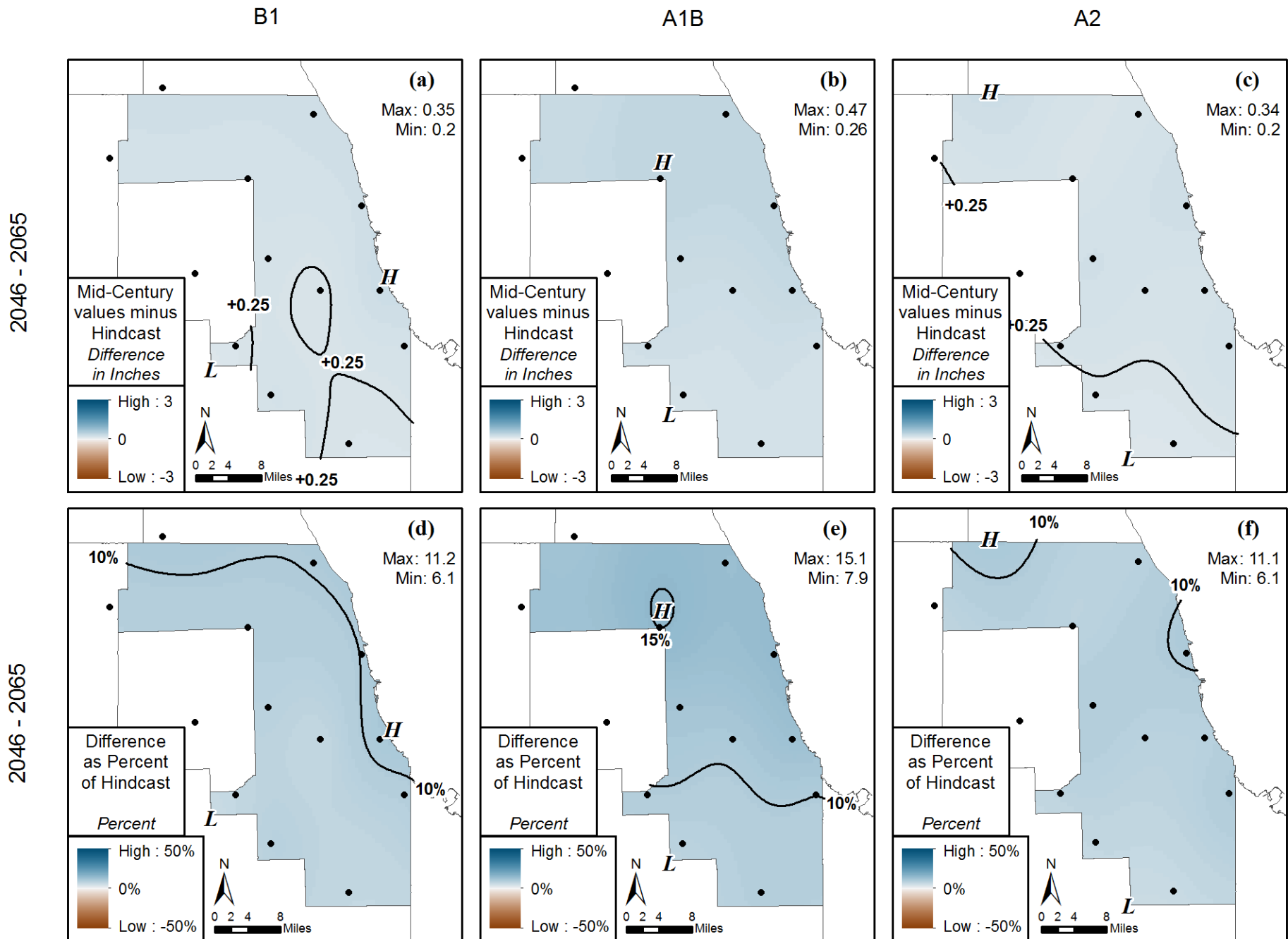
Figure 28. Differences between projected 2-year, 24-hour isohyetals for mid-21st century and 1961-2000 hindcast. Top row shows absolute differences in inches, and the bottom row shows percent differences. Three columns show results for 3 IPCC CMIP3 climate scenarios (B1, A1B, and A2).
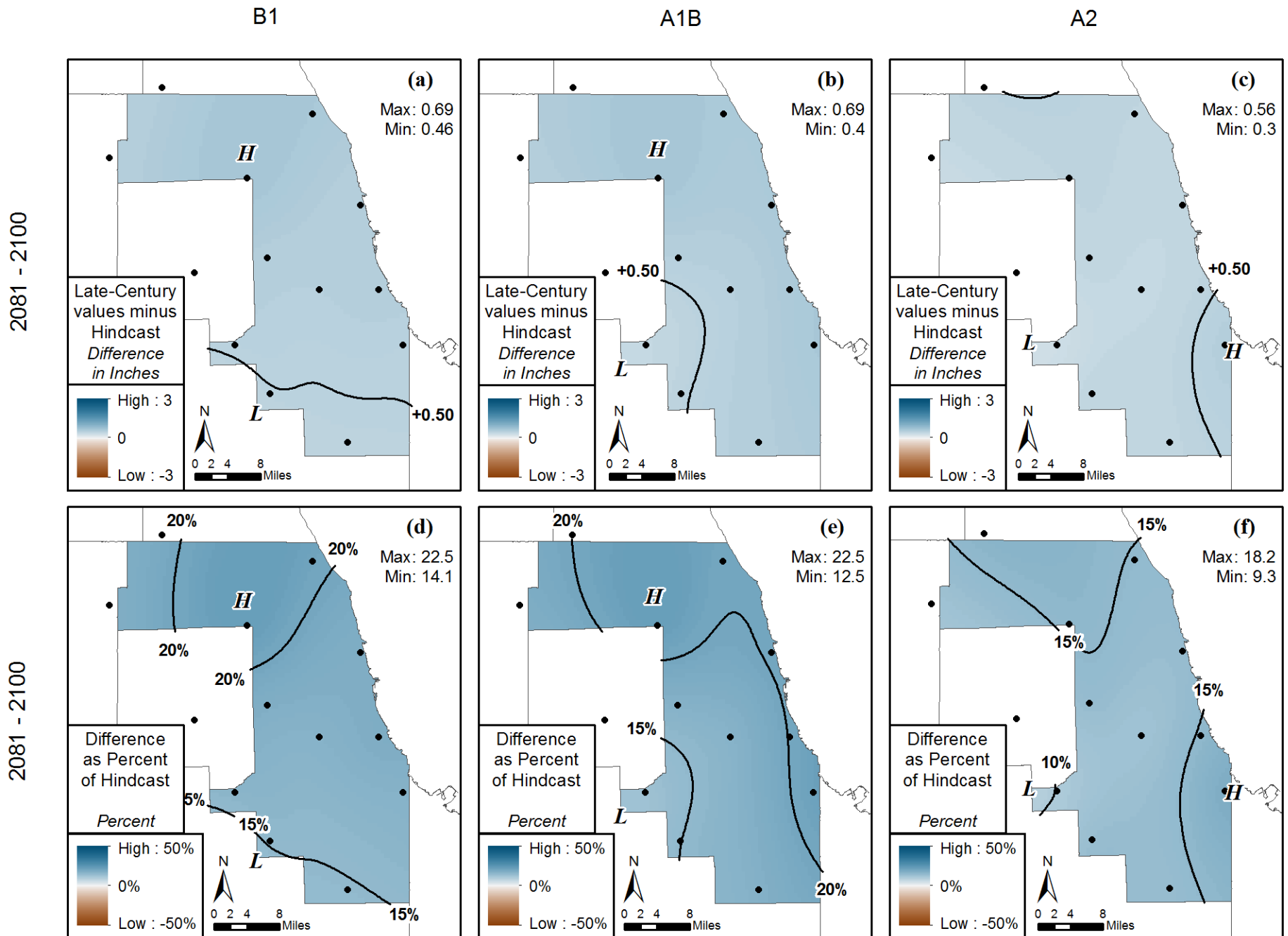
Figure 29. Differences between projected 2-year, 24-hour isohyetals for late-21st century and 1961-2000 hindcast. Top row shows absolute differences in inches, and the bottom row shows percent differences. Three columns show results for 3 IPCC CMIP3 climate scenarios (B1, A1B, and A2).
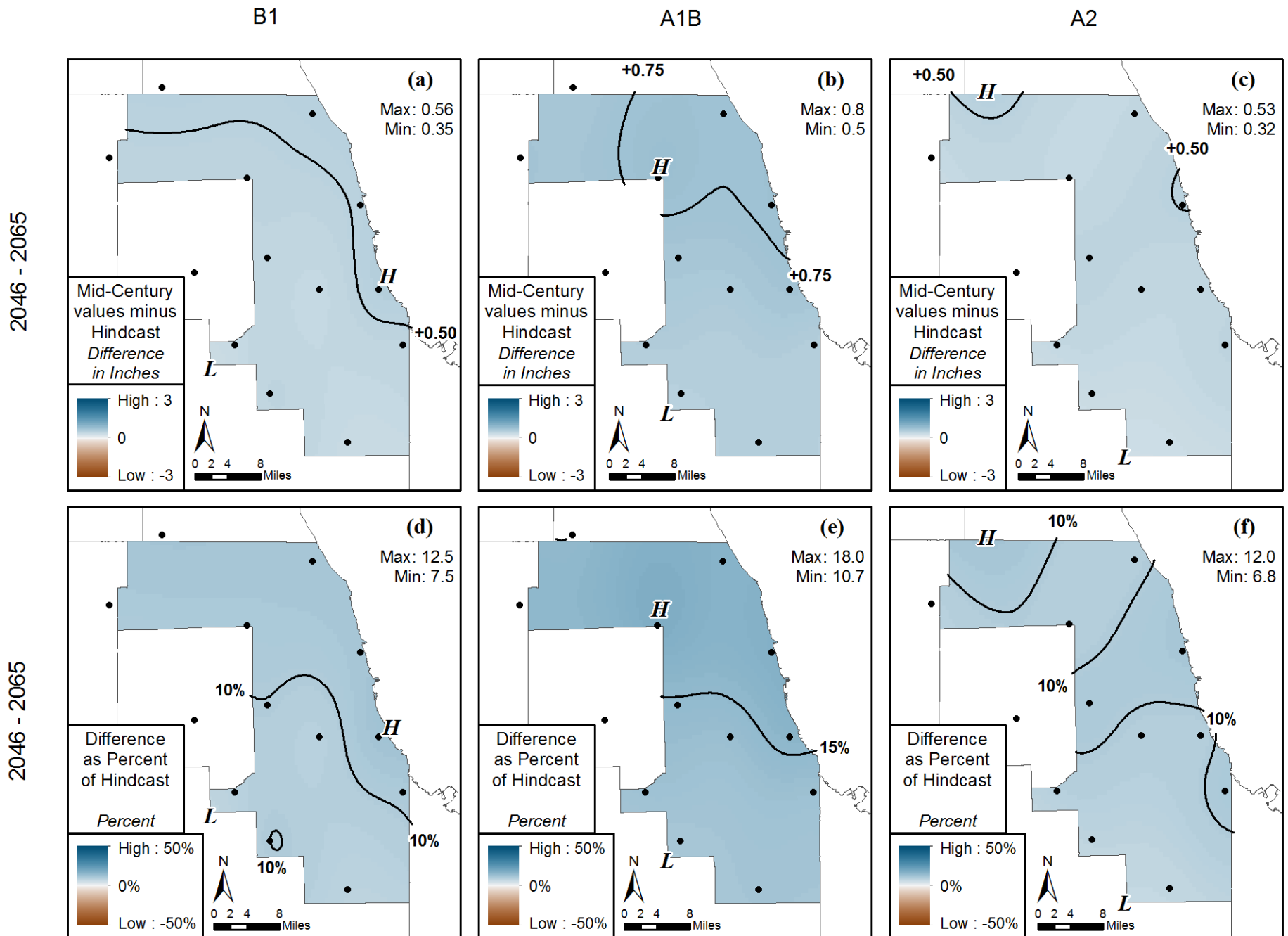
Figure 30. Differences between projected 10-year, 24-hour isohyetals for mid-21st century and 1961-2000 hindcast. Top row shows absolute differences in inches, and the bottom row shows percent differences. Three columns show results for 3 IPCC CMIP3 climate scenarios (B1, A1B, and A2).
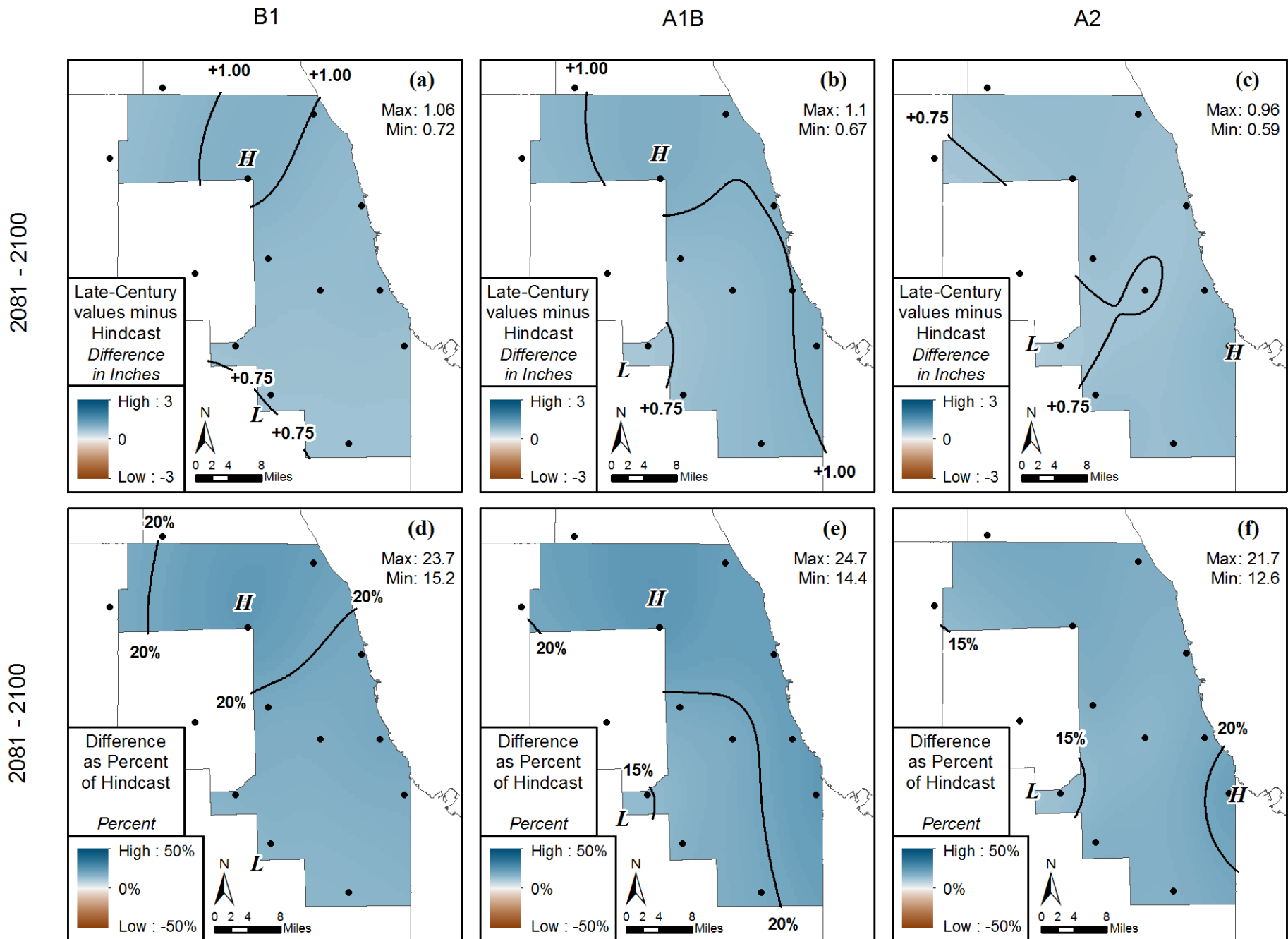
Figure 31. Differences between projected 10-year, 24-hour isohyetals for late-21st century and 1961-2000 hindcast. Top row shows absolute differences in inches, and the bottom row shows percent differences. Three columns show results for 3 IPCC CMIP3 climate scenarios (B1, A1B, and A2).
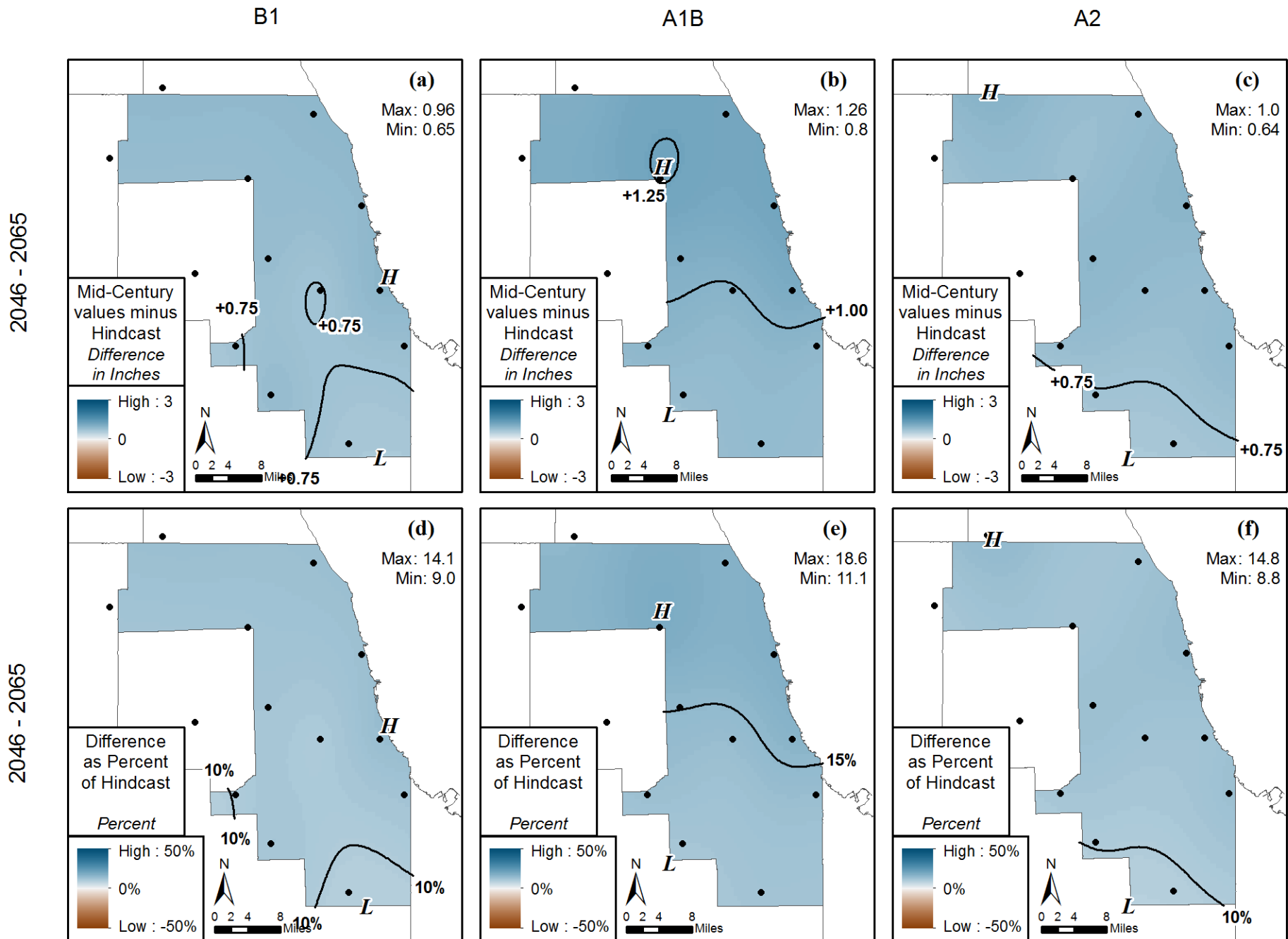
Figure 32. Differences between projected 100-year, 24-hour isohyetals for mid-21st century and 1961-2000 hindcast. Top row shows absolute differences in inches, and the bottom row shows percent differences. Three columns show results for 3 IPCC CMIP3 climate scenarios (B1, A1B, and A2).
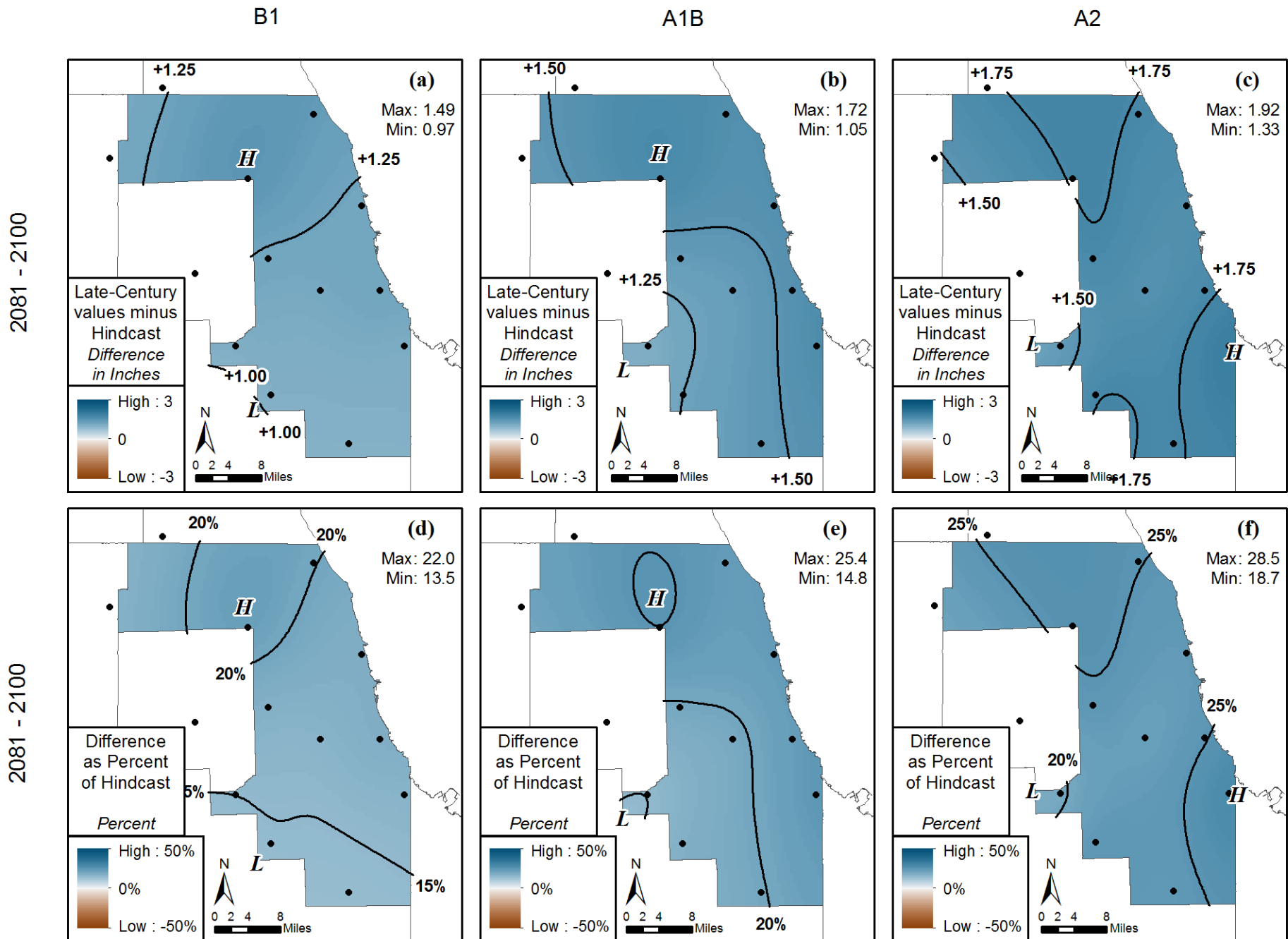
Figure 33. Differences between projected 100-year, 24-hour isohyetals for late-21st century and 1961-2000 hindcast. Top row shows absolute differences in inches, and the bottom row shows percent differences. Three columns show results for 3 IPCC CMIP3 climate scenarios (B1, A1B, and A2).

Appendix E: Projected Rainfall Frequency Tables for Cook County (2-year, 5-year, 10-year, 25-year, 50-year, and 100-year recurrence intervals)

Table 7. Frequency analysis for 1961-2000 calculated based on observed data

	2-year	5-year	10-year	25-year	50-year	100-year
Barrington 3 SW IL	3.05	3.74	4.31	5.16	5.94	6.83
Elgin IL	3.09	3.79	4.37	5.24	6.03	6.93
Wheaton 3 SE IL	3.40	4.17	4.82	5.77	6.64	7.63
Joliet IL	3.06	3.76	4.34	5.19	5.97	6.87
Joliet Brandon Rd Dam IL	3.24	3.98	4.59	5.50	6.33	7.28
Park Forest IL	3.17	3.89	4.49	5.37	6.18	7.11
Hobart 2 WNW IN	3.09	3.79	4.38	5.24	6.03	6.94
Gary IN	2.98	3.65	4.22	5.05	5.81	6.68
Site 19 (Chicago, IL)	3.21	3.94	4.55	5.45	6.27	7.21
Chicago Midway Airport 3SW IL	3.41	4.18	4.82	5.77	6.64	7.64
Chicago Botanical Garden IL	3.15	3.86	4.46	5.33	6.14	7.06
Site 7 (Chicago, IL)	3.07	3.76	4.34	5.20	5.98	6.88
Site 8 (Westbrook, IL)	3.09	3.80	4.38	5.25	6.04	6.94
Site 15 (Lemont, IL)	3.35	4.11	4.74	5.67	6.53	7.51
Site 20 (Orland Park, IL)	3.26	4.00	4.61	5.52	6.36	7.31
Chicago O'Hare Int. Airport IL	3.03	3.72	4.29	5.14	5.92	6.80
Chicago University IL	2.85	3.50	4.04	4.84	5.57	6.40

Table 8. Frequency analysis (in inches) for 1961-2000 calculated as a weighted mean of ensemble of climate models

	2-year	5-year	10-year	25-year	50-year	100-year
Barrington 3 SW IL	3.06	3.82	4.43	5.26	5.98	6.76
Elgin IL	3.14	3.92	4.54	5.40	6.14	6.94
Wheaton 3 SE IL	3.22	4.02	4.65	5.53	6.29	7.10
Joliet IL	3.22	4.01	4.65	5.53	6.29	7.11
Joliet Brandon Rd Dam IL	3.23	4.03	4.67	5.55	6.31	7.13
Park Forest IL	3.29	4.11	4.76	5.66	6.43	7.27
Hobart 2 WNW IN	3.13	3.91	4.53	5.38	6.12	6.92
Gary IN	3.05	3.80	4.41	5.24	5.96	6.73
Site 19 (Chicago, IL)	3.07	3.83	4.43	5.27	5.99	6.76
Chicago Midway Airport 3SW IL	3.22	4.01	4.65	5.53	6.28	7.10
Chicago Botanical Garden IL	3.14	3.92	4.54	5.40	6.13	6.92
Site 7 (Chicago, IL)	3.11	3.88	4.50	5.35	6.08	6.87
Site 8 (Westbrook, IL)	3.20	3.99	4.63	5.50	6.26	7.07
Site 15 (Lemont, IL)	3.24	4.04	4.68	5.56	6.32	7.14
Site 20 (Orland Park, IL)	3.26	4.06	4.71	5.60	6.36	7.19
Chicago O'Hare Int. Airport IL	3.09	3.85	4.46	5.31	6.03	6.81
Chicago University IL	3.12	3.88	4.50	5.35	6.09	6.88

Table 9. Multi-model ensemble average (in inches) for scenario A1B for mid-21st century

	2-year	5-year	10-year	25-year	50-year	100-year
Barrington 3 SW IL	3.43	4.36	5.09	6.09	6.92	7.81
Elgin IL	3.55	4.50	5.25	6.28	7.14	8.04
Wheaton 3 SE IL	3.56	4.52	5.28	6.31	7.18	8.10
Joliet IL	3.46	4.39	5.12	6.12	6.96	7.85
Joliet Brandon Rd Dam IL	3.44	4.37	5.11	6.10	6.94	7.83
Park Forest IL	3.59	4.56	5.32	6.36	7.23	8.15
Hobart 2 WNW IN	3.44	4.36	5.09	6.08	6.91	7.79
Gary IN	3.37	4.27	4.98	5.95	6.76	7.62
Site 19 (Chicago, IL)	3.38	4.29	5.01	5.99	6.81	7.69
Chicago Midway Airport 3SW IL	3.56	4.52	5.28	6.31	7.17	8.08
Chicago Botanical Garden IL	3.57	4.53	5.29	6.32	7.19	8.11
Site 7 (Chicago, IL)	3.56	4.52	5.27	6.30	7.16	8.07
Site 8 (Westbrook, IL)	3.58	4.54	5.31	6.35	7.21	8.14
Site 15 (Lemont, IL)	3.55	4.51	5.27	6.30	7.16	8.08
Site 20 (Orland Park, IL)	3.53	4.49	5.24	6.26	7.12	8.03
Chicago O'Hare Int. Airport IL	3.55	4.51	5.26	6.29	7.15	8.06
Chicago University IL	3.52	4.46	5.21	6.23	7.09	7.99

Table 10. Multi-model ensemble average (in inches) for scenario A2 for mid-21st century

	2-year	5-year	10-year	25-year	50-year	100-year
Barrington 3 SW IL	3.41	4.27	4.96	5.94	6.80	7.76
Elgin IL	3.39	4.25	4.94	5.91	6.76	7.72
Wheaton 3 SE IL	3.49	4.38	5.09	6.09	6.98	7.97
Joliet IL	3.34	4.18	4.86	5.82	6.67	7.61
Joliet Brandon Rd Dam IL	3.33	4.17	4.85	5.81	6.65	7.59
Park Forest IL	3.51	4.39	5.10	6.10	6.98	7.95
Hobart 2 WNW IN	3.37	4.22	4.90	5.87	6.72	7.66
Gary IN	3.32	4.16	4.83	5.79	6.62	7.55
Site 19 (Chicago, IL)	3.37	4.23	4.91	5.87	6.71	7.65
Chicago Midway Airport 3SW IL	3.49	4.37	5.09	6.09	6.98	7.96
Chicago Botanical Garden IL	3.41	4.28	4.97	5.95	6.82	7.79
Site 7 (Chicago, IL)	3.43	4.30	5.00	5.99	6.86	7.82
Site 8 (Westbrook, IL)	3.51	4.40	5.11	6.12	7.02	8.01
Site 15 (Lemont, IL)	3.50	4.38	5.09	6.10	6.98	7.97
Site 20 (Orland Park, IL)	3.49	4.37	5.08	6.08	6.95	7.93
Chicago O'Hare Int. Airport IL	3.35	4.19	4.87	5.83	6.68	7.62
Chicago University IL	3.39	4.24	4.93	5.90	6.76	7.72

Table 11. Multi-model ensemble average (in inches) for scenario B1 for mid-21ˢᵗ century.

	2-year	5-year	10-year	25-year	50-year	100-year
Barrington 3 SW IL	3.39	4.26	4.95	5.92	6.75	7.68
Elgin IL	3.44	4.32	5.03	6.00	6.85	7.79
Wheaton 3 SE IL	3.47	4.37	5.08	6.07	6.92	7.86
Joliet IL	3.41	4.29	4.99	5.96	6.80	7.73
Joliet Brandon Rd Dam IL	3.38	4.25	4.94	5.90	6.74	7.66
Park Forest IL	3.53	4.43	5.15	6.14	7.00	7.95
Hobart 2 WNW IN	3.35	4.20	4.88	5.82	6.64	7.54
Gary IN	3.36	4.22	4.90	5.85	6.67	7.57
Site 19 (Chicago, IL)	3.35	4.22	4.90	5.85	6.67	7.58
Chicago Midway Airport 3SW IL	3.46	4.35	5.05	6.04	6.90	7.84
Chicago Botanical Garden IL	3.46	4.35	5.06	6.05	6.90	7.85
Site 7 (Chicago, IL)	3.43	4.31	5.01	5.99	6.83	7.77
Site 8 (Westbrook, IL)	3.48	4.37	5.09	6.08	6.95	7.90
Site 15 (Lemont, IL)	3.47	4.36	5.07	6.06	6.92	7.87
Site 20 (Orland Park, IL)	3.54	4.45	5.18	6.19	7.06	8.03
Chicago O'Hare Int. Airport IL	3.38	4.25	4.94	5.90	6.73	7.65
Chicago University IL	3.45	4.34	5.05	6.03	6.88	7.82

Table 12. Multi-model ensemble average (in inches) for scenario A1B for late-21st century

	2-year	5-year	10-year	25-year	50-year	100-year
Barrington 3 SW IL	3.68	4.64	5.41	6.46	7.35	8.30
Elgin IL	3.71	4.68	5.45	6.51	7.41	8.37
Wheaton 3 SE IL	3.73	4.71	5.49	6.56	7.46	8.43
Joliet IL	3.60	4.54	5.29	6.32	7.19	8.12
Joliet Brandon Rd Dam IL	3.63	4.58	5.33	6.36	7.24	8.17
Park Forest IL	3.86	4.87	5.67	6.77	7.71	8.71
Hobart 2 WNW IN	3.81	4.81	5.60	6.69	7.62	8.61
Gary IN	3.71	4.69	5.46	6.52	7.43	8.40
Site 19 (Chicago, IL)	3.73	4.70	5.48	6.54	7.44	8.40
Chicago Midway Airport 3SW IL	3.75	4.74	5.52	6.59	7.49	8.46
Chicago Botanical Garden IL	3.78	4.77	5.56	6.64	7.55	8.53
Site 7 (Chicago, IL)	3.75	4.73	5.51	6.58	7.49	8.46
Site 8 (Westbrook, IL)	3.75	4.73	5.51	6.58	7.49	8.46
Site 15 (Lemont, IL)	3.65	4.61	5.37	6.40	7.28	8.22
Site 20 (Orland Park, IL)	3.75	4.73	5.51	6.58	7.48	8.44
Chicago O'Hare Int. Airport IL	3.77	4.76	5.55	6.62	7.53	8.51
Chicago University IL	3.74	4.72	5.50	6.57	7.47	8.44

Table 13. Multi-model ensemble average (in inches) for scenario A2 for late-21st century

	2-year	5-year	10-year	25-year	50-year	100-year
Barrington 3 SW IL	3.56	4.51	5.28	6.38	7.36	8.48
Elgin IL	3.53	4.48	5.25	6.34	7.31	8.41
Wheaton 3 SE IL	3.56	4.51	5.29	6.41	7.41	8.55
Joliet IL	3.48	4.42	5.18	6.26	7.23	8.32
Joliet Brandon Rd Dam IL	3.57	4.53	5.31	6.42	7.42	8.55
Park Forest IL	3.75	4.76	5.58	6.75	7.81	9.00
Hobart 2 WNW IN	3.69	4.68	5.48	6.63	7.66	8.84
Gary IN	3.57	4.53	5.31	6.42	7.41	8.53
Site 19 (Chicago, IL)	3.62	4.60	5.39	6.52	7.53	8.68
Chicago Midway Airport 3SW IL	3.62	4.59	5.38	6.51	7.52	8.68
Chicago Botanical Garden IL	3.61	4.58	5.37	6.50	7.51	8.66
Site 7 (Chicago, IL)	3.55	4.50	5.27	6.38	7.36	8.48
Site 8 (Westbrook, IL)	3.65	4.63	5.43	6.58	7.61	8.78
Site 15 (Lemont, IL)	3.56	4.52	5.30	6.41	7.40	8.53
Site 20 (Orland Park, IL)	3.70	4.70	5.52	6.68	7.73	8.92
Chicago O'Hare Int. Airport IL	3.56	4.52	5.30	6.42	7.42	8.57
Chicago University IL	3.59	4.56	5.34	6.46	7.45	8.58

Table 14. Multi-model ensemble average (in inches) for scenario B1 for late-21st century.

	2-year	5-year	10-year	25-year	50-year	100-year
Barrington 3 SW IL	3.65	4.59	5.32	6.30	7.12	7.99
Elgin IL	3.69	4.64	5.38	6.38	7.21	8.09
Wheaton 3 SE IL	3.82	4.81	5.58	6.62	7.48	8.40
Joliet IL	3.62	4.55	5.28	6.26	7.08	7.96
Joliet Brandon Rd Dam IL	3.58	4.50	5.22	6.20	7.01	7.87
Park Forest IL	3.78	4.76	5.52	6.54	7.40	8.30
Hobart 2 WNW IN	3.62	4.55	5.27	6.25	7.08	7.95
Gary IN	3.57	4.49	5.21	6.18	6.99	7.84
Site 19 (Chicago, IL)	3.59	4.51	5.23	6.20	7.01	7.87
Chicago Midway Airport 3SW IL	3.76	4.73	5.48	6.50	7.36	8.26
Chicago Botanical Garden IL	3.80	4.78	5.53	6.56	7.41	8.32
Site 7 (Chicago, IL)	3.67	4.62	5.36	6.37	7.20	8.09
Site 8 (Westbrook, IL)	3.77	4.75	5.50	6.53	7.38	8.28
Site 15 (Lemont, IL)	3.75	4.72	5.47	6.48	7.32	8.22
Site 20 (Orland Park, IL)	3.75	4.72	5.47	6.49	7.34	8.24
Chicago O'Hare Int. Airport IL	3.78	4.75	5.51	6.53	7.39	8.29
Chicago University IL	3.68	4.63	5.37	6.37	7.21	8.09

Appendix F. Projected Changes in 90% Upper Confidence Interval of Isohyetal Maps for Cook County (2-year, 10-year, and 100-year recurrence intervals)
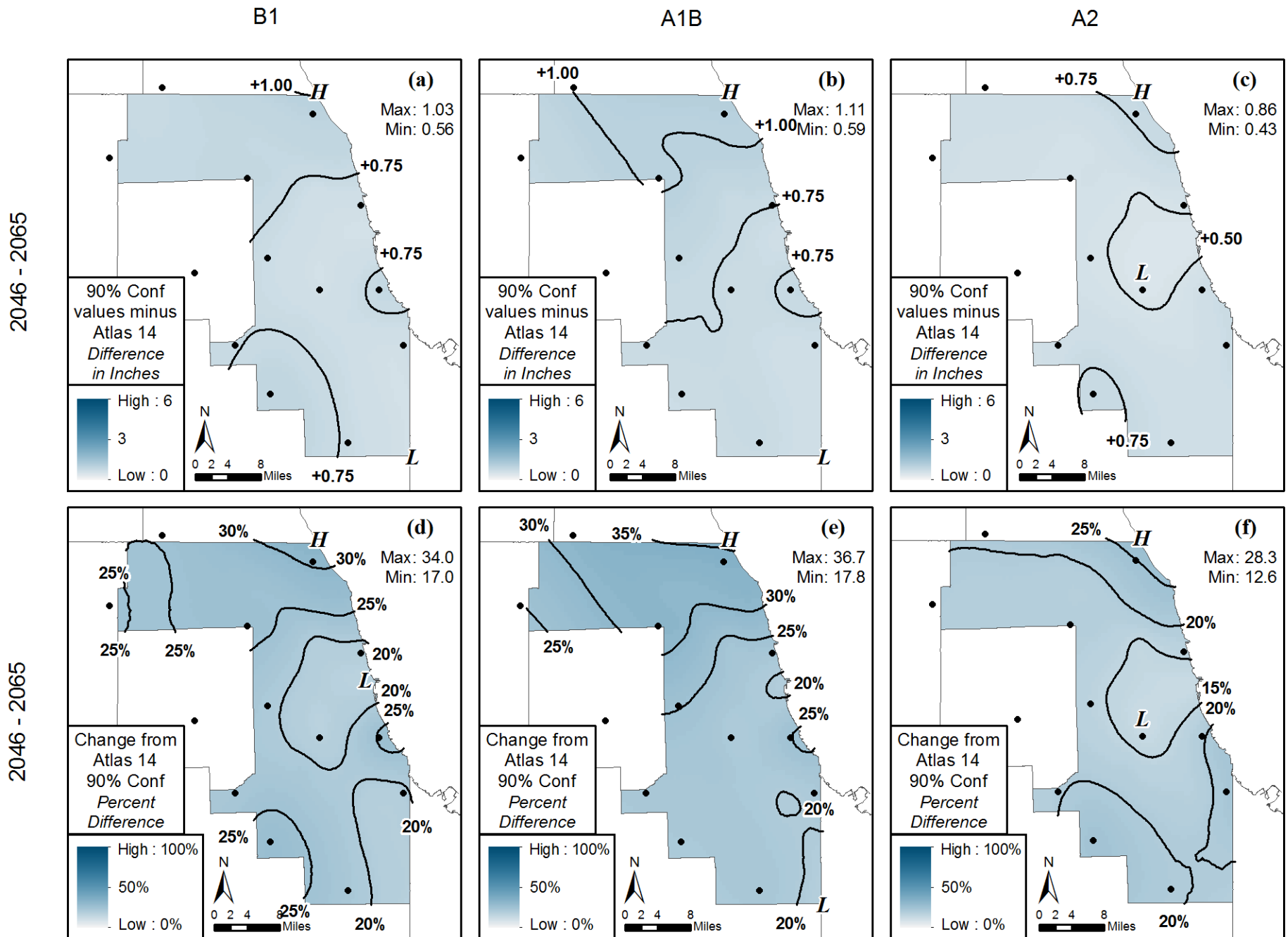
Figure 34. Differences between projected 2-year, 24-hour 90% Upper Confidence interval isohyetals for mid-21st century and Atlas 14 (Bonnin et al. 2006). Top row shows absolute differences in inches, and the bottom row shows percent differences. Three columns show results for 3 IPCC CMIP3 climate scenarios (B1, A1B, and A2).
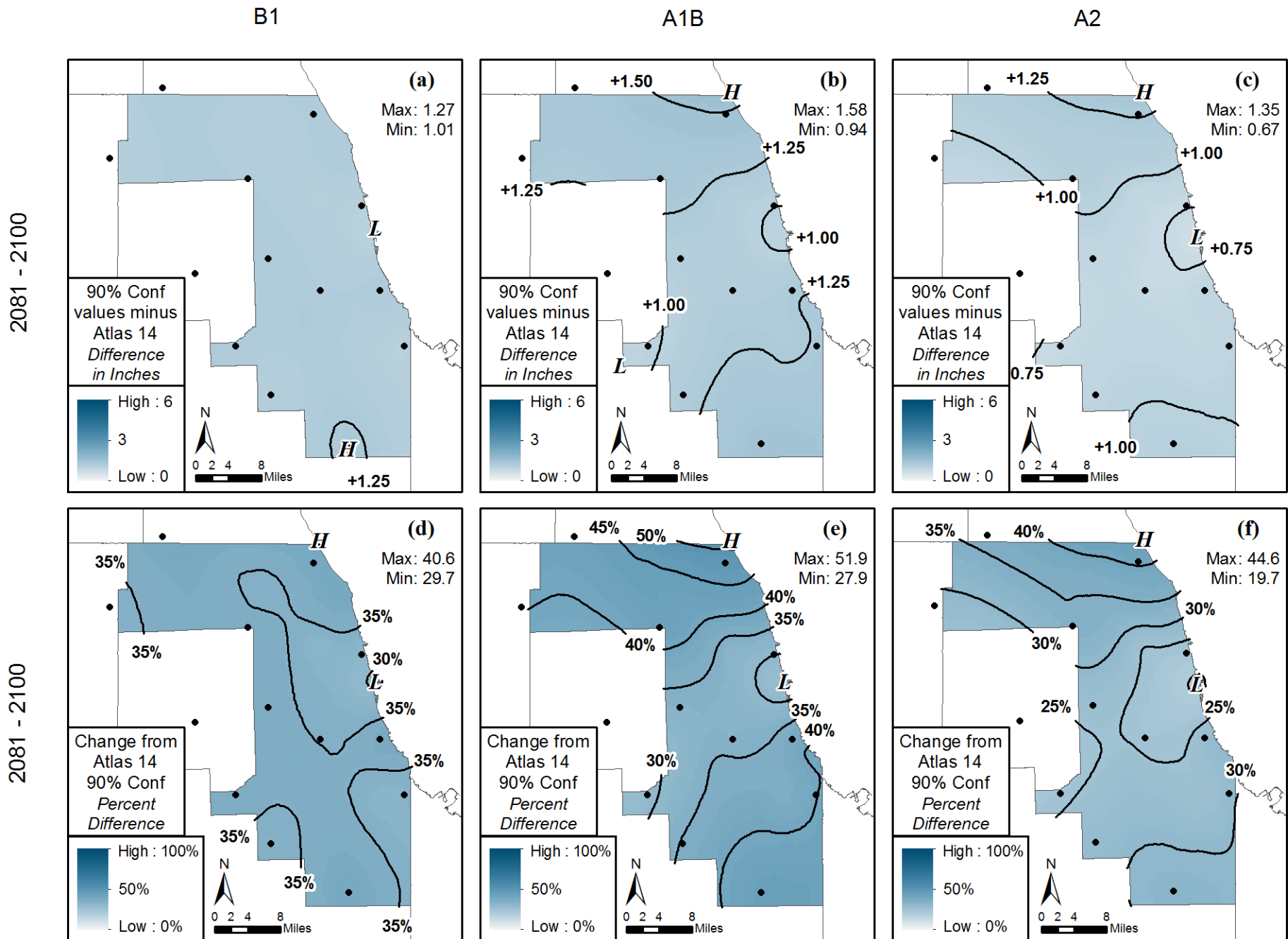
Figure 35. Differences between projected 2-year, 24-hour 90% Upper Confidence interval isohyetals for late-21st century and Atlas 14 (Bonnin et al. 2006). Top row shows absolute differences in inches, and the bottom row shows percent differences. Three columns show results for 3 IPCC CMIP3 climate scenarios (B1, A1B, and A2).
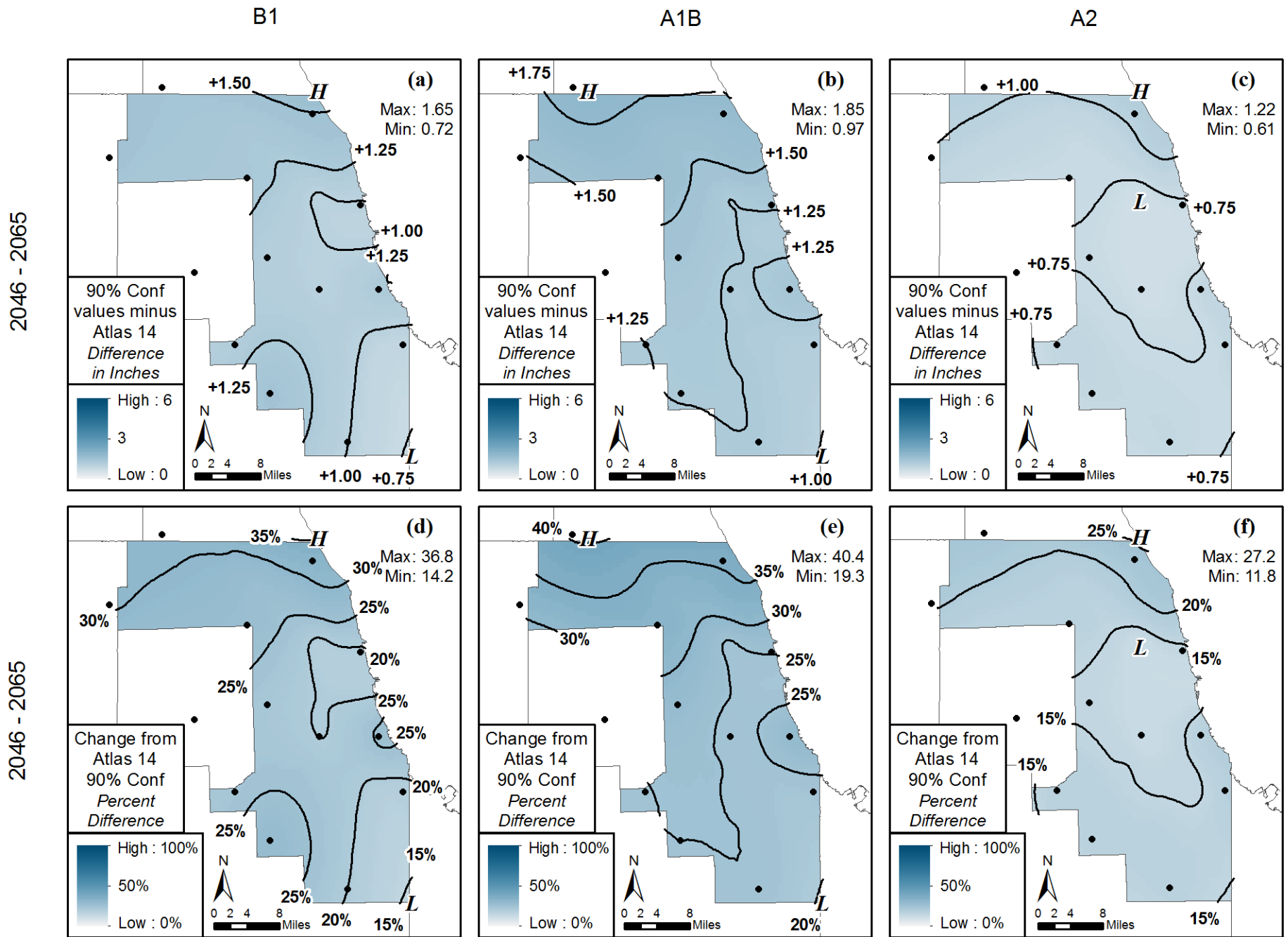
Figure 36. Differences between projected 10-year, 24-hour 90% Upper Confidence interval isohyetals for mid-21st century and Atlas 14 (Bonnin et al. 2006). Top row shows absolute differences in inches, and the bottom row shows percent differences. Three columns show results for 3 IPCC CMIP3 climate scenarios (B1, A1B, and A2).
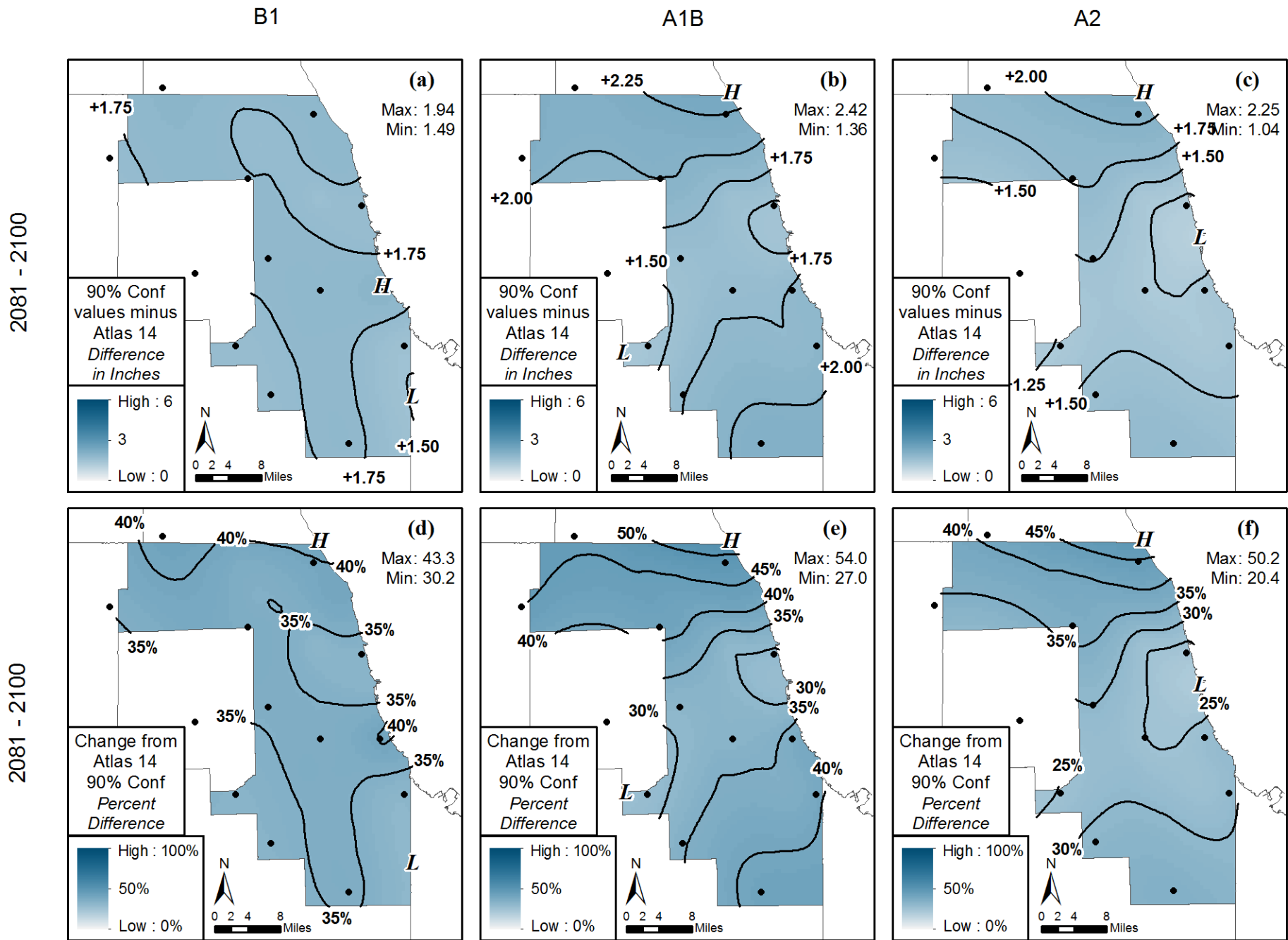
Figure 37. Differences between projected 10-year, 24-hour 90% Upper Confidence interval isohyetals for late-21st century and Atlas 14 (Bonnin et al. 2006). Top row shows absolute differences in inches, and the bottom row shows percent differences. Three columns show results for 3 IPCC CMIP3 climate scenarios (B1, A1B, and A2).

65
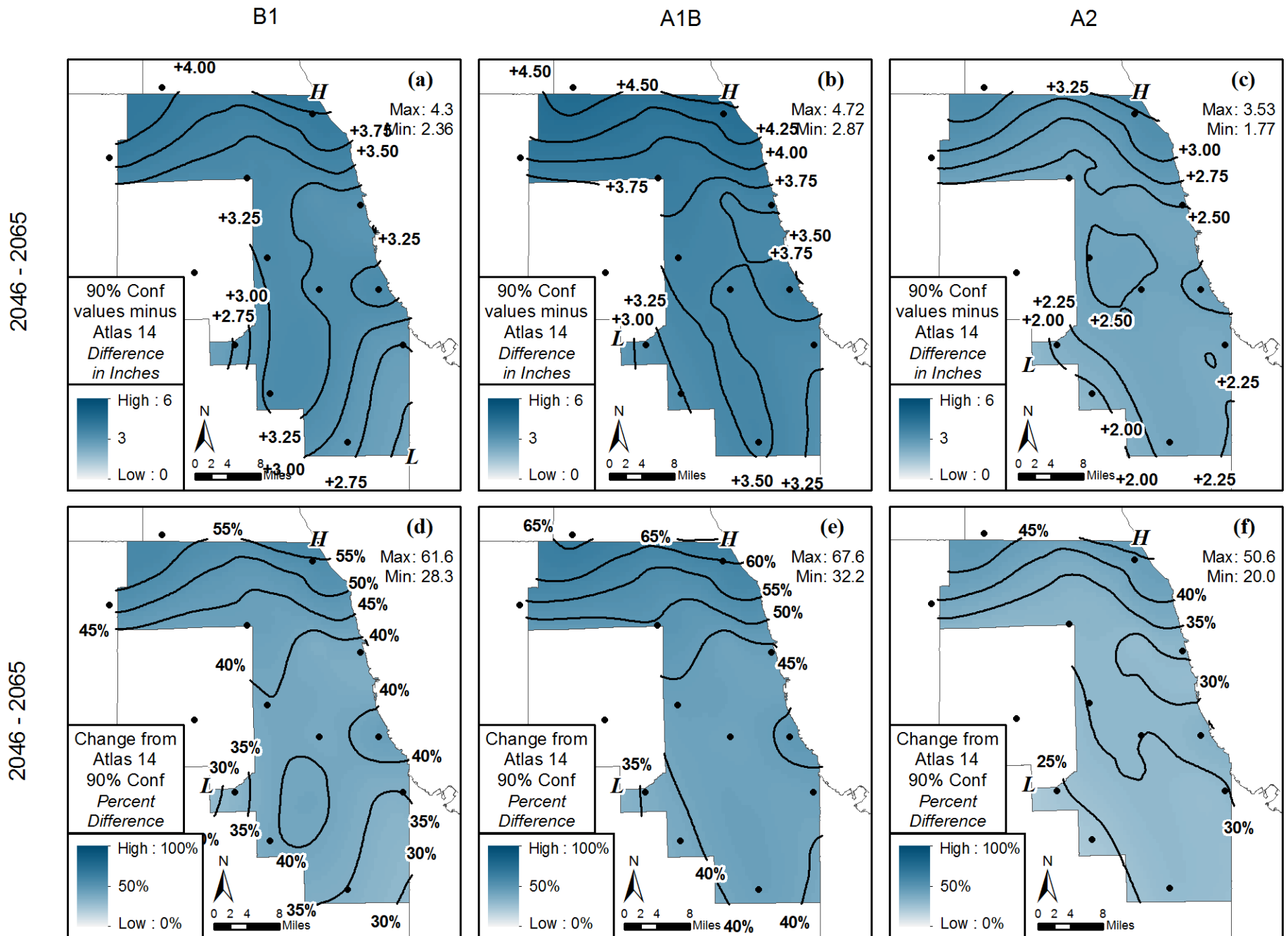
Figure 38. Differences between projected 100-year, 24-hour 90% Upper Confidence interval isohyetals for mid-21st century and Atlas 14 (Bonnin et al. 2006). Top row shows absolute differences in inches, and the bottom row shows percent differences. Three columns show results for 3 IPCC CMIP3 climate scenarios (B1, A1B, and A2).
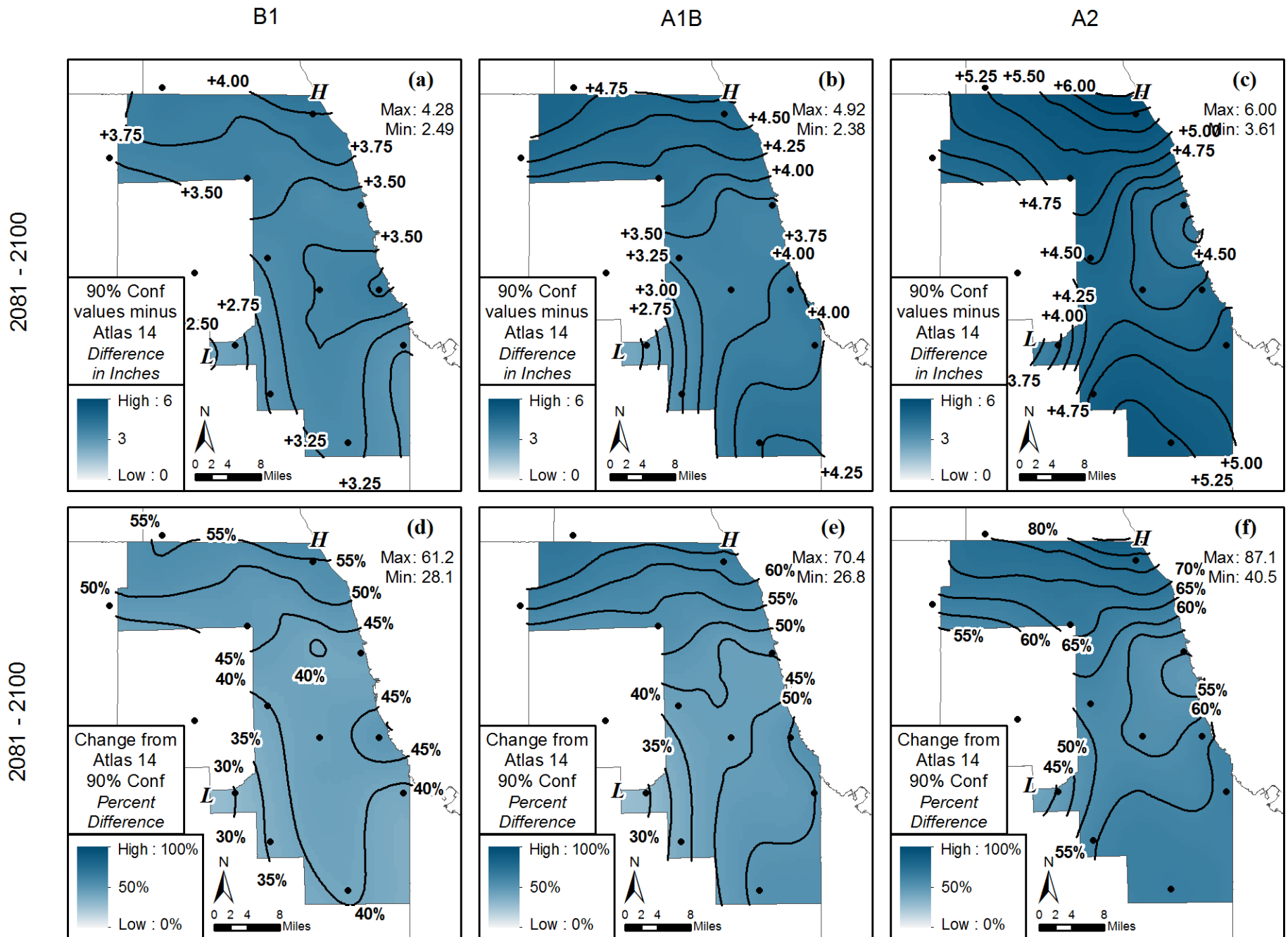
Figure 39. Differences between projected 100-year, 24-hour 90% Upper Confidence interval isohyetals for late-21st century and Atlas 14 (Bonnin et al. 2006). Top row shows absolute differences in inches, and the bottom row shows percent differences. Three columns show results for 3 IPCC CMIP3 climate scenarios (B1, A1B, and A2).